APPLYING THE PULSED ION CHAMBER METHODOLOGY TO FULL RANGE REACTOR POWER MEASUREMENTS

By

BRUCE J. KAISER

A DISSERTATION PRESENTED TO THE GRADUATE COUNCIL OF THE
UNIVERSITY OF FLORIDA
IN PARTIAL FULFILLMENT OF THE REQUIREMENTS FOR THE
DEGREE OF DOCTOR OF PHILOSOPHY

UNIVERSITY OF FLORIDA
1977

ACKNOWLEDGEMENTS

The author is especially indebted to his committee chairman Dr. William Ellis, whose input, guidance, and encouragement in this long endeavor proved invaluable. Thanks is also extended the other members of his committee, Dr. E. E. Carroll, Dr. N. J. Diaz, Dr. G. R. Dalton, Dr. W. Mauderli, and Dr. C. K. Day for their interest and support.

Much of the work to be described herein was performed at the Hanford Engineering and Development Laboratory. The author is deeply indebted to Dr. Cliff Day and the Instrument Technology group at Westinghouse Hanford whose avid support made the work possible.

Acknowledgement is expressed for the financial support received from a University of Florida teaching assistantship and a Northwest College and University Association for Science fellowship.

Finally, words fail to express the thanks which is extended to the author's wife, Michele. Her patience, love, and financial support proved to be the difference between success and failure.

TABLE OF CONTENTS

LIST OF TABLES

LIST OF FIGURES

FIGURES (Cont'd)

FIGURES (Cont'd)

FIGURES (Cont'd)

Abstract of Dissertation Presented to the Graduate Council of the University of Florida in Partial Fulfillment of the Requirements for the Degree of Doctor of Philosophy

APPLYING THE PULSED ION CHAMBER METHODOLOGY
TO FULL RANGE REACTOR POWER MEASUREMENTS

By

Bruce J. Kaiser

June, 1977

Chairman: Dr. William H. Ellis
Major Department: Nuclear Engineering Sciences

A computer based/controlled PIC solid state electronic system is presented in its entirety. Its operation is described and evaluated both as a plasma diagnostic instrument and a basic reactor power measurement system. The system, in conjunction with two sets of matched ionization chambers (one with a 93% enriched ^{235}U coating the other without), is evaluated in terms of response in radiation fields of 10^2 to 3×10^6 R/hr at temperatures ranging from 25°C to 475°C. Two different sets of chambers were used, one containing Ar-5%N_2, the other Ne. Gamma compensation to within $\sim \pm$ 5% proved feasible, at a given temperature from, 10^3 to 3×10^6 R/hr.

The chambers' responses altered over the temperature range used. The PIC signal for neon at 3×10^6 R/hr and 25°C was 2.03V where at 432°C it was 4.75V. For the Ar - 5% N_2 chambers under the same conditions the signal increased from 1.9V to 2.74 volts. The Ar-N_2 chamber temperature response was expected. The Ne temperature response was constant up to

282°C as predicted. However, at this temperature the signal began to show a slow increasing trend which continued up to the maximum temperature used, 475°C. This requires more study.

CHAPTER I
INTRODUCTION

The need for dependable and accurate monitoring of neutron flux (reactor power) presents the nuclear engineer with one of his most difficult design tasks. For safety reasons, commercial reactors of all types require the flux to be monitored over at least twelve decades with ±10% accuracy. This range, even under optimum environmental conditions, requires a minimum of two detector operational modes. However, in all cases, three modes are used to insure overlap (redundancy) and thus the safe operation of the reactor. In addition to the range requirements, the detectors must operate consistently and accurately under the most adverse environmental conditions. These, depending on the situation, include high temperatures, excessive background radiation levels, and high neutron flux levels, over extended periods of time (months).

For the most part, adequate monitoring systems exist for those nuclear plants which are in use at the present time. However, the limits of these current systems are exceeded when one attempts to apply them to the needs of the fast breeder reactor or the new generation of large core light water reactors. These new plants require fast response, in-core detection systems. Unfortunately, the in-core environment is extreme in both the temperature and flux domains and, as yet, no system has functioned adequately under such conditions.

To delineate the exact nature of the problems faced, one must carefully examine the reactor power measurement systems presently being

utilized. Such an examination will not only suggest where, and possibly how, improvement can be made in current systems, but it will also point to the pressing need for a full range, high temperature single sensor system.

The first division between neutron sensing systems comes from whether they utilize in-core or ex-core sensors. Examining figure 1-1 we see why such a division exists. There is a difference of a factor of 10 in temperature and a factor of 10^3 in gamma and neutron fluxes between the two regions. It is apparent that those systems designed for in-core monitoring must be an extremely hearty breed. For this reason, only one of the four major reactor types (PWR, HTGR, LMFBR, and BWR) has the neutron flux level safety control monitors in-core. The BWR, due to its large volume and particular design characteristics (large cruciform control rods and boiling water) requires in-core flux monitoring for safety reasons. This requirement, coupled with the lack of dependable in-core systems, together, comprise one of the most difficult problems the BWR engineer faces today.

Figure 1-1 also serves to define the upper limit operating specifications for both the in-core and ex-core environment. The lower limits corresponding to reactor shutdown are depicted in figure 1-1 as well. The great range in reactor power makes the use of a single sensor and circuit impossible with current technology. Thus a detector of any given design is of use only over a specific part of the flux range and must be complimented with other sensor-circuit designs. Overlapping one or two decades of each design sacrifices part of their useful range but insures smooth transfer of control and safety functions from one control circuit to the next.

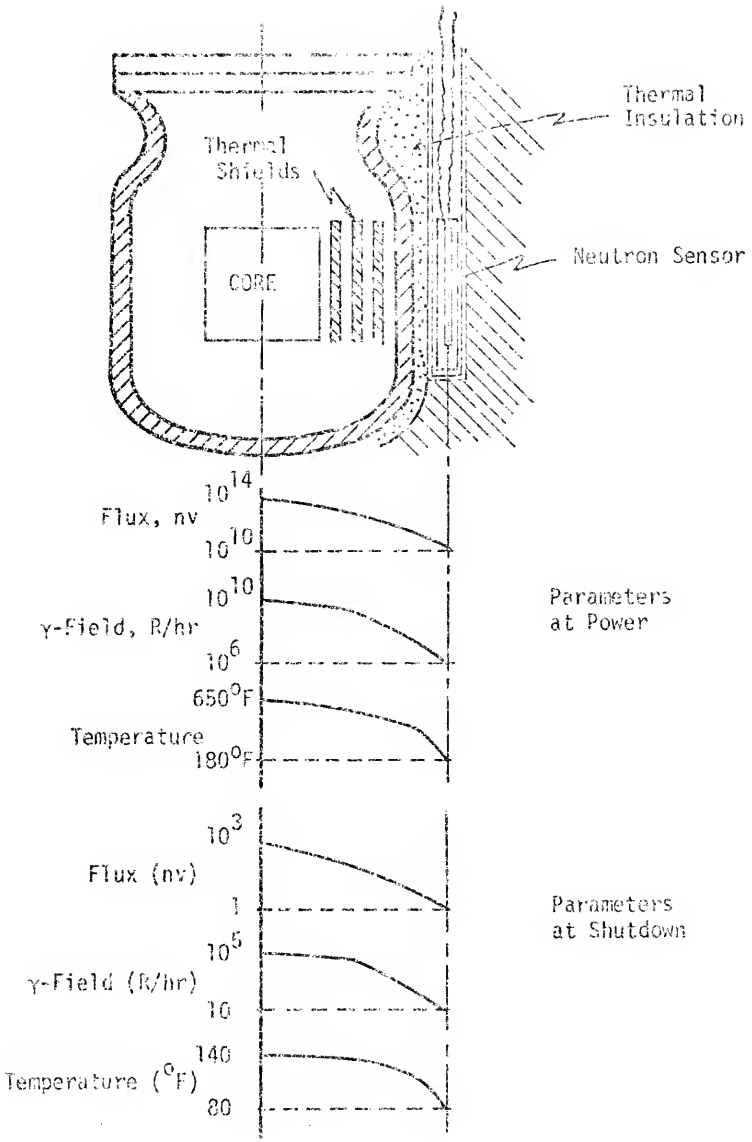

Figure 1-1. Typical environmental profile for neutron sensors in a PWR at full power and at shutdown.

Three ranges are used to divide neutron flux levels found in reactors from startup to full power; the source, intermediate, and full or operating power range. Figures 1-2 and 1-3 show the limits of these ranges, along with the typical neutron detectors used in common ex-core and BWR in-core control systems.

It is apparent from figure 1-3 that the source range monitoring system must utilize sensitive detection methods. Proportional and fission counting systems offer the greatest sensitivity with maximum gamma discrimination. Three neutron sensitive materials are commonly used in the proportional counters; $^{10}BF_3$ gas, ^{3}He gas and ^{10}B as a lining. Each has its advantages and disadvantages. $^{10}BF_3$ offers high sensitivity but the necessary high polarizing voltages cause rapid degradation of the gas in high flux environments. The ^{3}He gas proportional counter offers greater sensitivity and stability than the $^{10}BF_3$, but has a smaller Q value, which makes the gamma sensitivity proportionately greater. The ^{10}B lined chamber is less sensitive than the $^{10}BF_3$ but more stable in high intensity fields. Fission chambers have their electrodes coated with uranium highly enriched in ^{235}U.

In both in-core and ex-core systems, the minimum allowable count rate for safety reasons is 1 to 10 counts per second. Thus, the detector's sensitivity in each case must be adjusted to insure that the shutdown reactor neutron flux results in a count rate of greater than 1 count per second. Due to the resolution limitations of such counting systems, their fastest possible response is on the order of 10^6 counts per second. To the point, a state of the art fission counter can accurately indicate neutron flux levels over six decades while immersed in a gamma flux as high as 10^5 R/hr. Although counting systems have their problems, no

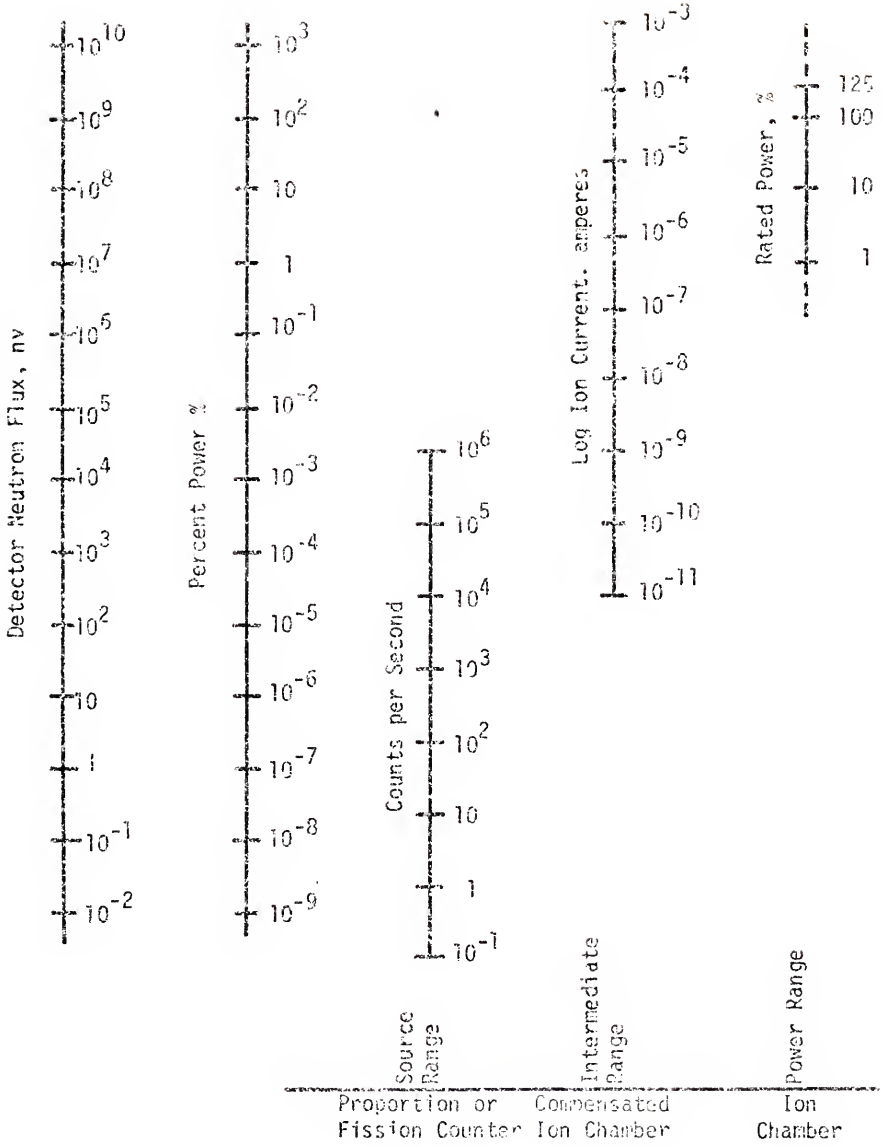

Figure 1-2. Typical ranges and detectors used in ex-core systems to cover the source, intermediate and power ranges.

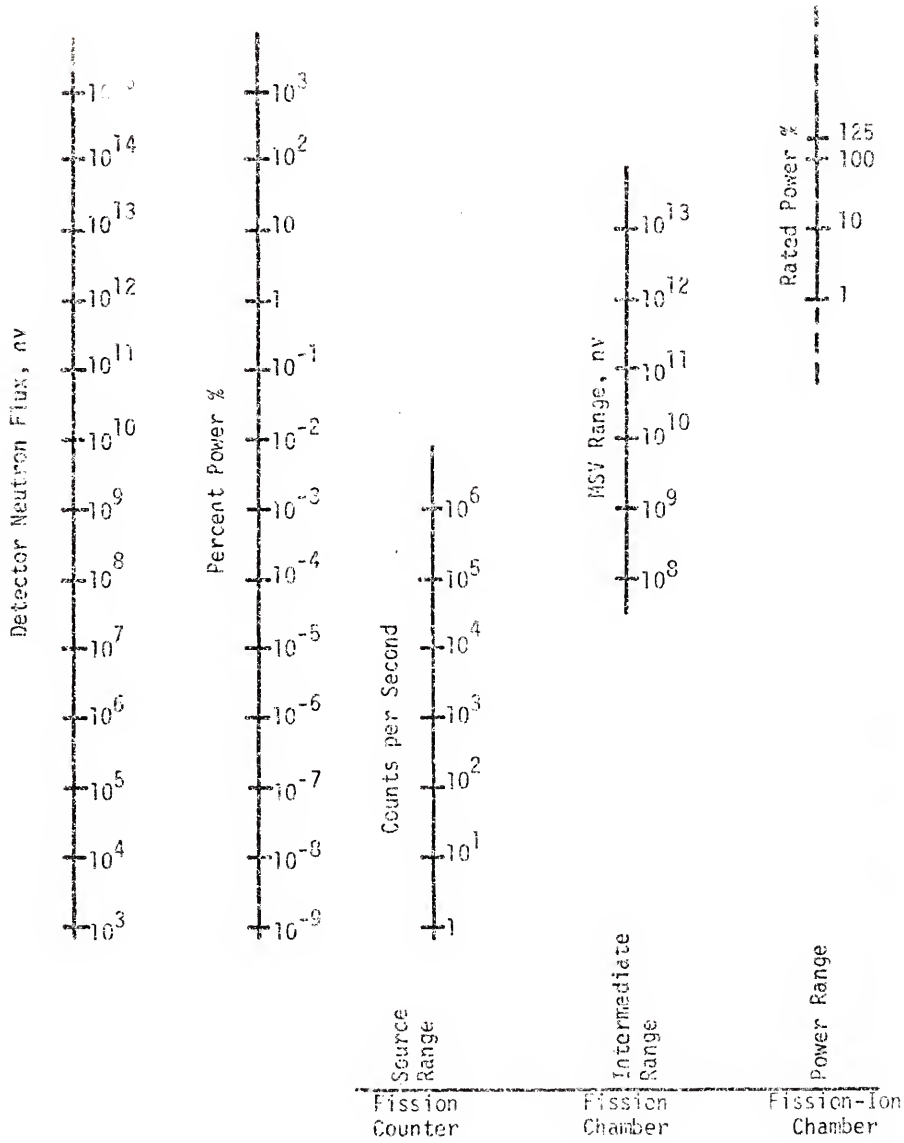

Figure 1-3. Typical ranges and detectors used in in-core systems to cover the source, intermediate and power ranges.

other system yet developed offers the required sensitivity in conjunction with the necessary gamma discrimination that they do. Counting systems, when stretched to their limits, cover only half of the twelve decade range.

The intermediate range instrumentation covers most of the remaining six decades, overlapping two to four decades of the source range and part or all of the power range. The sensors used to span this range are ionization chambers of various designs with boron or fissile electrode coatings. When simple fission (or boron) chambers are used, the associated signal processing circuitry is designed so that the resulting system's output is some measure of the mean square voltage (mean of the squares of the deviation from the mean), abbreviated MSV. Since Poisson statistics govern the pulses from a nuclear radiation sensor, a measure of the mean square voltage is a direct measure of the mean counting rate. This method has just recently[1] been developed and offers at least three important advantages over the conventional compensated ionization chambers:[2] increased gamma discrimination (100 times more than the CIC), improved operation when chambers and cables are exposed to elevated temperatures, and more efficient use of sensors.

Compensated ion chambers (CIC) are the sensors commonly used to cover the intermediate range. Such chambers provide signals which have the gamma induced component reduced by a factor of 20 to 100 times over that of a conventional ionization chamber. The methodology employed to achieve this is simple. The CIC is constructed with two separate sensitive volumes; one, having the confining electrode surfaces coated with neutron sensitive material, is sensitive to both gammas and neutrons, and the other, having no such coatings, is sensitive to only gammas. The

sensitivity of the two volumes is adjusted so that they are equally responsive to gammas. Thus, when the radiation induced ionization from both volumes is collected and subtracted, the resultant signal is, in theory, that induced solely by the neutron interactions. Such a procedure is necessary because, while the prompt gamma flux is proportional to the neutron flux, the gamma flux due to radioactive decay is not. Thus, all gamma response must be negated as much as possible. This, however, is true only for the intermediate range. At high power levels, when the neutron field is much more intense than the background gamma field, no compensation is necessary. Because of this fact, conventional ionization chambers are used as the control monitors from 1 to 100% of reactor power.

The use of a gamma-compensated detector extends the reactor control range, compared to that of an uncompensated chamber, by approximately two decades. The reason this extension is so small lies in the fact that with fixed voltages compensation is exact at only one given reactor power level. This point has also given rise to the recent practice of operating with fixed voltages and designing safety systems that avoid total control dependence on more than two decades of compensation.

The upper limit of any ionization chamber's operation is fixed by either recombination affects, which cause nonlinear responses, or by the inability to apply sufficient collection voltage to the electrodes. The flux level at which either of these occur depends on the overall design of the sensor. Leakage current through the insulators, due to the applied voltage, becomes the limiter for measuring low neutron flux levels. In addition to insulation leakage, the lower limit of the ionization chamber

operation may be affected by background current caused by the activation of chamber materials, neutron sensitive material reaction product activity, or background alpha current for fission chambers.

It was mentioned at the beginning that present monitoring systems are adequate, and they are, but just barely so. Points which are difficult to get across in a summary of this kind are the complexity, failure rate, and field engineering problems that these systems present. The in-core BWR system is a case in point. How is one to calibrate, normalize, and keep in operating condition the hundreds of detectors present in the core of an operating reactor? The need for a distinct system to cover each of the three flux ranges makes things just that much more difficult.

It is apparent that a single sensor, full range reactor power measurement system, which could cover the entire flux range without being stretched to its limit, would vastly improve the situation. Such a system should function in the source range as a counter, with inherent gamma compensation through pulse height discrimination, and should smoothly switch to the intermediate range measurements with substantial overlap to insure a linear transition. At intermediate flux levels, the system should be capable of both gamma compensation and minimization of leakage current contributions to the signal, especially at the elevated temperatures encountered in the in-core environment. Build up of neutron sensitive material reaction products should not adversely affect the system. For power measurements, the range of operation should not be restricted by recombination effects. To be of use, such a system must provide a linear (or log) output over the entire power range under all expected environmental conditions. The Pulsed Ionization Chamber (PIC) technique, which

is to be the topic of this dissertation research report, and which was developed and investigated by Ellis and his students at the University of Florida, appears to have most, if not all, of the above mentioned characteristics.

The promise of the PIC methodology for meeting the real needs and future requirements, alluded to above, is considered to constitute more than adequate justification for undertaking a research program for further developing the PIC system towards practical nuclear power reactor applications. Therefore, to better impliment the concepts and demonstrate the desired operational characteristics, the development of a much more sophisticated and practical solid state PIC pulsed high voltage and control system would need to be undertaken.

Thus, the main goal in initiating the research described in the subsequent chapters of this dissertation was to develop and evaluate a single sensor compensated PIC system, capable of full range in-core reactor power measurements. In order to establish an initial base on which to develop this research topic, a review of the PIC system's basic operational characteristics and previous research results therewith is presented in the following chapter.

CHAPTER II
PULSED IONIZATION CHAMBER OPERATIONAL THEORY

The Pulsed Ionization Chamber (PIC) mode, which was originally developed for plasma diagnostic purposes, is a new mode of operating gas filled ionization chambers.[3] In its initial stages, the PIC mode was applied to the measuring of ionization densities and recombination parameters in gas filled chambers exposed to neutron radiation. The logical deduction made at that time was that if the PIC output was known as a function of the neutron flux, then such output could be used to measure unkown fluxes. This was proven to some extent as reported by Markwell[4] who demonstrated the basic PIC performance over eight decades of reactor power, figure 2-1.

The PIC methodology involves the periodic application of a single polarity voltage collection potential across the electrodes of an ionization chamber. Sufficient time is allowed between high voltage pulses for the ionization density in the gas filled gap, between the chamber electrodes, to approach its asymptotic steady state limit. The application of the collection voltage results in the collection of first the electrons and subsequently the ions of the equilibrium ionization density, n. The fact that the electrons are collected approximately a thousand times faster than the ions makes it feasible to use the collection of only one of these charged particle types in measuring the steady state ionization density. Which of these is used depends almost entirely on the chamber

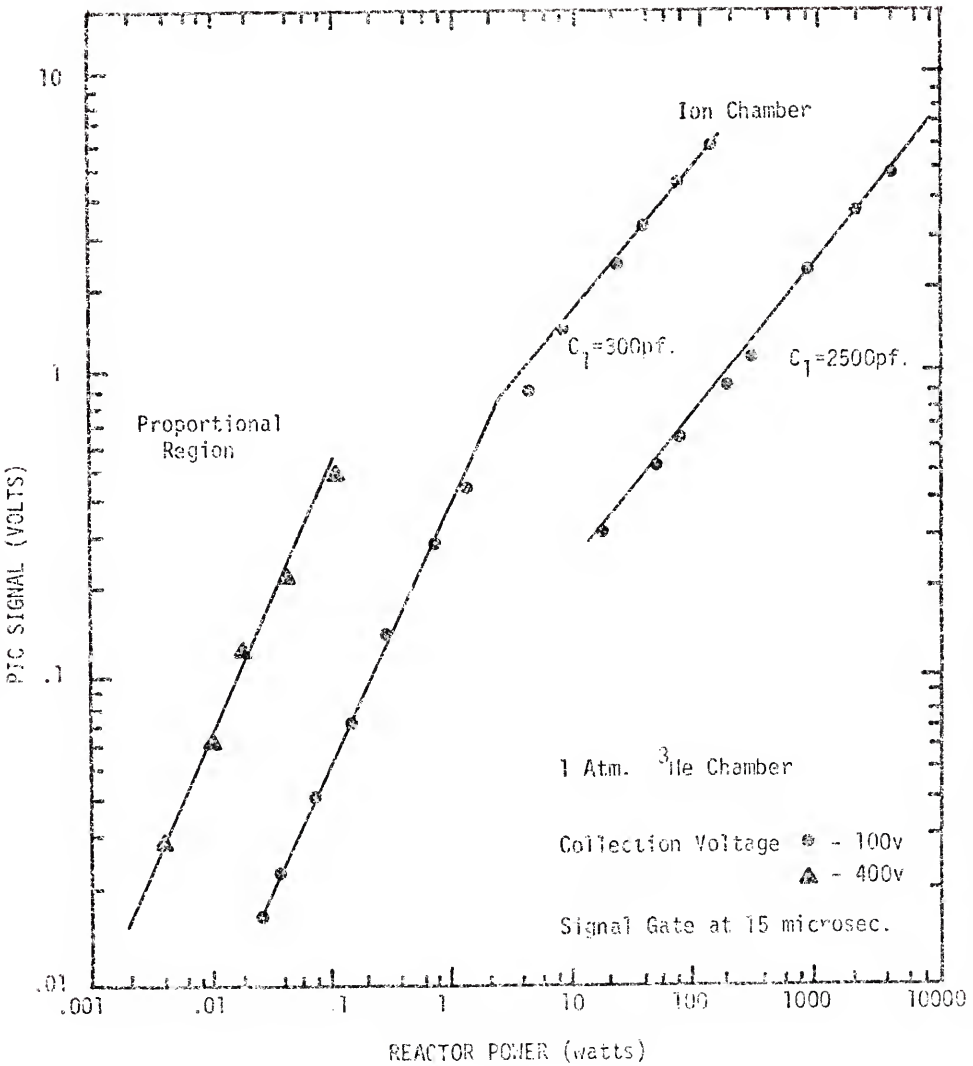

Figure 2-1. Results of PIC system with 1 atm. ^{3}He chamber.

design, and the fill gas composition and pressure. For the research reported here, the ions were the species used in order that some of the problems associated with electron kinetics[6] could be avoided. The theory derived and presented in the following paragraphs will revolve around ion collection rather than electron collection used in earlier works.

There are two factors basic to the feasibility and usefulness of the PIC system for the field of radiation measurement. The first of these is that the ionization density in a chamber, when it is exposed to ionizing radiation, grows rapidly (10 to 100 milliseconds) to an asymptotic limit dependent on the source intensity. The second factor is that it must be possible to theoretically relate the measured voltage signal, due to the collection of ions, to the asymptotic ionization density, and thus the source intensity.

The description of the positive ion and electron densities growth to their asymtotic value lies in the following gas kinetics equations;

$$\frac{\partial n_-}{\partial t} = \nabla \cdot (D_{e-} \nabla n_-) - \alpha_1 n_- - \alpha_2 n_- n_+ + S, \qquad (2\text{-}1)$$

$$\frac{\partial n_+}{\partial t} = \nabla \cdot (D_{e+} \nabla n_+) - \alpha_2 n_- n_+ + S, \qquad (2\text{-}2)$$

where: n_+ = positive ion density (cm^{-3}),

n_- = negative ion density (cm^{-3}),

α_1 = first order electron loss coefficient,

α_2 = second order loss coefficient,

S = ionization source rate (ion-pairs/second),

and D_e = effective diffusion coefficient which is functionally dependant on the radial position of n in cylindrical geometry because of the variance of n in that direction.

It should be noted that these coupled equations, when used, generally constitute a nonlinear pair of equations with no possible analytical solution. However, for the densities of interest in this study, the equations may be markedly simplified. The two ion density regions of interest are those controlled by the free diffusion regime and the ambipolar-volume recombination regime.

Second order loss mechanisms can be neglected at ion densities where free diffusion dominates and the asymtotic form of equation 2-2 reduces to;

$$D_+\nabla^2 n_+ + S = 0 \ . \qquad (2\text{-}3)$$

When this equation is applied to cylindrical geometry and is subject to the boundary conditions,

$$n_+(a) = n_+(b) = 0,$$

where a and b are the outside boundary of the inside electrode and the inside boundary of the outer electrode, respectively, the exact solution is:

$$n_+(r) = \frac{S}{4D_+ \ln(b/a)} [(b^2-a^2)\ln r - \ln (b/a)r^2 + a^2\ln b - b^2\ln a]. \qquad (2\text{-}4)$$

At ion densities greater than $\sim 10^8$ cm^{-3} ambipolar diffusion is controlling the mechanism for spatial distribution of charged particles and volume recombination becomes the major loss mechanism. Because of ambipolar diffusion, the ion-electron diffusional losses become approximately

equal, thus validating the approximation $n_+ = n_-$ at such densities. This approximation leads to,

$$D_a \nabla^2 n_+ - \alpha_2 n_+^2 + S \quad 0, \tag{2-5}$$

which is the decoupled ion density equation for $n \geq 10^8$. This equation, when written in cylindrical coordinates, is the Emden differential equation which can be solved using only numerical methods.[6]

The PIC voltage signal amplitude $v(t_c)$, at the time t_c, when all of the ions are collected, for a large RC cathode circuit time constant (large with respect to t_c), and for coaxial detector electrode geometry, is analytically and experimentally related to the steady state ionization density, n_+, in the chamber gas by,

$$v(t_c) = \frac{2\pi l e}{C} \int_a^b r\, n_+(r) dr, \tag{2-6}$$

where; l = length of the chamber,

C = cathode circuit capacitance,

e = the unit of electron charge.

The final link in relating the measured voltage peak signal $v(t_c)$ to the neutron and gamma flux, is provided by the equations;

$$S_n = \frac{\overline{E_o N_a \phi}}{W}, \tag{2-7}$$

and

$$S_\gamma = q I_\gamma, \tag{2-8}$$

where; $\bar{E}$ = the average energy deposited in the gas per neutron interaction,

w = the mean energy required to create an electron-ion pair,

$\bar{\sigma}$ = average neutron interaction cross section,

N_a = atom density of the neutron sensitive material,

ϕ = the flux density in the vicinity of the detector,

g = gas ionization efficiency which is for a given radiation field and chamber design

I = gamma source intensity.

The ion source rate, S, is directly relatable to the relatively easily measured experimental valve I_{ss}, the steady state ionization current. I_{ss} is measured by applying a constant collection potential to chamber electrodes and measuring the current between those electrodes which result from the ionizing radiation.

In particular,

$$S = \frac{I_{ss}}{eU} , \qquad (2\text{-}9)$$

where, e = the unit of electronic charge,

U = the sensitive volume of the chamber.

Equations 2-4 through 2-9 thus provide a direct, relatively simple relationship between the PIC output signal $v(t_c)$ and the ionizing radiation field strengths, and, as such, serve as the theoretical basis for this entire endeavor. With the aid of the author, detailed numerical calculations were performed by Heravi[6] for a miniature fission chamber filled with neon and argon. Some of the results, are presented in figures 2-2 through 2-5. The curves in figures 2-2 and 2-3 represent the radial

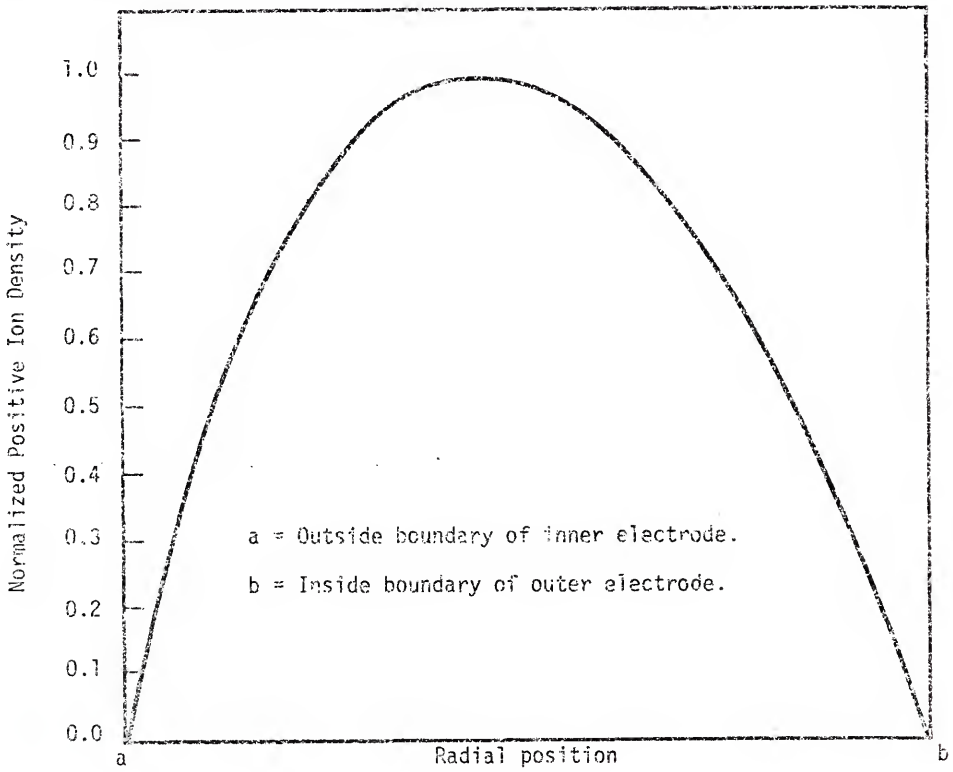

Figure 2-2. Charge density within a 1 atm. argon-filled miniature fission chamber S = 10^7 ion pairs/sec, 300°K.

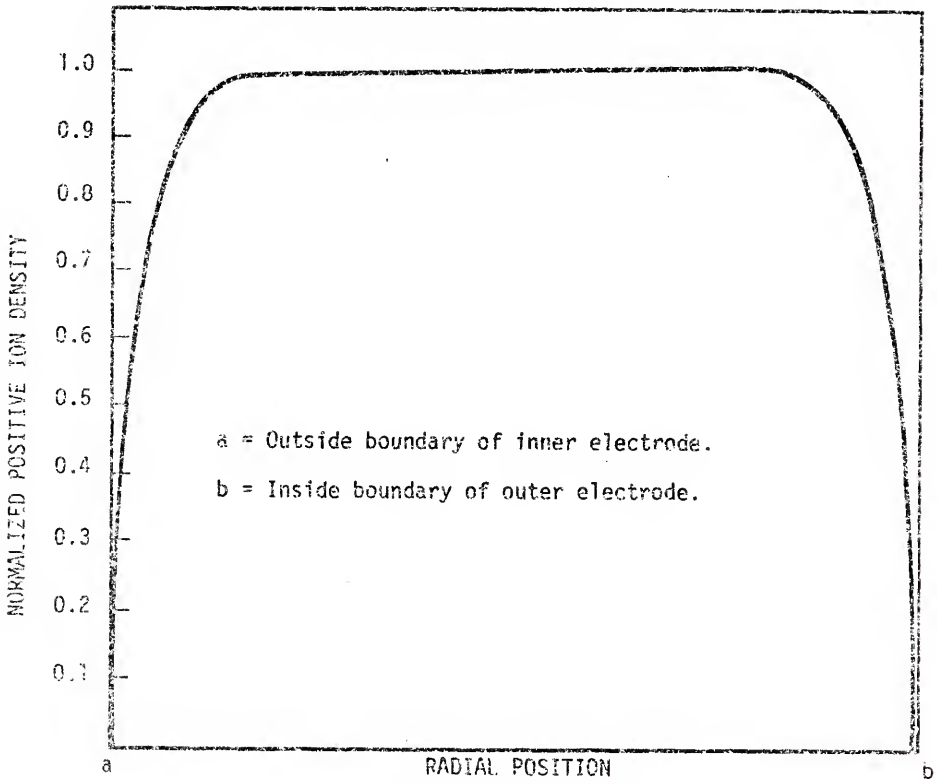

Figure 2-3. Charge density within a 1 atm. argon-filled miniature fission chamber. $S = 10^{13}$ ion pairs/sec, 300°K.

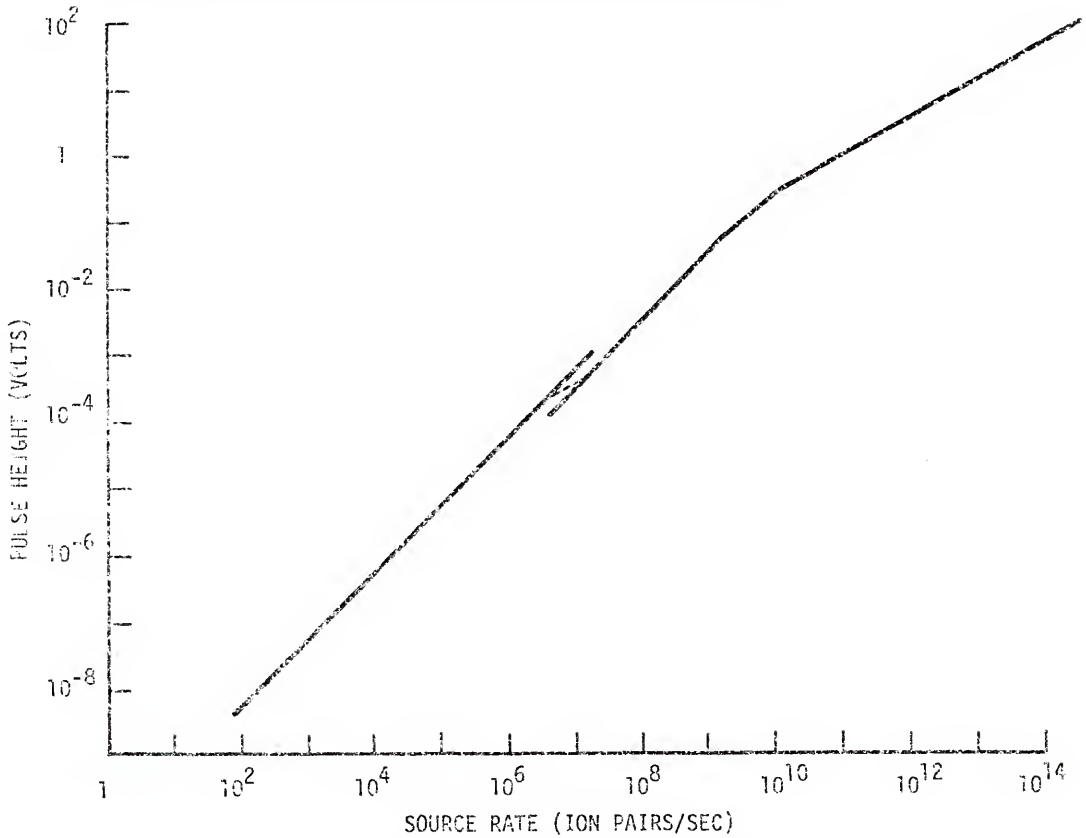

Figure 2-4. Pulse height versus source rate. 1 atm. argon-filled miniature fission chamber, 300°K.

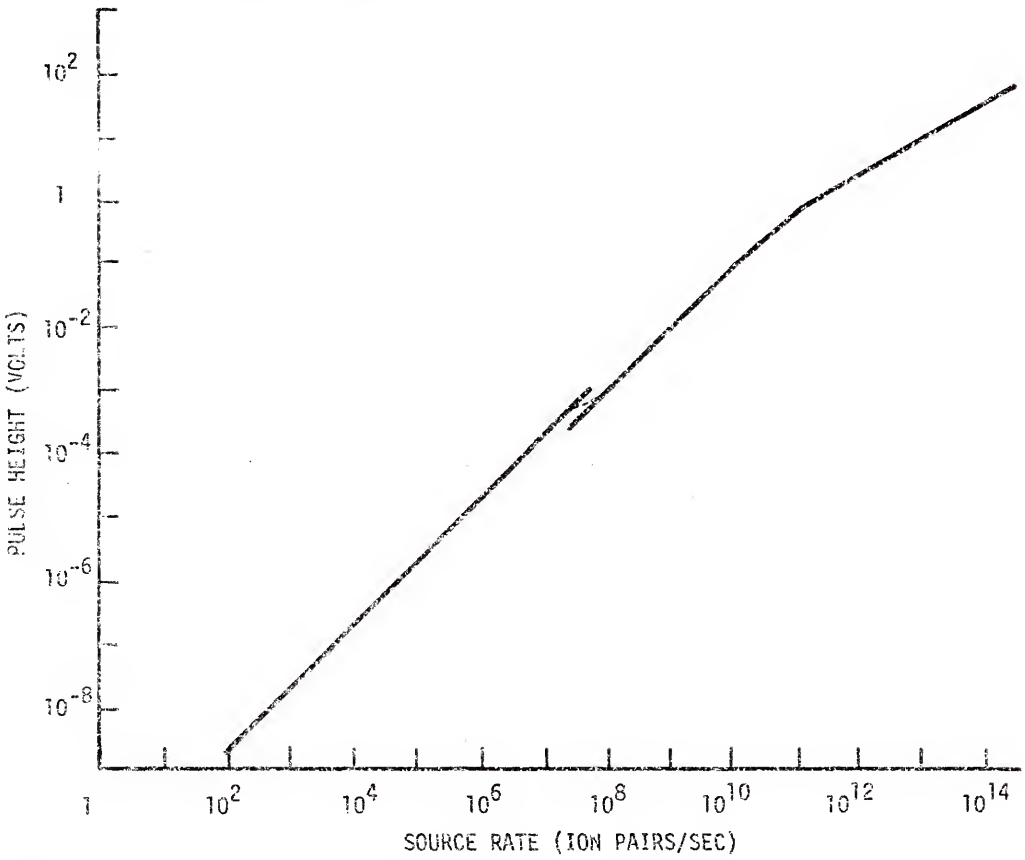

Figure 2-5. Pulse height versus source rate. 1 atm. neon-filled miniature fission chamber, 300°K.

charge distribution in an argon filled chamber for low and high ionization source rates, respectively. The severe flattening of the distribution of n at the higher source rate is due to volume recombination. Figures 2-4 and 2-5 depict the theoretically determined $v(t_c)$ versus S for argon and neon gas filled miniature fission chambers. In both cases the response is at first linearly controlled by free diffusional losses. At approximately 10^6 ion pair/sec, ambipolar diffusion becomes the controlling factor and there is a lateral shift in the linear response due to the more rapid ambipolar diffusional loss mechanism. Above 10^8 ion pairs/sec volume recombination becomes the controlling loss mechanism and the response becomes second order. These results were, to some extent, experimentally validated by Markwell.[4] Figure 2-1 shows measurements taken in the University of Florida Training Reactor (UFTR) with a PIC system. Over seven decades of reactor flux were measured. Both first and second order gas kinetic response region are observed, as was predicted. A milliwatt was the minimum measurable reactor power, due to the noise and time jitter of that PIC system. The upper limit of 10 Kw was then the maximum output of the UFTR. Note that care must be taken in directly relating the experimental and numerical data shown, since the former deals with the collection of electrons and the later with the collection of ions.

The effective replication of the characteristics of the sets of data, resulting from either gamma or neutron caused ionization, indicates the basic dependence of the PIC operation on the ionized gas kinetics, regardless of which radiation induced the ionization. Thus, although a neutron sensitive chamber results in a signal which is comprised of both neutron

and gamma induced ionization, by matching this detector with one that is sensitive to gammas only, compensation is possible, at least at a given temperature, as was shown by Cooper.[7] Some of his experimental results are shown in figure 2-6.

Conventional in-core ionization chambers suffer greatly from high temperature induced leakage current effects as shown in[4] figure 2-7. The departure from linearity of the ionization current, as a function of reactor power at low flux levels, results from temperature enhanced leakage current. The PIC method's ability to greatly reduce such current effects was shown by Ellis and Imani and reported in Markwell's thesis.[4] Figure 2-8 shows their results. The change in signal output for increased temperatures was shown to be due to the change of the recombination coefficient with temperature. However, such a change would complicate the application of the PIC methodology to reactor power measurements. Fortunately, however, Sanders[8] results indicate that this drawback could possibly be averted in chambers using neon as a fill gas, since neon's recombination coefficient was reported to be independent of temperature over the range of 70°F (25°C) to 572°F (300°C).

Even though the previously developed PIC systems were adequate for the proof-of-principle application described above, they fell far short of being prototypic of a practical reactor power measurement system. The bases for such a practical design was set forth by Ellis.[9] The principle technique of his system involved direct analog signal processing in combination with direct logic system gating resulting in live time feedback range and operational mode control. The major advantage of this approach, in terms of reactor safety and control, would be its fast response time characteristics. However, it would suffer from the inherent disadvantage

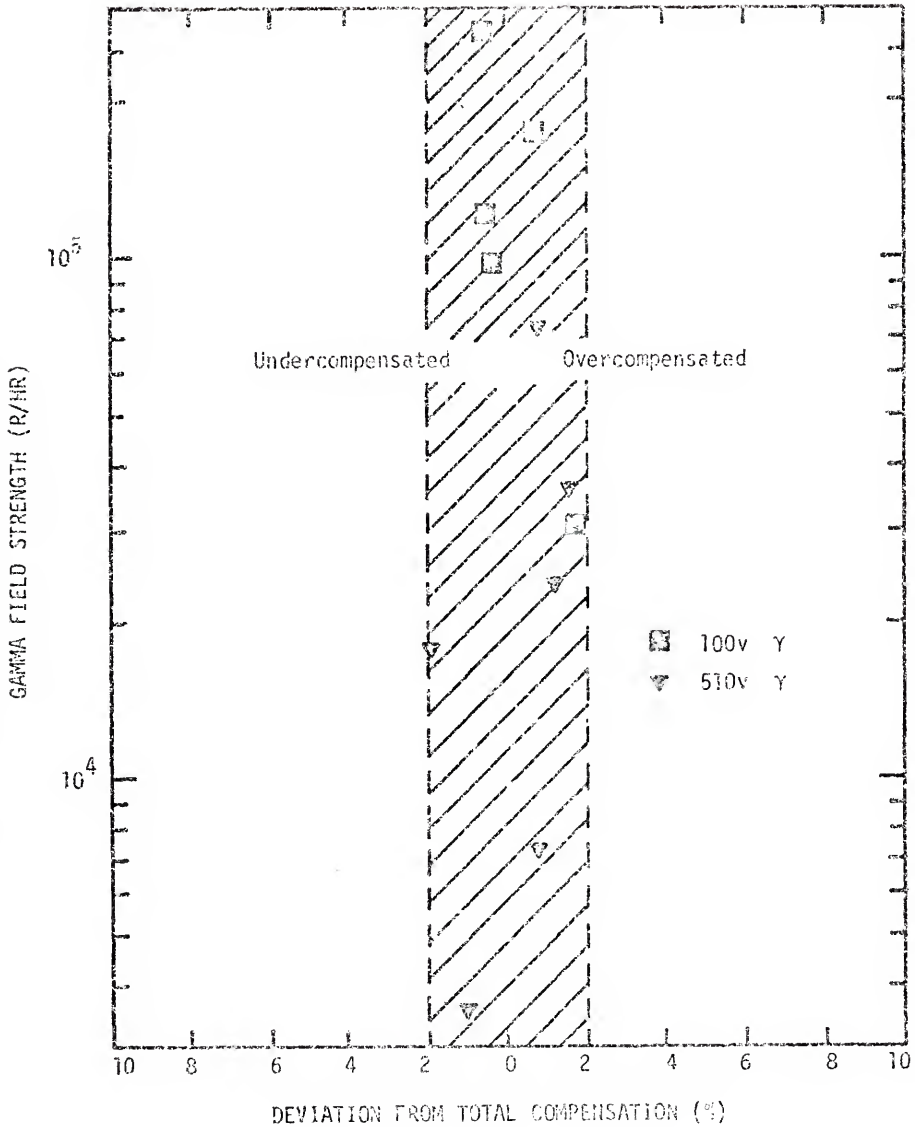

Figure 2-6. Gamma compensation as a function of gamma field strength.

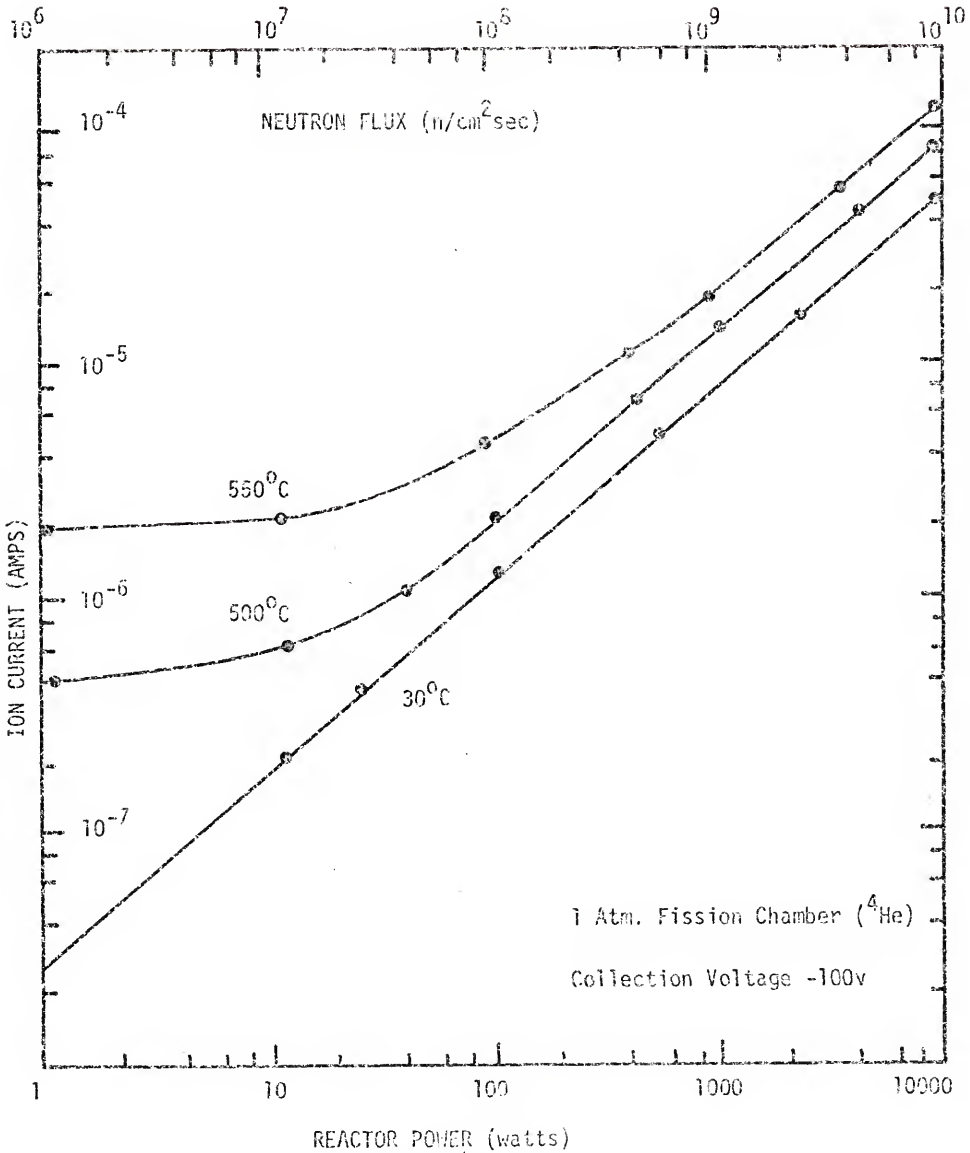

Figure 2-7. Mean level ionization current as a function of reactor power (neutron flux) and gas temperature for a 1 atm. ^{4}He-filled fission chamber.

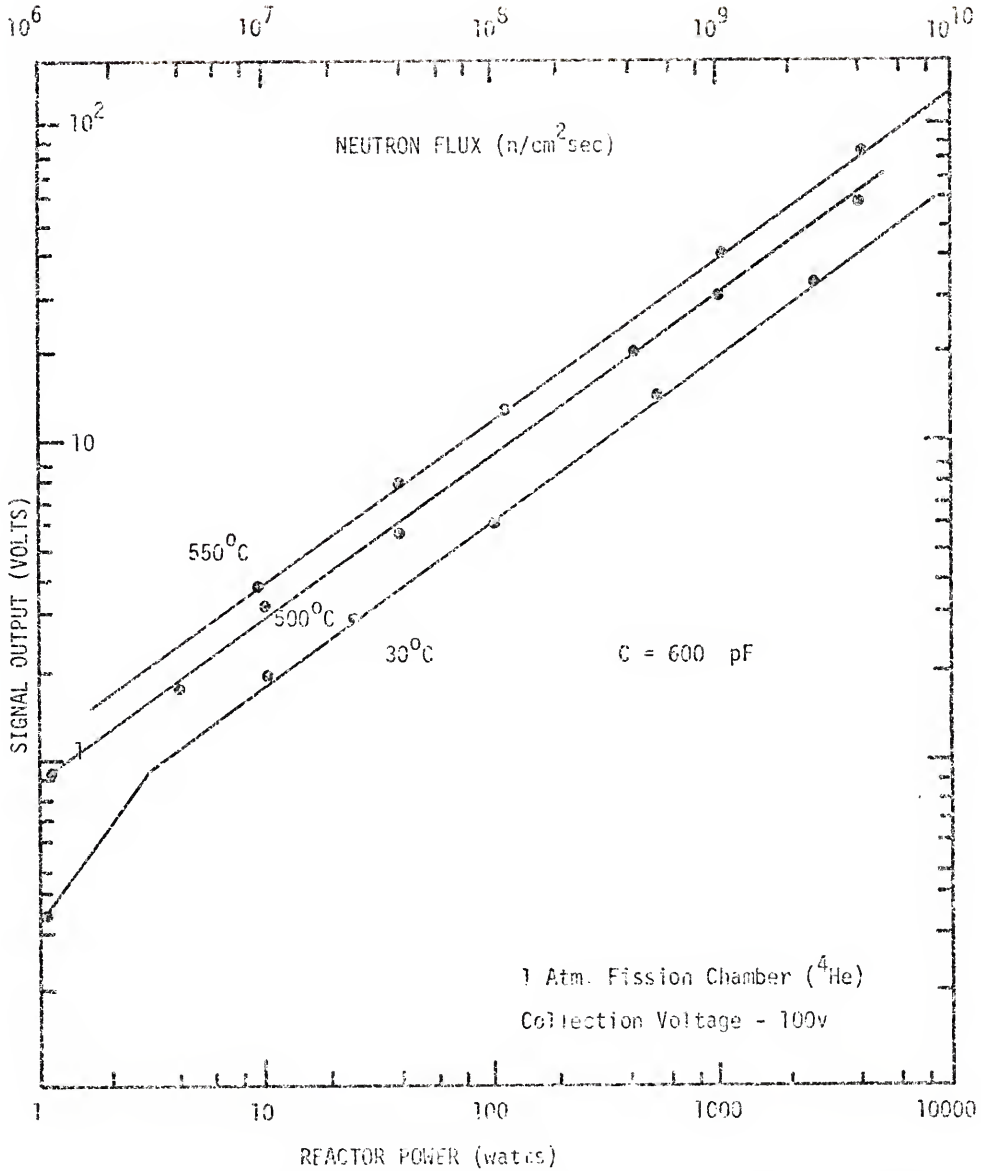

Figure 2-8. Pulsed ionization chamber signal voltage as a function of reactor power (neutron flux) and gas temperature for a 1 atm. ^{4}He-filled fission chamber.

of voltage level instabilities and drift characteristics of analog systems and the inflexibility which is associated with hard-wired signal processing and control systems.

State-of-the-art digital data processing and control systems are capable of speeds more than adequate for reactor application with the PIC system. Use of such a system would result in both greater system stability and adaptive flexibility. However, such a high speed computer for developing a prototypic system might incur an unnecessary expense, since the performance capabilities of a high speed digital computer PIC reactor control system could be adequately demonstrated through the use of a more readily available digital computer having less stringent response and processing characteristics. Thus, for this reason, a more moderately priced, but adequate unit was sought. The HP9821, having the desired characteristics, was adapted as a component of the prototypic digital computer based PIC power reactor control system (PDCPIC) which was designed and built for this dissertation.

In the following chapter the general design and operational characteristics of the PDCPIC are presented in detail. This is followed in Chapter IV by a presentation of the experimental techniques used to evaluate the system in terms of gamma compensation and detector temperature response; two important operational characteristics which needed further study. The results of these tests are then evaluated. Finally, in Chapter V, the author's conclusions are put forward and the areas requiring additional research are stated.

CHAPTER III
PIC POWER REACTOR MEASUREMENT SYSTEM[9]

The potential benefit of the research, if not already clear, will be clarified in the following general description of a PIC full range, in-core, single sensor, reactor power measurement system.

Three operational modes are to be used to cover the expected power range: count rate, compensated PIC, and gamma only PIC operation. Based on available performance data, a decade or more overlap between these modes for safety purposes should be easily attainable.

The count rate mode, as summarized earlier, is the best low flux measuring, high gamma discrimination method available. Integration of it into the PIC scheme requires only the coupling of the count rate system to the detector cathode and applying a constant collection bias to that electrode as depicted in figure 3-1. Such a configuration would cover the in-core flux range of 10^3 to 10^9 neutrons/cm^2/sec.

The CIC mode, as previously mentioned, has some serious drawbacks; the PIC compensated mode, because of its insensitivity to leakage current, should offer a wider, more stable range of response. The in-core compensated PIC system would cover a 6 decade range; 10^7 to 10^{13} neutrons/cm^2/sec. The operation of this mode could prove to be quite complex and will be discussed later.

Above approximately 10^9 neutrons/cm^2/sec, the field strength from the prompt fission gammas begins to exceed that resulting from radioactive

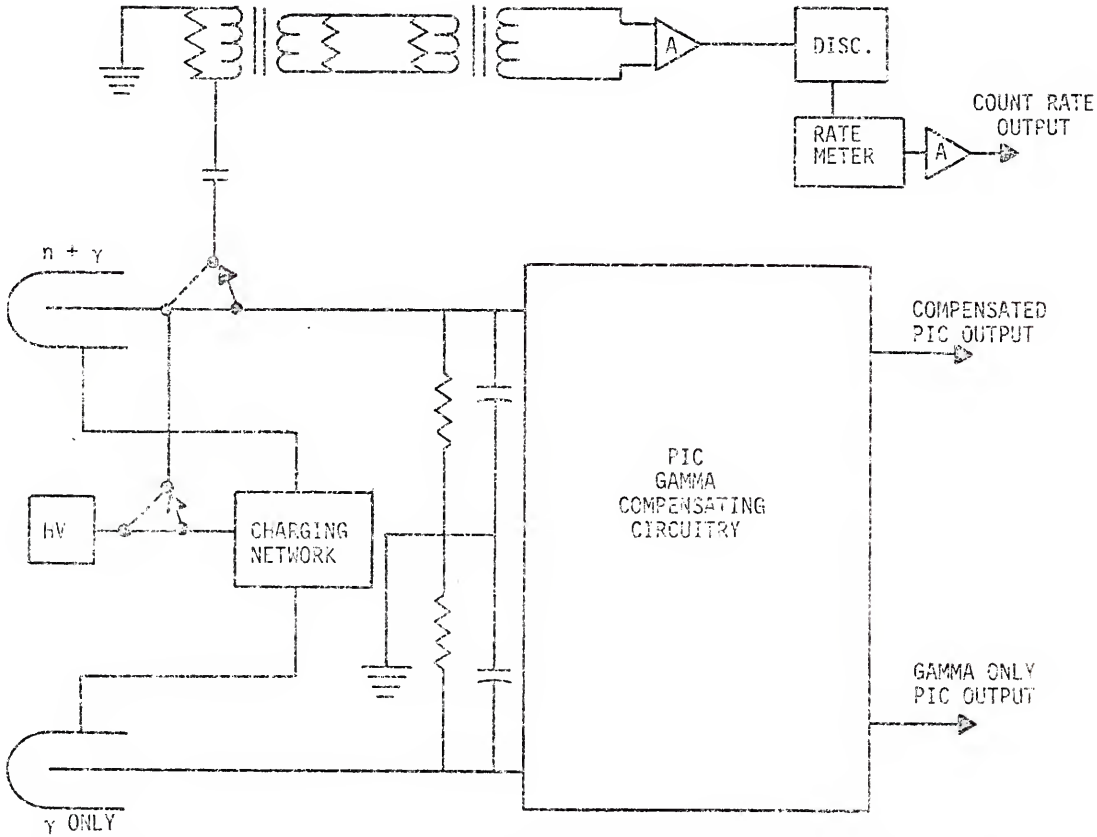

Figure 3-1. Block diagram of full range single sensor reactor power measurement system.

decay of the fission product inventory. Thus, above 10^{11} neutrons/cm^2/sec, the output of the gamma-only section of the compensated chamber can be used to determine the power level of a reactor. Depending on the overall detector design, fluxes as high as 10^{17} could be measured using this technique. Thus, a single sensor system utilizing the modes described, with the proper sensor, would indicate reactor power over the full expected range of operation, encompassing a possible neutron flux range of 10^3 to 10^{17} neutrons/cm^2/sec.

To design and assemble such a system from the basis which existed at the initiation of this program would not only have been difficult but also impractical. While verification of some of the basic PIC responses were performed, the entire range and depth of its response had not been proven as a whole. For instance, neither full range gamma compensation nor the chamber's response to temperature variations of greater than approximately 280°C had been examined fully.

For this reason the prototypic system described below was designed not only for demonstrating the operational characteristics of the PIC instrumentation, but also to allow the gamma compensation capability to be better evaluated and the temperature characteristics measurements to be extended and reverified. The assembling of such a prototypic system not only indicates the feasibility of constructing the entire reactor grade system, but also offers a vehicle for examining, in depth, all the PIC methodology characteristics.

PIC Electronic System

The PIC electronic system is composed of 5 basic units; the high voltage pulser (HVP), the raw data acquisition system (RDA), a computer

controlled PIC to steady state mode switching system, the computer interface modules and finally the HP9821 computer system. A system block diagram is given in figure 3-2. Photographs of it assembled are shown in Figure 3-3. With the exception of two analog to digital converters, a picoammeter, certain power supplies, and the HP9821 system, the electronics were designed and built by the experimenter. Because of the newness of the design approach taken and the resulting improvement over all previous PIC electronics, its design and operation are carefully outlined below.

The solid state high voltage pulser is depicted in figure 3-4. There were two basic design goals for this unit. The first was to apply a 350 volt potential across a detector-cable system totaling approximately 500 pf capacitance in approximately 500 nsec., The second goal was to return the cathode, which was essentially grounded in order to meet the first requirement, to a high impedance state within 100 nsec after full voltage applications so that little of the collected charge would be lost. These two goals were to be accomplished using solid state electronics. Time jittering components previously used[3,4,6,7,8,9] such as mercury wetted relays were to be avoided at all cost.

Figure 3-5 gives a simplified description of the basic pulser operation. A close study of it makes following the circuit description below easier.

The integrated circuit (IC) used throughout the entire system is an SN74121, monostable multivibrator. This 14 pin IC is triggered by a +5 to 0V transition input at pins 3 and/or 4. Pins 1 and 6 provide the resulting negative going (+5 to 0V) and positive going (0 to 5V) output pulses, respectively. The pulse widths are controlled by the capacitive

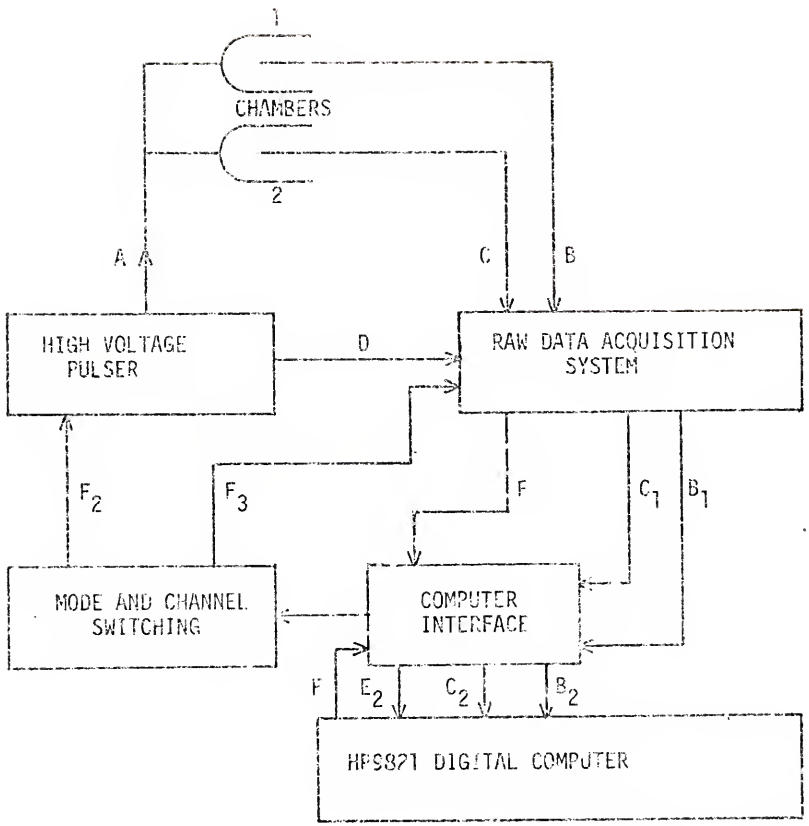

LEGEND

A	HIGH VOLTAGE PULSE OR HIGH VOLTAGE
B and C	$v(t_c)$ or I_{ss} (ANALOG)
B_1 and C_1	$v(t_c)$ or I_{ss} (BCD)
B_2 and C_2	$v(t_c)$ or I_{ss} (ASCII)
D	DATA ACQUISITION TRIGGER SIGNAL
E and E_1	DATA READY SIGNAL
F, F_1, F_2, and F_3	MODE AND CHANNEL SWITCHING SIGNALS

Figure 3-2. Block diagram of the prototypic digital computer based PIC reactor power control system.

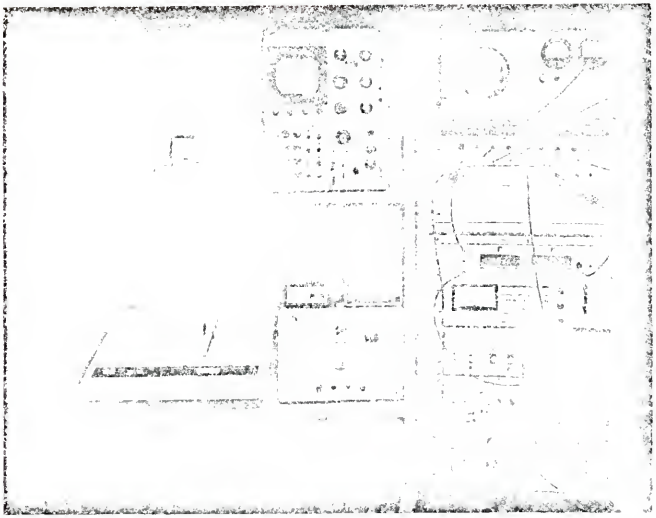

A. COMPLETE DIGITAL COMPUTER BASED PIC SYSTEM.

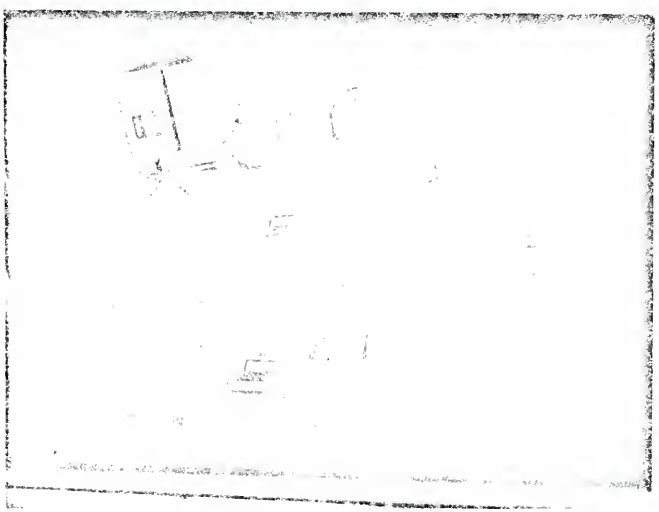

B. SOME OF THE INTERNAL CIRCUITRY OF THE HVP AND RDA.

Figure 3-3. Photographs depicting the PIC system.

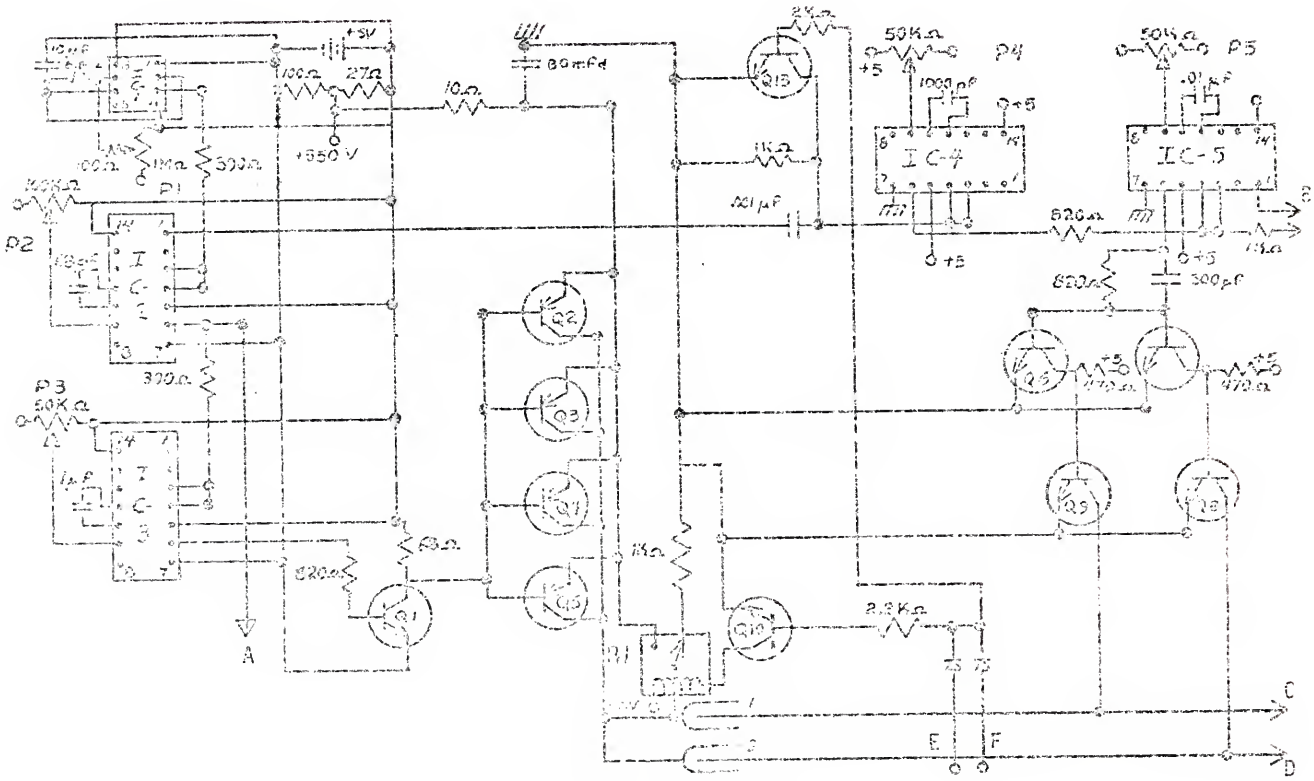

Figure 3-4. The PIC solid state high voltage pulser (HVP).

PIC EQUIVALENT CIRCUIT

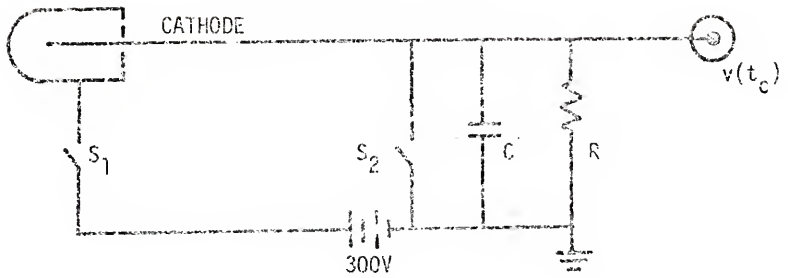

EVENT	TIME ELAPSED
(1) S_1 CLOSES	0
(2) S_2 CLOSES	0
(3) S_2 OPENS	.1 to .8 μsec
(4) SIGNAL PEAK DUE TO ION COLLECTION IS MEASURED	1 to 150 μsec
(5) S_1 OPENS	1 to 100 msec
(6) IONIZATION DENSITY BUILDS UP TO ITS EQUILIBRIUM VALUE	∿90 msec
(7) S_1 CLOSED BEGINNING A NEW CYCLE	

OPERATION PULSING SEQUENCE

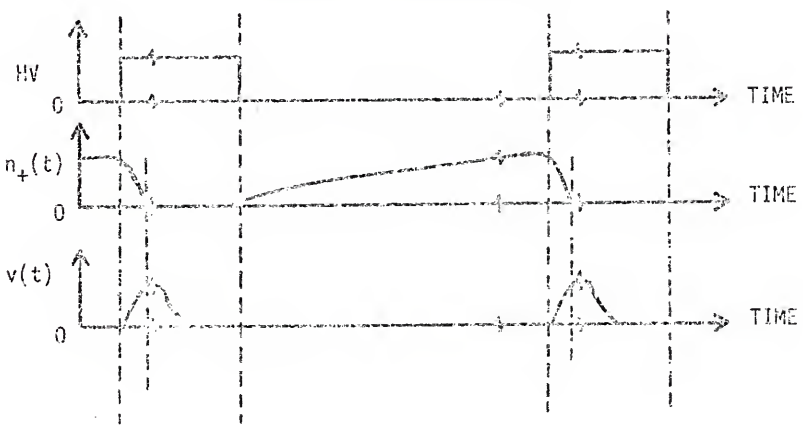

Figure 3-5. PIC equivalent circuit with pulsing sequence.

load across pins 10 and 11 and resistive load between pin 9 and +5 volt supply. Note that since both outputs 1 and 6 appear simultaneously, utilizing the positive rather than the negative output to trigger the next 74121, at inputs 3 and/or 4, results in it being triggered at the end of the input pulse. Thus its output is delayed by the width of the input pulse. This fact was often used in the design of the system now described.

The pulsing-sampling rate of the entire computer based PIC system is controlled, within limits, by the SN555 timing IC. The falling edge of its positive output is used to trigger IC-2, an SN74121 monostable multivibrator. (Note all the remaining designated ICs are SN74121.) IC-2 provides the necessary variable time delay between the application of HV and triggering of the cathode impedance circuitry. The trailing edge of the positive output pulse of IC-2, whose width is controlled by P-2, serves to trigger IC-3. The positive output of IC-3 is then fed into the driving transistor Q-1, which inverts the pulse and drives the high voltage transistors Q-2 through Q-5, rapidly to their low impedance state, thus applying voltage to the outer shell of the chamber.

The leading edge of the negative output of IC-2 triggers IC-4. Note that this occurs sometime before the high voltage is applied. IC-4 provides the necessary variable time of occurrence required so that the pulse which forces the cathode switching transistor into a high impedance state may be positioned to occur immediately after the chamber has been charged to its full potential. The trailing edge of the positive output pulse of IC-4, whose width is controlled by P-4, serves to trigger IC-5. The positive output of IC-5 is then fed into the driving transistors Q-6

and 7. These invert the pulse and drive the two switching transistors Q-8 and 9, forcing them into a high impedance (~20MΩ) state.

On examining the circuit closely, one notes that the power supply for Q-1 and the IC's 1, 2, and 3, is floating about 350V. The reason for this lies in the way the high voltage transistors Q-2 through 5 are used. In particular, note that to get Q-2 into a non-conducting state the base must be at a higher potential than the emitter, which is at 350 volts. To achieve this using a 5 volt pulsing system, one has simply to float that pulsing sytem about 350 volts. Thus a voltage of 352 or 347 volts can be placed on the base of Q-5 forcing it off or on, respectively.

The critical parts to this unit are the high voltage and the cathode impedance switching transistors. The ones used in both cases are state-of-the-art and were selected only after an extensive search. The cathode impedance switching transistors had to have the capability of conducting a large current (~ .5 amp) at low voltage for a short period of time (~ 500 nsec) and yet return to a high impedance state in ~ 100 nsec. Although this is out of specification for almost all transistors due a basic design problem, the 2N2857 performed perfectly under these conditions. The high voltage transistors had to meet the same basic requirement as those just listed, except, in addition, they had to be able to isolate 350 volts. The 2N3743, although not as fast as desired, performed quite well. The HVP could drive a 360 pf capacitive chamber-cable load to 350 volts in 800 nsec and switch from low to high impedance in 50 nsec.

The Raw Data Acquisition system (RDA) had two basic tasks; measure the PIC output voltage $v(t_c)$ and the steady state current I_{ss} for the two chambers and present the results to the computer interface in binary coded decimal (BCD) format. The main components of the RDA system depicted

in figure 3-6 are; 2 OEI track and holds (T-H), two analog to digital (A-D) converters, a 419 Keithly picoammeter, two 318 operational amplifiers (op amps), and four 302 op amps. The logic of this system is given below.

The $v(t_c)$ signal coming from the cathode of the chamber, when the system is in the PIC mode, is fed into a 302 op amp with a gain of one. The signal is then attenuated by a factor of 2 in gain, by using a resistor network, and fed into the positive differential input of a 318 op amp. The signal is reduced by a factor of two because of the fact that the 318 op amp is much more stable when operated at a gain of approximately 2. The use of the 318 op amp allows one to apply a zeroing d-c shift to the input as well as to adjust the gain so that the entire PIC system has a gain of one. The signal from the 318 op amp then serves as the input of the OEI 5892 track and hold (T-H). The T-H takes a 400 nsec sample at a given time after the collection voltage is applied to the chambers. The time at which the sample is taken is set by the experimenter by adjusting P-6 of IC-6. Note that IC-6 is tripped by the negative going pulse of IC-5 and thus for given pot settings, has a definite time relationship with respect to the time of application for the collection potential. IC-7 serves as the T-H sample pulse width controller.

The output of the T-H is then fed into the first analog to digital converter (A-D1) which presents the data to the computer interface in the required BCD format.

Once both data channels have been read in the PIC mode, the computer then switches the mode relays so that a constant d-c collection potential is applied to the chambers and the cathode of each chamber is, in its

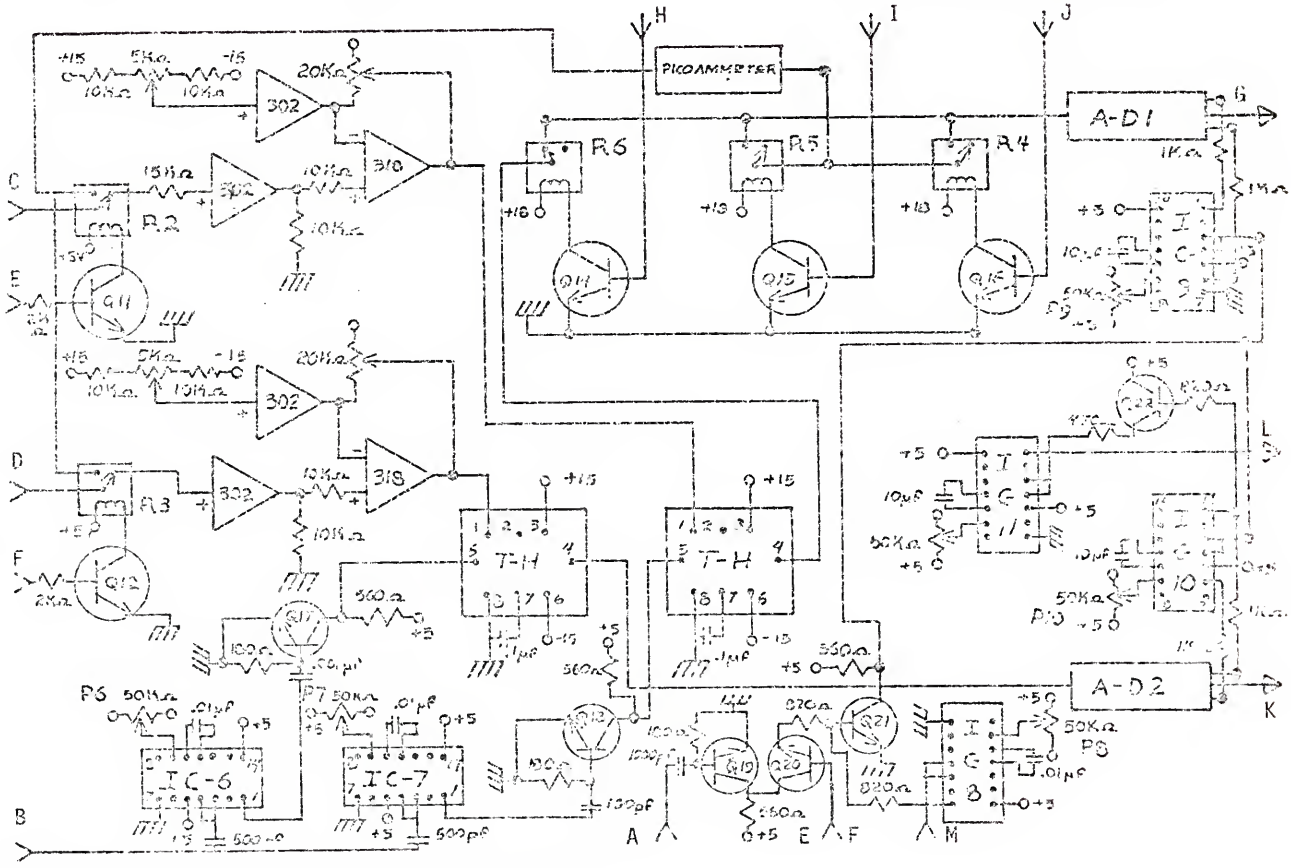

Figure 3-6. The PIC raw data acquisition system.

time, fed into the 419 picoammeter. The output of the ammeter is fed into A-D1 which is read by the computer. The computer examines the reading to determine whether the ammeter is on the right scale. If it is not, the computer raises or lowers the ammeter range by one decade and reexamines the resulting 419 output. This is done until the meter reading indicates the ammeter has the right range setting. This data are then stored and the computer switches to the second channel and repeats the above sequence to obtain a correct current reading. Thus data are is recorded in both PIC and steady state modes automatically. Once this is done the chambers are exposed to a different intensity radiation field by moving the chambers closer or farther from the source, and the computer is then given a command to repeat the above sequence.

The channel and mode switching system (CMS) is composed of transistors reed relays, and diodes. It is an integral part of both the HVP and RDS system and, as such, is included in their schematics. Switching from PIC to steady state mode is accomplished when the computer, through the interface, provides a positive 3 volt output which is applied to the base of Q-10 and Q-11 or Q-12. This results in relays R1 and 2 or 3 closing. Note R2 is closed when the current from channel 1 is being measured and R3 is closed for measurement of the current from channel 2. Note also that, when the current is being measured in each channel, the PIC mode cathode circuitry is disconnected. The coaxial switch serves to route data to A-D1 as described below.

R-6 is closed in the PIC mode for measurment of $v(t_c)$ from chamber 1. The $v(t_c)$ signal from chamber 2 is routed through A-D2 when the system is in the PIC mode. R-5 is closed as well as R-1 and R-2 when measuring

the I_{ss} from chamber 1. R-4 is closed as well as R-1 and R-3 when measuring I_{ss} from chamber 2.

The timing sequence for one data recording cycle in the PIC mode begins when the cathode impedance circuitry is tripped to its high state by IC-4. The positive going pulse of IC-4 is fed into IC-8. The negative output of IC-8 is then inverted by O-21 and then fed to IC-9 and IC-10. The pulse width of IC-8 is set such that it is slightly greater in width than that of those used in the T-H triggering circuitry from IC-6 and 7. This is to ensure that the A-D converters are commanded to read their inputs only after the T-H has the data sample ready for them. IC-9 and IC-10 provide the pulses necessary to activate the A-D's. Since the A-D converters require 250 msec to sample, the output pulses of IC-9 and IC-10 are set accordingly. IC-11, which is triggered by IC-10 at the end of its pulse, indicates to the computer, through the interface, that the data is ready to be read. The IC-11 pulse width is set so as to allow the HP9821 250 msec to record the data from both A-D converters.

When the system is in the steady state mode, only A-D1 is read by the computer, as described earlier. The codes used by the computer to control the system and output the resulting data are given in the Appendix. The system operated flawlessly over the 3 months of evaluation. No major deficiencies were found. The systems response remained both linear and free of gain drift with the calibrating accuracy of $\pm 2\%$.

Detector Selection

The fundamental part of any nuclear radiation measuring system is the detector. The capability of a system, even with the most sophisticated electronics, is ultimately determined by the sensor. The only detector

proven capable of approaching the limits set forth in the beginning of this chapter is the ^{235}U fission chamber. It gives the maximum possible gamma discrimination, with relatively low burnup and has been proven to operate under the most adverse conditions, all of which are necessary characteristics for the PIC application. For these reasons two matched pairs of RSN-34A-M1 fission chambers were obtained. A scale diagram is shown in Figure 3-7. Of each pair, one had a coating of 93% ^{235}U. Thus one chamber of each set was sensitive to both neutrons and gammas, while the other was sensitive only to gammas. As a consequence they formed a gamma compensating pair. One set was filled at the manufacturing facility with 1 atmosphere (STP) of a high purity Ar-5%N_2 gas mixture. The other set was ordered with fill tubes attached. They were pumped down to 2 x 10^{-8} torr at 300°C, cooled, and then filled to 2 atmospheres with research grade high purity neon. The argon-nitrogen gas mixture was used because of its proven characteristics in conventional fission chamber operation. Neon on the other hand, was reported to have a volume recombination coefficient that was independent of temperature; a desired gas characteristic of the PIC reactor power measurement system.

These chambers, along with the previously described PIC system, were then evaluated. Chapter IV describes the experimental procedures used to accomplish this, as well as the results obtained.

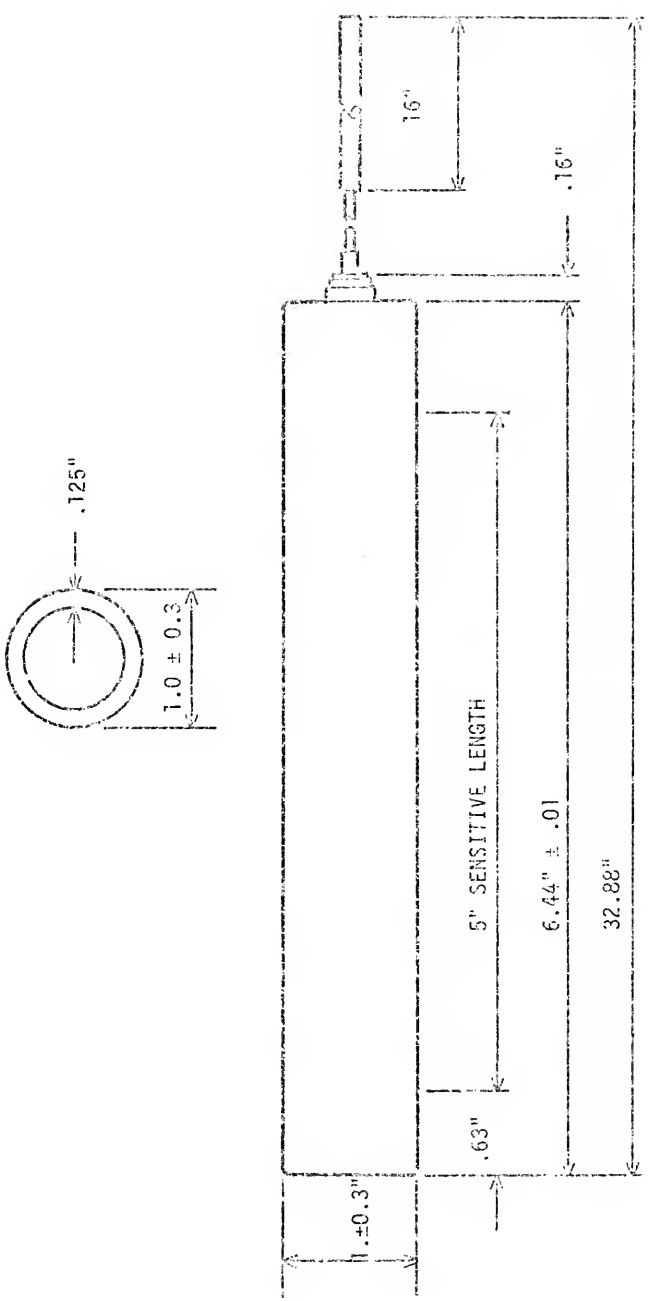

Figure 3-7. RSN-34A-M1 fission chamber used in this research.

CHAPTER IV
EXPERIMENTAL PROCEDURES, RESULTS AND METHODS OF DATA PROCESSING

Initial System Setup

The limiting factor of the sampling rate of the system described in the previous chapter was the analog to digital conversion speed of components used. One complete data reading required 250 msec. Because of this limit the system's pulse rate was set at 1.55/sec.

The high voltage pulse width was set at 15 msec, which was more than sufficient to sweep the chambers free of the ions which constituted the steady state charge density. The collection time for the Ne^+ ions in the RSN-34A-M1 chamber, with a 200 volt collection potential applied, was 100 usec. For the Ar-N_2 chambers, with a 300V collection potential applied, the ion collection time was found to be 150 usec. A time of 630 msec was allowed for the ionization in the chamber to reach its equilibrium value. This was found to be more than sufficient, since the ionization density reaches its steady state value in less than 100 msec.

The maximum possible collection potentials were used in each case to ensure rapid collection of the ions. The neon filled chambers had 200 volts applied, because, above 235 volts, their response was observed to suffer from breakdown. The Ar-N_2 filled chambers were operated at 350 volts, because as stated earlier, that was the upper limit of the HVP.

The system was run continuously for two months, with linearity, gain and zero drift being monitored periodically during that time. The linearity

and gain were checked over the full voltage and current range of interest by injecting known signals. Over the entire period of operation the system's response remained both linear and at a constant gain within a ±2% accuracy. On the other hand, zero drift in the PIC mode was found to be a strong function of the ambient temperature of the HVP. The impedance switching transistors Q-8 and Q-9 were identified as the cause. Their temperature coefficient was approximately 10 mV/°C. For the measurements taken, baseline drift was carefully monitored to ensure false readings were not obtained.

Experimental Measurements & Results

Gamma Compensation

After carefully ascertaining the system's linearity and verifying its calibration, measurements of exposure rate versus $v(t_c)$ were begun. The radiation source utilized was the Westinghouse Hanford 230 kCi ^{60}Co irradiation facility, which is depicted in figure 4-1. A plot of the radiation intensity versus vertical position for the port used is shown in figure 4-2. The data points were obtained using an RSG-8A gamma ionization chamber. The curve represents a seventh order polynominal fit of the data;

$$\log(R/hr) = 6.226 + .4033\chi - .1939\chi^2 + .02524\chi^3 - 2.2067\times10^{-3}\chi^4 + 1.682\times10^{-4}\chi^5 - 3.3963\times10^{-6}\chi^6 + 4.0521\times10^{-8}\chi^7,$$

where χ is the digital position of the chambers in the irradiation port. χ ranges from 1 to 22. Note this curve fit equation was used in the PIC System Data Recording Code given in the Appendix.

The first system response to be examined was its ability to gamma compensate. To do this the matched pair of Ar-N_2 chambers were utilized.

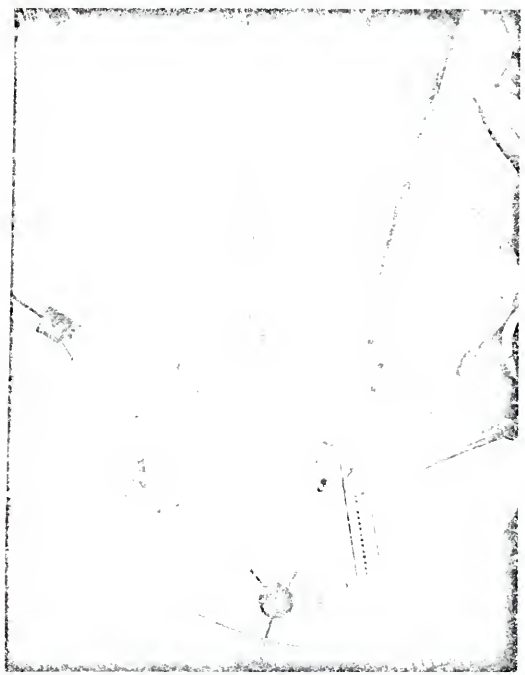

Figure 4-1. Westinghouse Hanford 230 kCi ^{60}Co irradiation facility.

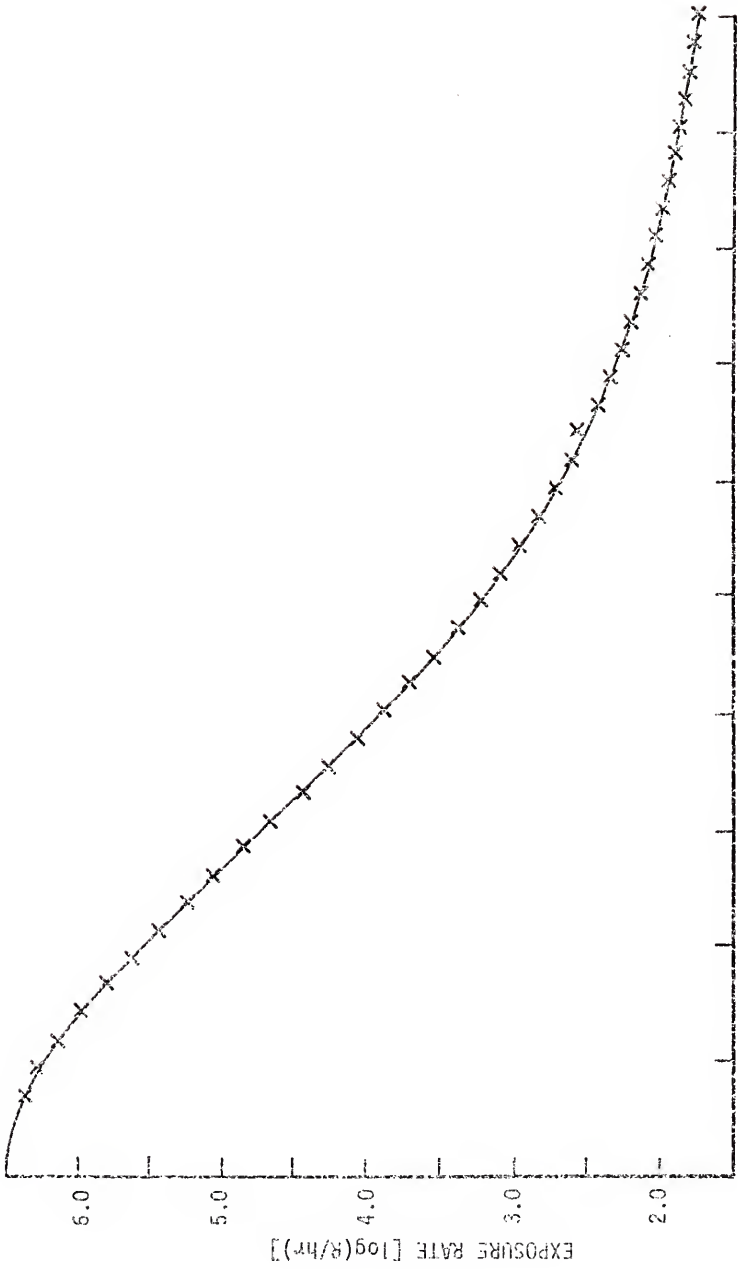

Figure 4-2. Exposure rate versus vertical position for port 6 of the ^{60}Co facility.

They were placed side by side in a cylindrical styrofoam mold and lowered in 6 inch increments down into the radiation port, while the computer system recorded $v(t_c)$ and I_{ss} of both chambers at each point. The code used to control the system is given in the Appendix under the title PIC System Data Recording Code. Note this code was used to take all the $v(t_c)$, R/hr, and I_{ss} data reported in this chapter. Typical plots of the $v(t_c)$, I_{ss}, and R/hr data taken are shown in figures 4-3, 4-4, and 4-5. It is immediately apparent from figures 4-3 and 4-4 that the chamber with the ^{235}U deposited on its walls was 3 times more sensitive to gamma radiation. This fact shows that the composition of the wall material has a strong effect on the gamma sensitivity of a given chamber. The non-linearity observed in the low-end response of the neutron sensitive chamber was due to ionization produced by the ^{234}U alpha activity in the uranium coating on its inner walls.

In the plot of $v(t_c)$ versus I_{ss} it can be seen that the curves for the two chambers lie virtually on top of each other. It shall be remembered that S, the ionization source strength is linearly related to I_{ss}, i.e.,

$$S = \frac{I_{ss}}{eU} ,$$

where e and U denote, the unit of electronic charge in coulombs and sensitive volume of the chamber, respectively.

Thus figure 4-5 shows that, at a given ion production rate S, regardless of which chamber is used, the resulting measured $v(t_c)$ is the same. This proves that the chambers and electronics for each channel are closely matched, a very basic requirement for gamma compensation. Note, however,

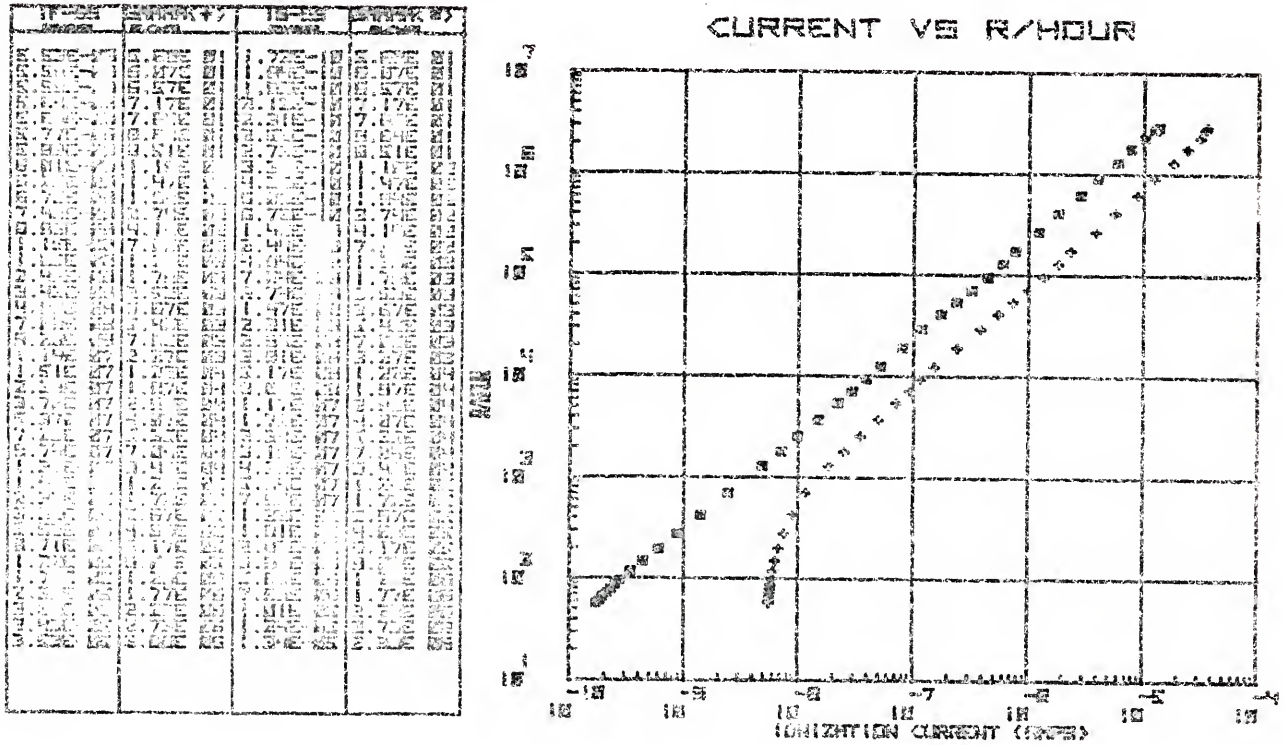

Figure 4-3. Steady state current versus exposure rate. 1 atm. Ar-5% N_2-filled RSN-34-M1 fission chambers.

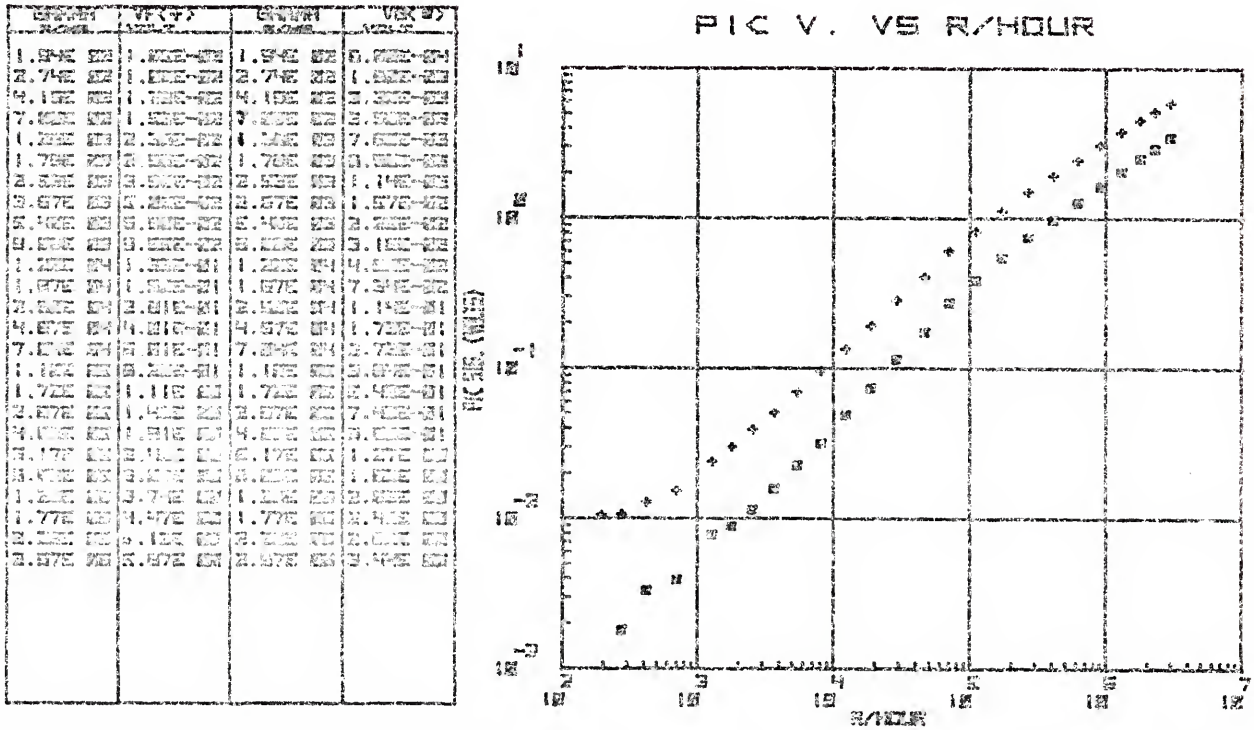

Figure 4-4. PIC voltage signal versus exposure rate. 1 atm. Ar-5% N_2-filled RSN-34-MI fission chambers.

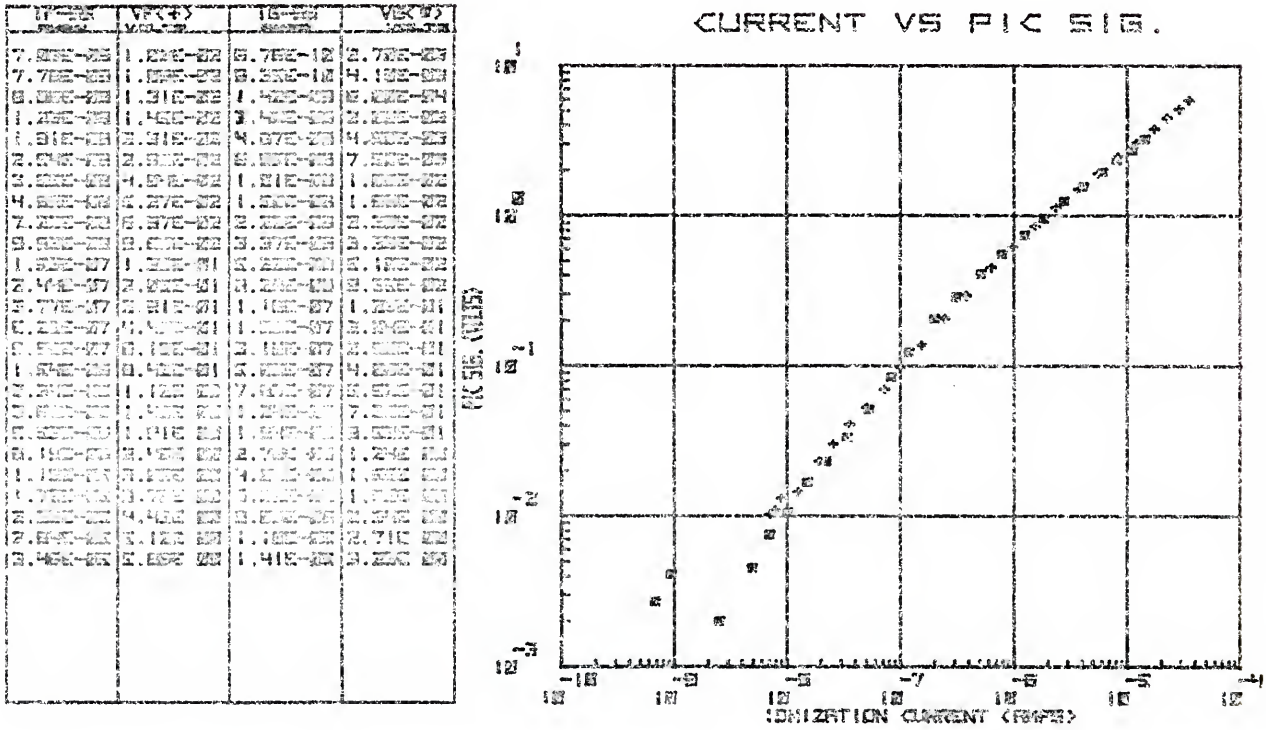

Figure 4-5. PIC voltage signal versus steady state current. 1 atm. Ar-5% N_2-filled RSN-34-M1 fission chambers.

as stated earlier, for a given exposure rate, the ionization rates in both chambers are not equal, due to the effect of the uranium wall coating in the neutron sensitive chamber.

Examining figure 4-4, one can see the presence of the linear and second order response regions of $v(t_c)$ versus R/hr as predicted by the theory given earlier. However, the presence of transition regions and their characteristics should be noted. In the fission chamber curve, this region extends from approximately 10^4 to at least 5×10^6 R/hr. The gamma chamber appears to have a much more defined transition region; from 10^5 to 10^6 R/hr. These effects are observed in figure 4-5 as well. The broad exposure range covered by the transition region, coupled with the fact that this region of response does not coincide between chambers, makes gamma compensation difficult. The gamma chamber signal cannot be simply multiplied by a constant and subtracted from the fission chamber to give full compensation over the full range of exposure rates, because, as seen, due to the increased gamma sensitivity of the fission chamber, the two chamber responses are not linearly related. Thus, to accomplish gamma compensation, using the chamber selected, more than simple differential gain controlled inputs, as were used by Cooper[7] and suggested by Ellis,[9] were required. To compensate using nonlinear electronics would have been complicated. On the other hand, compensating through computer methods appeared relatively simple and straight forward.

Computer based compensation was accomplished as follows. The chamber responses shown in figure 4-4 were curve fitted to eighth order polynominals, using Chebyshev Polynominals.[10] A description of the code is contained in the Appendix. The resulting equations were;

$$\chi = 5.161 + 1.4986y \quad .4590y^2 - .2015y^3 - .4586y^4 \qquad (4\text{-}1)$$
$$+ .2038y^5 + .3682y^6 + .08162y^7 - .009803y^8,$$

$$\chi = 5.6355 + 1.5321z + .1500z^2 - .3241z^3 + .048842^4 \qquad (4\text{-}2)$$
$$+ .4138z^5 + .2519z^6 + .05276z^7 + .002576z^8,$$

where; χ = log R/hr,

y = log $v_f(t_c)$,

z = log $v_\gamma(t_c)$,

$v_f(t_c)$ = the PIC voltage signal from the fission chamber,

$v_\gamma(t_c)$ = the PIC voltage signal from the gamma chamber.

A code was then written for the HP9821 which caused it to record the $v(t_c)$ signals from the chambers, at given exposure rates, compute the measured R/hr from equation 4-1 or 4-2 for the corresponding chamber, subtract the results, compute the compensation error and finally output all results. The code is listed in the Appendix under the title of Compensation Code.

Table 4-1 contains a set of typical results of this application. The sixth column in the table plotted in figure 4-6 indicates the compensation results. The first six values are as large as they are for two reasons. The first is that the curve fit did not fit the low data points well and, second, the system's electronic stability was ±2mV, which, as one can see, has a large effect on the computed R/hr values at the low exposure rates. The remainder of the values in that column, nevertheless, indicate that, at least for fixed temperatures, reasonable compensation can be obtained. The fluxuations that do exist are due to curve fitting, chamber positioning, and the precision of the measuring system. The last of these was measured at ±1%. The other two were difficult to accurately determine, but combined, are on the order of ±5%.

TABLE 4-1
GAMMA COMPENSATION DATA

Known KR/hr	$V_f(t_c)$ mV	Calculated From Fission Chamber KR/hr	$V_\gamma(t_c)$ mV	Calculated From Gamma Chamber KR/m	± Chamber Compensation Error
.273	12.0	.361	1.2	.003	99.1
.418	13.3	.484	1.2	.003	99.3
.699	16.0	.732	3.0	.304	58.4
1.277	24.0	1.376	5.8	1.062	22.9
1.781	29.7	1.809	7.1	1.402	22.5
2.533	38.5	2.510	10.9	2.390	4.7
3.668	51.7	3.673	16.1	3.783	-3.0
5.403	69.8	5.460	22.6	5.575	-2.1
8.078	93.6	8.019	32.0	8.192	-2.2
12.24	132.5	12.41	49.6	12.99	-4.7
18.75	189.2	18.90	73.2	19.16	-1.4
28.98	280.9	29.47	115.0	29.7	-0.9
46.66	400.0	43.96	175.8	45.47	-3.4
70.44	596.3	71.43	276.5	74.53	-4.34
110.2	818.0	109.4	388.1	112.5	-2.9
171.9	1119.	174.0	548.9	178.7	-2.7
266.6	1490.	274.2	748.2	279.0	-1.7
408.9	1919.	416.8	979.0	418.2	-0.3
616.8	2442.	626.6	1281.	633.6	-1.1
908.4	3070.	926.6	1640.	930.3	-0.4
1294.	3741.	1303.	2036.	1303.	0.0
1767.	4461.	1781.	2481.	1777.	+0.2
2277.	5149.	2324.	2918.	2302.	+1.0
2974.	5899.	3037.	3458.	3045.	-0.3

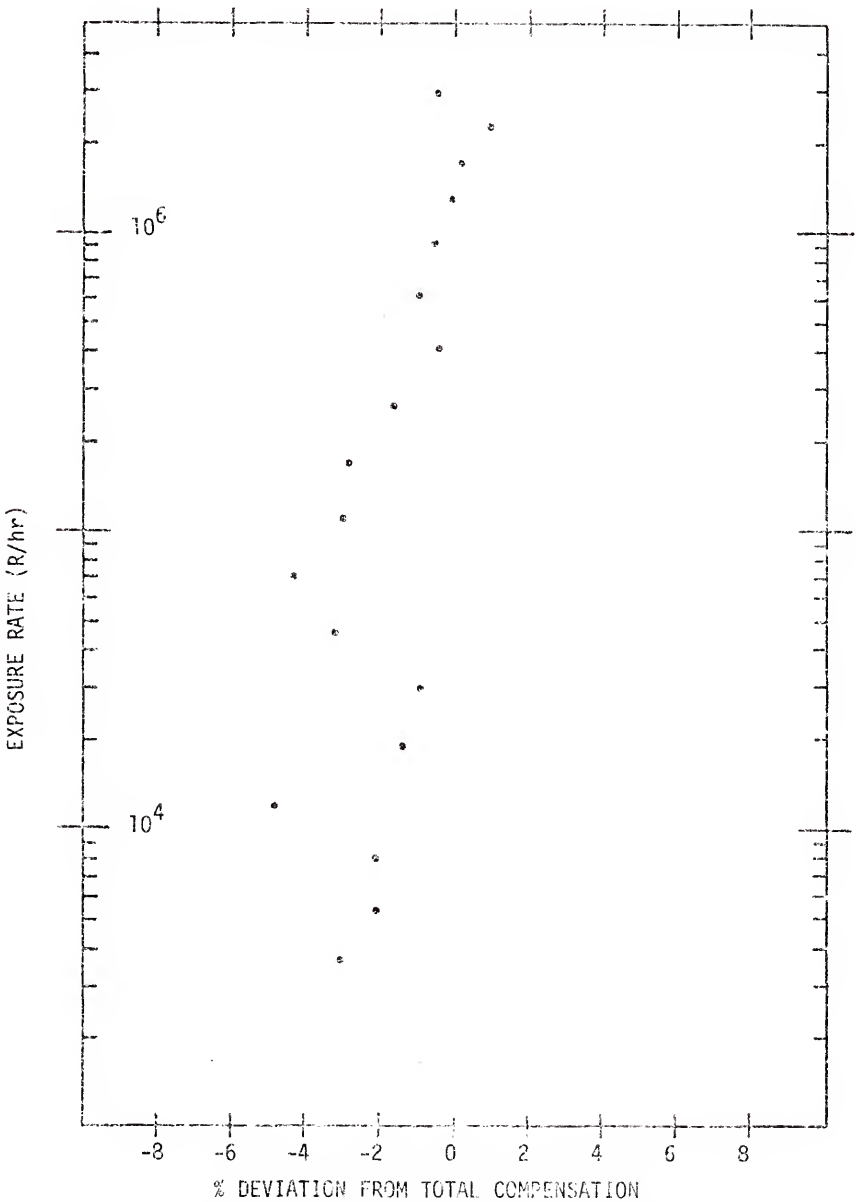

Figure 4-6. Gamma compensation as a function of exposure rate.

PIC Chamber Temperature Response

Once gamma compensation was proven feasible, using the computer based method, $v(t_c)$ for both chamber sets was examined as a function of temperature at various exposure rates. This was accomplished by constructing the 3.8 inch diameter, double tubed oven shown in figure 4-7. The Ar-N_2 chambers were inserted into the oven and connected to the long RG62-U leads from the PIC HVP by 2-foot lengths of high temperature mineral (SiO_2) insulated cables. However, when the Ne-filled chamber measurements were taken, air coax was used in place of the mineral cables because they suffered from voltage breakdown at 400°C. The oven was capable of reaching temperatures up to 550°C when used in conjunction with a 120 volt variac.

The cylindrical oven-chamber assembly was placed in the same port as was used for the gamma compensation experiment. The data were then taken for both the Ar-N_2 and Ne chamber pairs. The most pertinent of this is displayed in figures 4-8 through 4-23.

Some basic chamber response characteristics are immediately apparent. The most obvious being the rise in leakage current as the temperature is increased. This fact accounts for the drastic change in the slope of the beginning data points as the temperature is increased. Note that the I_{ss} values became next to useless as the temperature was increased, because the leakage current far exceeds the current caused by the radiation. On the other hand $v(t_c)$, even at the highest temperatures, maintains its basic functional response to the exposure rate. (Note, in figures 4-7 through 4-22 the tabulated values from top to bottom correspond to vertical port positions 14, 13, 12, 11.5, 11, 10.5, 10, 9.5, 9, 8.5, 8, 7.5, 7, 6.5, 6, 5.5, 5, 4.5, 4, 3.5, 3, 2.5, and 1.5, in that order.)

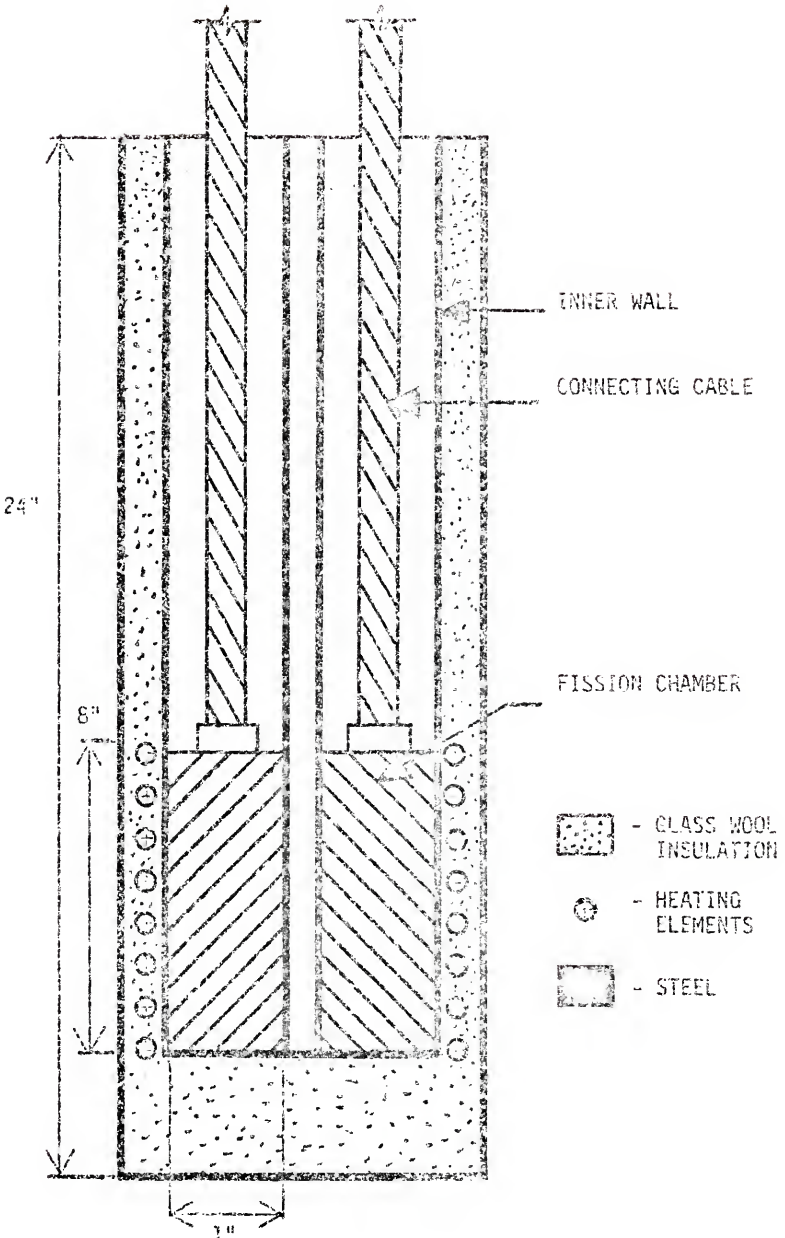

Figure 4-7. Cross sectional view of the oven built to accommodate a matched pair of RSN-34-M1 chambers. Maximum temp. 550°C.

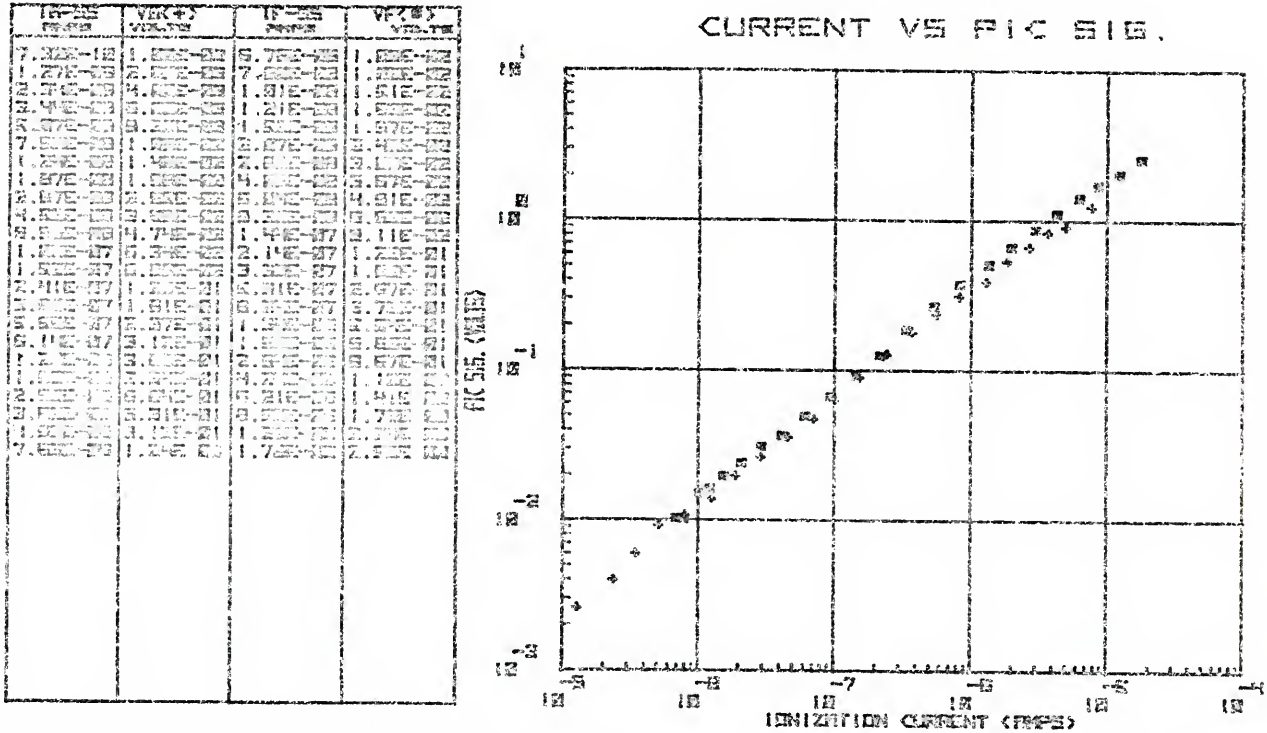

Figure 4-8. PIC signal versus steady state ionization current for 2 atm. Ne-filled gamma sensitive (+) and neutron-gamma sensitive (□) chambers at the temperature 25°C.

IG-SS (AMPS)	VG(+) VOLTS	IF-SS (AMPS)	VF(⊡) VOLTS
[illegible].51E-10	4.[illegible]E-04	5.77E-0[illegible]	1.[illegible]E-02
1.13E-09	1.40E-03	7.[illegible]E-03	1.13E-02
2.21E-09	4.[illegible]E-03	1.[illegible]E-08	1.4[illegible]E-02
3.21E-09	4.[illegible]E-03	1.[illegible]E-08	1.[illegible]E-02
4.[illegible]E-09	[illegible]	1.34E-08	2.[illegible]E-02
7.[illegible]E-09	1.1[illegible]E-02	2.11E-08	2.[illegible]E-02
1.[illegible]E-08	2.[illegible]E-02	2.[illegible]E-08	4.07E-02
1.[illegible]E-08	2.79E-02	4.[illegible]E-08	4.[illegible]E-02
2.81E-08	3.73E-02	6.[illegible]E-08	6.13E-02
4.4[illegible]E-08	5.01E-02	9.3[illegible]E-08	8.15E-02
6.7[illegible]E-08	7.21E-02	1.3[illegible]E-07	1.[illegible]E-01
1.0[illegible]E-07	8.[illegible]E-02	2.17E-07	1.40E-01
1.[illegible]E-07	1.17E-01	3.3[illegible]E-07	1.[illegible]E-01
2.4[illegible]E-07	1.[illegible]E-01	5.1[illegible]E-07	2.71E-01
4.[illegible]E-07	2.21E-01	[illegible]	3.[illegible]E-01
6.1[illegible]E-07	2.[illegible]E-01	1.3[illegible]E-06	5.[illegible]E-01
8.21E-07	3.[illegible]E-01	1.34E-06	6.87E-01
1.4[illegible]E-06	4.77E-01	2.[illegible]E-06	8.[illegible]E-01
2.[illegible]E-06	6.10E-01	4.21E-06	1.17E 00
2.97E-06	7.91E-01	6.[illegible]E-06	1.4[illegible]E 00
4.1[illegible]E-06	9.71E-01	8.[illegible]E-06	1.[illegible]E 00
6.72E-06	1.1[illegible]E 00	1.[illegible]E-05	2.1[illegible]E 00
8.[illegible]E-06	1.3[illegible]E 00	1.72E-05	2.64E 00

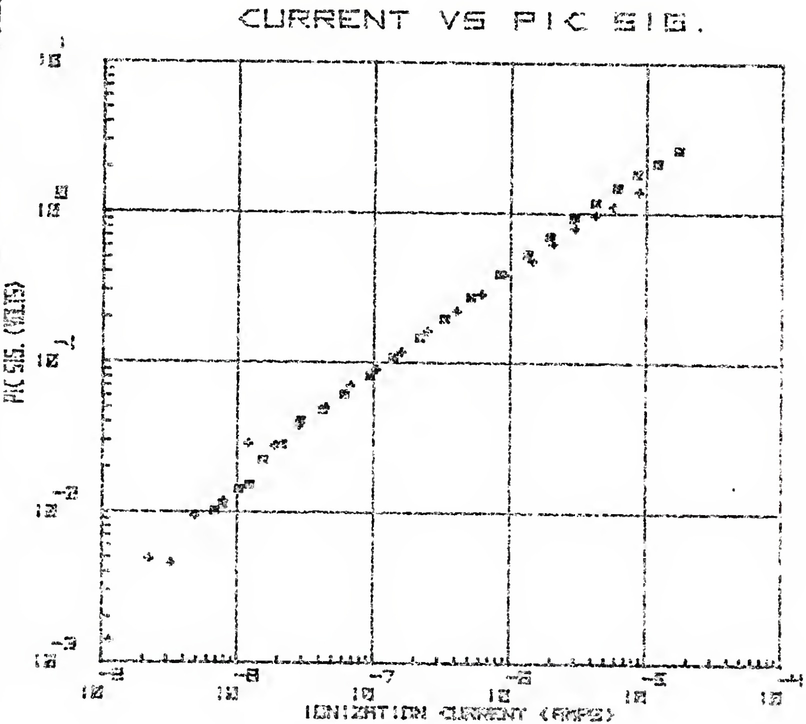

Figure 4-9. PIC signal versus steady state ionization current for 2 atm. Ne-filled gamma sensitive (+) and neutron-gamma sensitive (⊡) chambers at the temperature 71°C.

IG-SS (AMPS)	VR(+) VOLTS	IP-SS (AMPS)	VR(-) VOLTS
6.28E-10	1.40E-03	7.05E-09	1.05E-02
1.22E-09	3.40E-03	8.14E-09	1.22E-02
2.35E-09	5.00E-03	1.05E-08	1.54E-02
3.17E-09	9.51E-03	1.25E-08	1.73E-02
4.67E-09	1.34E-02	1.53E-08	2.54E-02
7.54E-09	1.71E-02	2.15E-08	3.12E-02
1.15E-08	2.57E-02	2.55E-08	3.54E-02
1.60E-08	3.37E-02	4.22E-08	5.13E-02
2.78E-08	4.12E-02	5.11E-08	5.34E-02
4.33E-08	5.55E-02	9.24E-08	6.41E-02
6.91E-08	7.80E-02	1.42E-07	1.13E-01
1.24E-07	9.79E-02	2.15E-07	1.45E-01
1.61E-07	1.37E-01	3.30E-07	1.93E-01
2.55E-07	1.74E-01	5.25E-07	2.83E-01
4.21E-07	2.53E-01	8.03E-07	3.21E-01
6.52E-07	3.22E-01	1.37E-06	5.50E-01
9.47E-07	4.11E-01	1.93E-06	7.15E-01
1.49E-06	5.34E-01	2.80E-06	9.52E-01
2.15E-06	6.78E-01	4.12E-06	1.23E 00
3.12E-06	8.90E-01	5.91E-06	1.57E 00
4.49E-06	1.15E 00	8.27E-06	1.89E 00
6.53E-06	1.50E 00	1.17E-05	2.92E 00
9.11E-06	1.84E 00	1.68E-05	3.87E 00

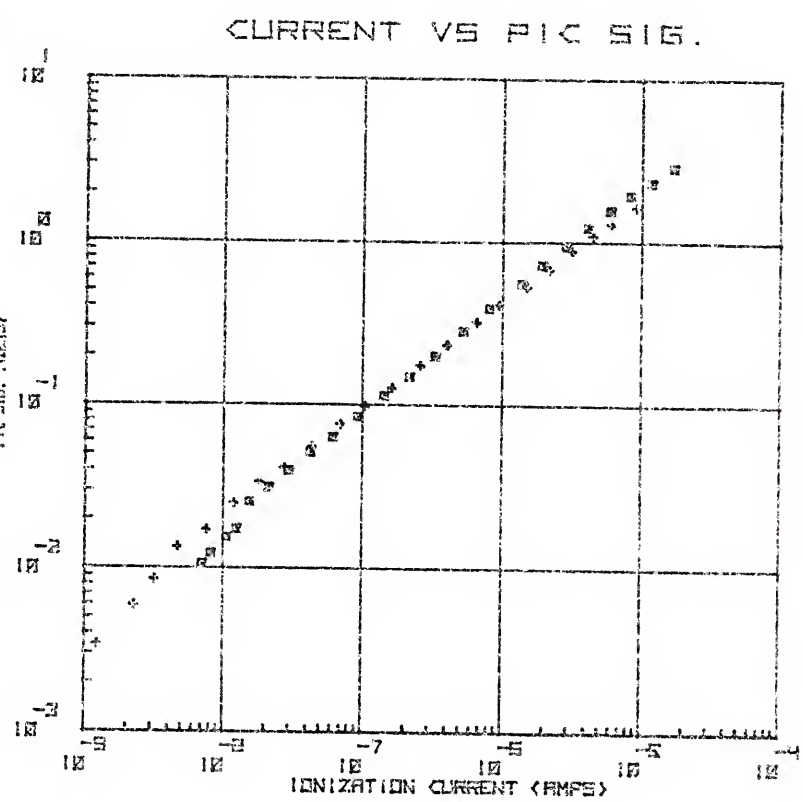

Figure 4-10. PIC signal versus steady state ionization current for 2 atm. Ne-filled gamma sensitive (+) and neutron-gamma sensitive (⊡) chambers at the temperature 129°C.

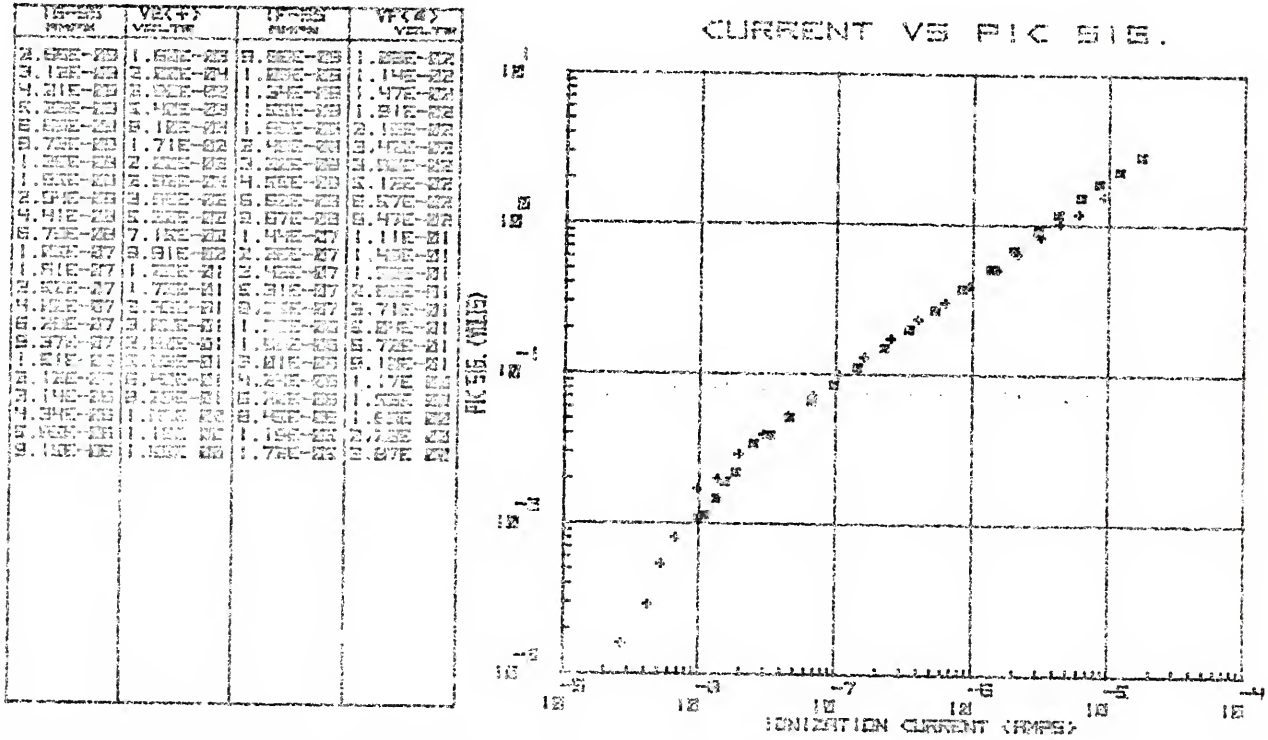

Figure 4-11. PIC signal versus steady state ionization current for 2 atm. Ne-filled gamma sensitive (+) and neutron-gamma sensitive (□) chambers at the temperature 179°C.

IG-SQ (AMPS)	VD(+) (VOLTS)	IF-SQ (AMPS)	VF(□) (VOLTS)
1.63E-08	1.43E-02	2.21E-08	1.23E-02
1.87E-08	1.50E-02	2.53E-08	1.37E-02
1.77E-08	1.51E-02	3.18E-08	1.49E-02
1.87E-08	1.65E-02	2.41E-08	2.25E-02
2.12E-08	1.42E-02	3.73E-08	2.67E-02
2.28E-08	1.85E-02	4.21E-08	3.13E-02
2.52E-08	2.57E-02	5.47E-08	3.85E-02
3.18E-08	3.03E-02	5.79E-08	4.01E-02
4.21E-08	4.72E-02	8.37E-08	5.97E-02
5.54E-08	5.18E-02	1.12E-07	8.81E-02
8.17E-08	8.81E-02	1.54E-07	1.21E-01
1.17E-07	1.18E-01	2.41E-07	1.54E-01
1.74E-07	1.60E-01	3.61E-07	2.04E-01
2.62E-07	2.11E-01	5.42E-07	2.67E-01
4.15E-07	2.83E-01	8.47E-07	3.67E-01
6.45E-07	3.81E-01	1.31E-06	4.81E-01
9.81E-07	4.57E-01	2.03E-06	6.41E-01
1.52E-06	5.52E-01	2.91E-06	8.20E-01
2.15E-06	6.85E-01	4.24E-06	1.02E 00
3.17E-06	8.59E-01	6.11E-06	1.37E 00
4.34E-06	1.04E 00	8.35E-06	1.67E 00
6.02E-06	1.24E 00	1.15E-05	2.01E 00
9.07E-06	1.55E 00	1.72E-05	2.57E 00

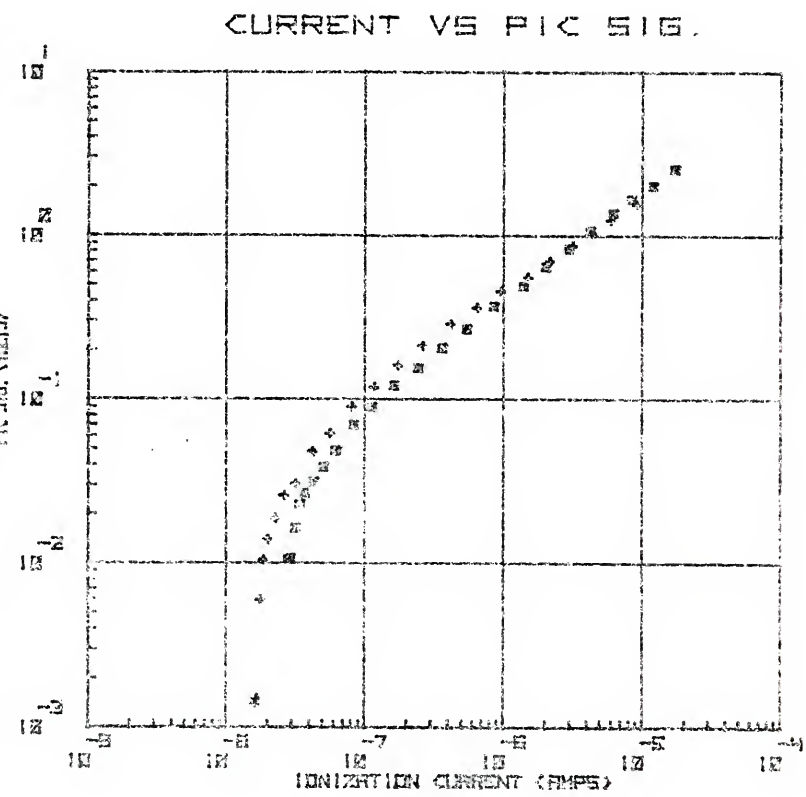

Figure 4-12. PIC signal versus steady state ionization current for 2 atm. Ne-filled gamma sensitive (+) and neutron-gamma sensitive (□) chambers at the temperature 217°C.

IE-SS (AMPS)	VE(+) VOLTS	IF-SS (AMPS)	VF(S) VOLTS
2.41E-07	4.12E-03	3.30E-07	1.27E-02
2.41E-07	2.58E-03	3.30E-07	1.93E-02
2.41E-07	5.33E-02	3.34E-07	1.57E-02
2.41E-07	9.58E-05	3.37E-07	2.10E-02
2.40E-07	1.07E-03	3.41E-07	2.33E-02
2.53E-07	1.50E-02	3.47E-07	2.67E-02
2.54E-07	2.47E-02	3.5[illegible]E-07	3.07E-02
2.55E-07	3.84E-02	3.5[illegible]E-07	3.50E-02
2.68E-07	5.81E-02	3.68E-07	7.03E-02
2.62E-07	8.49E-02	4.16E-07	3.46E-02
3.45E-07	1.22E-01	4.60E-07	1.31E-01
3.41E-07	1.71E-01	5.32E-07	1.75E-01
5.55E-07	2.50E-01	6.48E-07	2.23E-01
4.77E-07	3.23E-01	8.17E-07	3.01E-01
5.2[illegible]E-07	4.52E-01	1.15E-06	4.09E-01
8.11E-07	5.88E-01	1.55E-06	5.24E-01
1.1[illegible]E-06	7.53E-01	2.10E-06	6.74E-01
1.6[illegible]E-06	9.70E-01	2.59E-06	8.72E-01
2.23E-06	1.22E 00	4.24E-06	1.12E 00
3.07E-06	1.50E 00	5.83E-06	1.36E 00
4.19E-06	1.80E 00	7.98E-06	1.73E 00
5.52E-06	2.12E 00	1.11E-05	2.07E 00
8.25E-06	2.51E 00	1.58E-05	2.52E 00

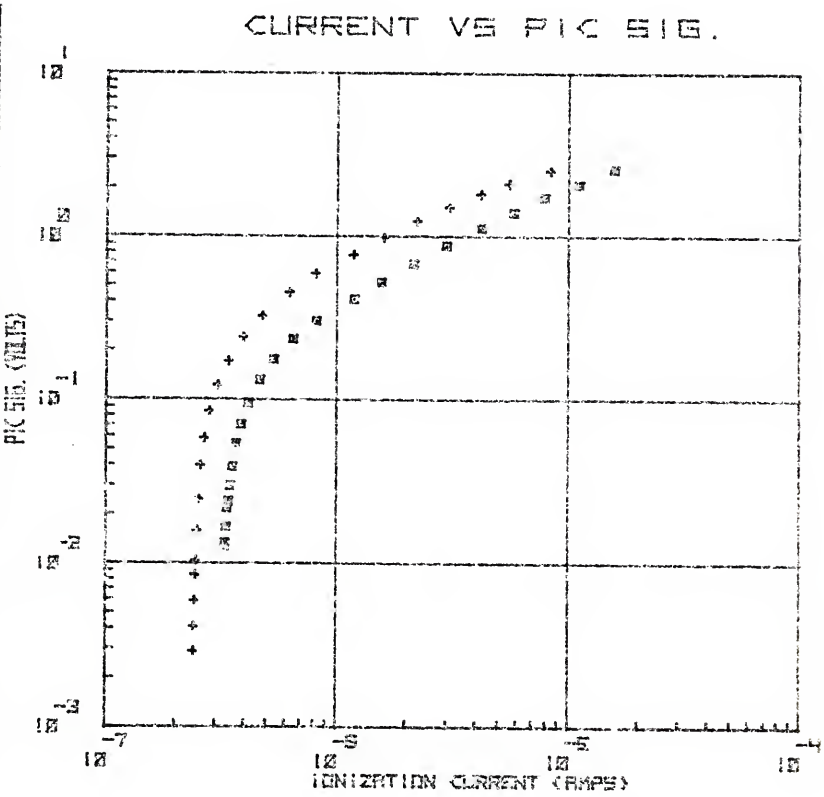

Figure 4-13. PIC signal versus steady state ionization current for 2 atm. Ne-filled gamma sensitive (+) and neutron-gamma sensitive (⊡) chambers at the temperature 282°C.

IG-SS AMPS	VB(+) VOLTS	IF-SS AMPS	VF(Ø) VOLTS
1.19E-06	3.00E-04	1.54E-06	1.02E-02
1.18E-06	2.00E-03	1.53E-06	1.05E-02
1.19E-06	4.10E-03	1.54E-06	1.44E-02
1.16E-06	6.50E-03	1.53E-06	1.81E-02
1.18E-06	1.31E-02	1.54E-06	2.36E-02
1.19E-06	2.12E-02	1.54E-06	3.23E-02
1.19E-06	3.04E-02	1.55E-06	5.93E-02
1.19E-06	4.51E-02	1.56E-06	5.30E-02
1.20E-06	7.02E-02	1.57E-06	7.40E-02
1.21E-06	1.08E-01	1.59E-06	1.06E-01
1.24E-06	1.54E-01	1.63E-06	1.50E-01
1.27E-06	2.25E-01	1.69E-06	2.19E-01
1.31E-06	3.02E-01	1.79E-06	2.99E-01
1.40E-06	4.18E-01	1.94E-06	4.15E-01
1.52E-06	5.53E-01	2.17E-06	5.53E-01
1.71E-06	7.50E-01	2.55E-06	7.71E-01
1.95E-06	9.47E-01	3.01E-06	9.79E-01
2.40E-06	1.23E 00	3.82E-06	1.27E 00
2.92E-06	1.51E 00	4.77E-06	1.55E 00
3.76E-06	1.99E 00	6.24E-06	1.93E 00
4.80E-06	2.75E 00	9.02E-06	2.50E 00
6.15E-06	2.65E 00	1.10E-05	2.76E 00
8.95E-06	3.28E 00	1.51E-05	2.35E 00

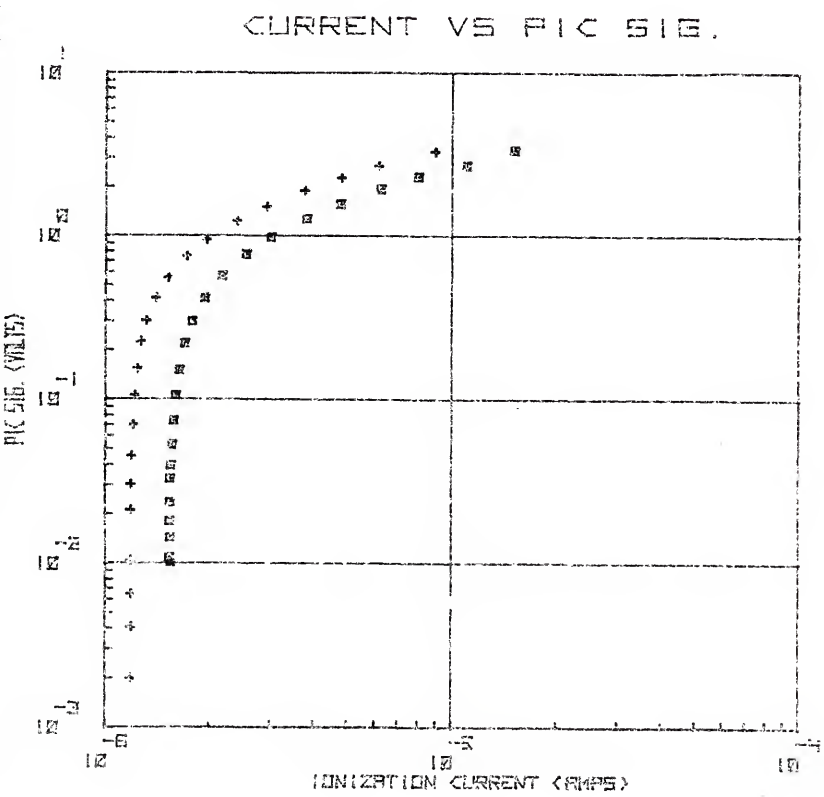

Figure 4-14. PIC signal versus steady state ionization current for 2 atm. Ne-filled gamma sensitive (+) and neutron-gamma sensitive (□) chambers at the temperature 326°C.

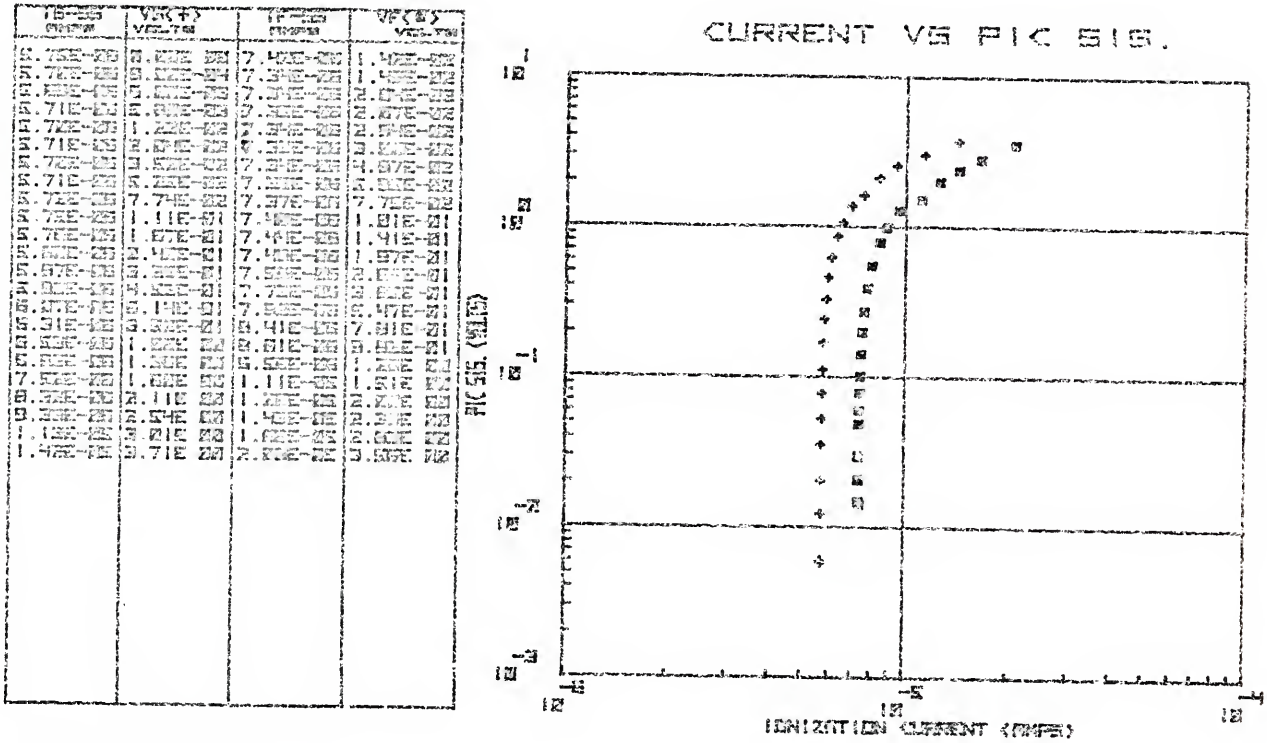

Figure 4-15. PIC signal versus steady state ionization current for 2 atm. Ne-filled gamma sensitive (+) and neutron-gamma sensitive (⊡) chambers at the temperature 380°C.

IG-GS AMPS	VG(+) VOLTS	IF-GS AMPS	VF(0) VOLTS
1.93E-05	5.60E-03	2.37E-05	6.60E-03
1.92E-05	4.50E-03	2.30E-05	1.16E-02
1.91E-05	7.30E-03	2.34E-05	1.53E-02
1.93E-05	1.1FE-02	2.37E-05	2.62E-02
1.51E-05	1.91E-02	2.30E-05	3.41E-02
1.91E-05	2.69E-02	2.30E-05	4.02E-02
1.91E-05	3.73E-02	2.36E-05	5.10E-02
1.91E-05	4.21E-02	2.34E-05	6.50E-02
1.91E-05	7.23E-02	2.35E-05	8.F3E-02
1.57E-05	1.02E-01	2.35E-05	1.22E-01
1.91E-05	1.44E-01	2.32E-05	1.67E-01
1.92E-05	2.07E-01	2.32E-05	2.40E-01
1.91E-05	2.91E-01	2.31E-05	3.47E-01
1.91E-05	3.91E-01	2.30E-05	4.67E-01
1.92E-05	5.23E-01	2.40E-05	6.65E-01
1.82E-05	7.23E-01	2.34E-05	9.71E-01
1.80E-05	9.31E-01	2.40E-05	1.28E 00
2.03E-05	1.29E 00	2.57E-05	1.71E 00
2.03E-05	1.53E 00	2.60E-05	2.15E 00
2.11E-05	1.85E 00	2.82E-05	2.74E 00
2.27E-05	2.31E 00	2.98E-05	3.27E 00
2.43E-05	2.83E 00	3.05E-05	3.85E 00
2.72E-05	3.57E 00	3.37E-05	4.21E 00

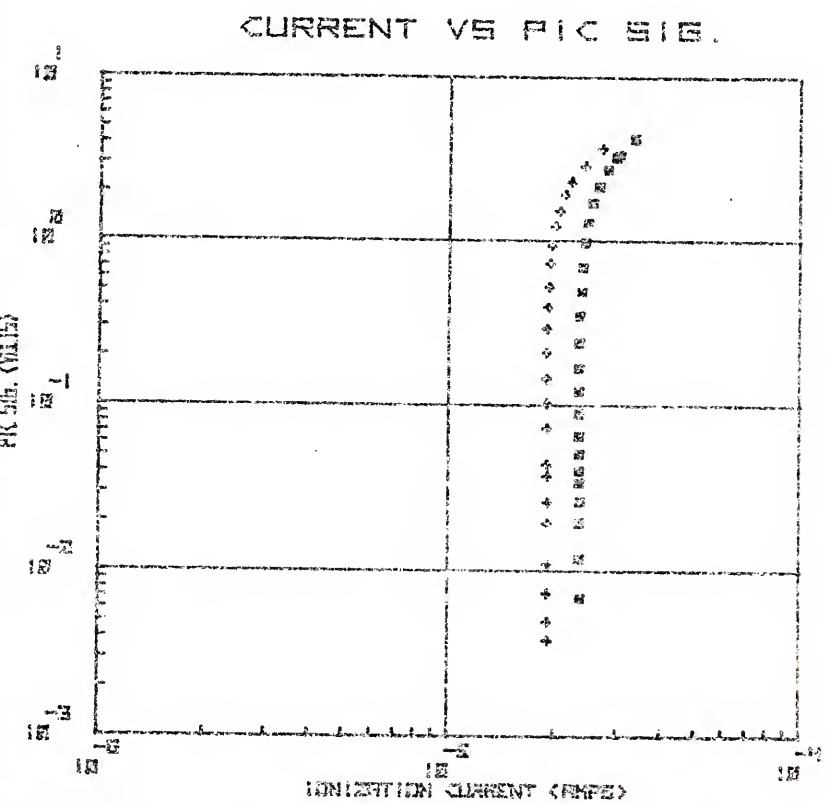

Figure 4-16. PIC signal versus steady state ionization current for 2 atm. Ne-filled gamma sensitive (+) and neutron-gamma sensitive (⊡) chambers at the temperature 432°C.

(F-S) AMPS	VF(F) VOLTS	(S-S) AMPS	VF(S) VOLTS
6.2[illegible]E-09	5.[illegible]E-02	4.[illegible]E-10	1.7[illegible]E-02
7.5[illegible]E-09	1.[illegible]E-01	1.[illegible]E-09	3.2[illegible]E-02
9.[illegible]E-09	2.2[illegible]E-01	1.77E-09	7.7[illegible]E-02
1.3[illegible]E-08	2.7[illegible]E-01	3.4[illegible]E-09	1.1[illegible]E-01
1.3[illegible]E-08	3.1[illegible]E-01	4.5[illegible]E-09	1.4[illegible]E-01
1.67E-08	4.0[illegible]E-01	5.2[illegible]E-09	2.2[illegible]E-01
2.1[illegible]E-08	4.7[illegible]E-01	7.7[illegible]E-09	3.5[illegible]E-01
3.0[illegible]E-08	5.8[illegible]E-01	1.1[illegible]E-08	5.6[illegible]E-01
4.2[illegible]E-08	8.17E-01	1.81E-08	5.1[illegible]E-01
5.2[illegible]E-08	8.5[illegible]E-01	2.6[illegible]E-08	5.0[illegible]E-01
6.1[illegible]E-08	1.1[illegible]E+01	4.57E-08	7.7[illegible]E-01
1.3[illegible]E-07	1.4[illegible]E+01	7.1[illegible]E-08	8.57E-01
2.8[illegible]E-07	1.8[illegible]E+01	1.6[illegible]E-07	1.2[illegible]E+01
3.17[illegible]E-07	2.5[illegible]E+01	1.72[illegible]E-07	1.7[illegible]E+01
4.70E-07	3.2[illegible]E+01	2.72[illegible]E-07	2.91E+01
7.1[illegible]E-07	4.4[illegible]E+01	4.37E-07	3.8[illegible]E+01
1.07[illegible]E-06	5.6[illegible]E+01	6.71E-07	5.2[illegible]E+01
1.61[illegible]E-06	7.1[illegible]E+01	1.0[illegible]E-06	6.21[illegible]E+01
2.25[illegible]E-06	8.5[illegible]E+01	1.4[illegible]E-06	5.61[illegible]E+01
3.21[illegible]E-06	1.1[illegible]E+02	2.2[illegible]E-06	8.4[illegible]E+01
4.58[illegible]E-06	1.2[illegible]E+02	3.0[illegible]E-06	1.0[illegible]E+02

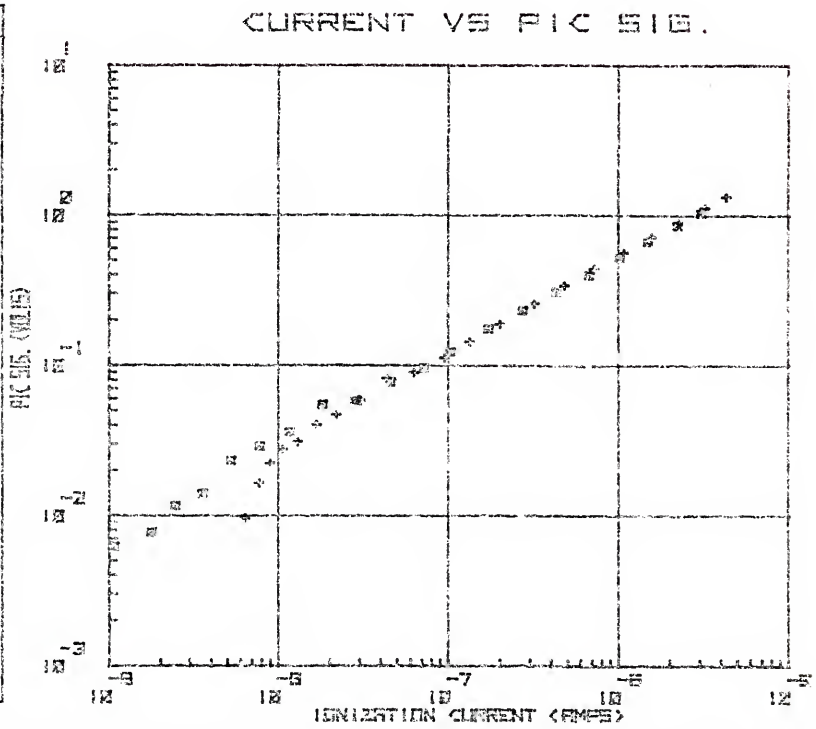

Figure 4-17. PIC signal versus steady state ionization current for 1 atm. Ar-5% N_2-filled neutron-gamma sensitive (+) and gamma sensitive (□) chambers at the temperature 25°C.

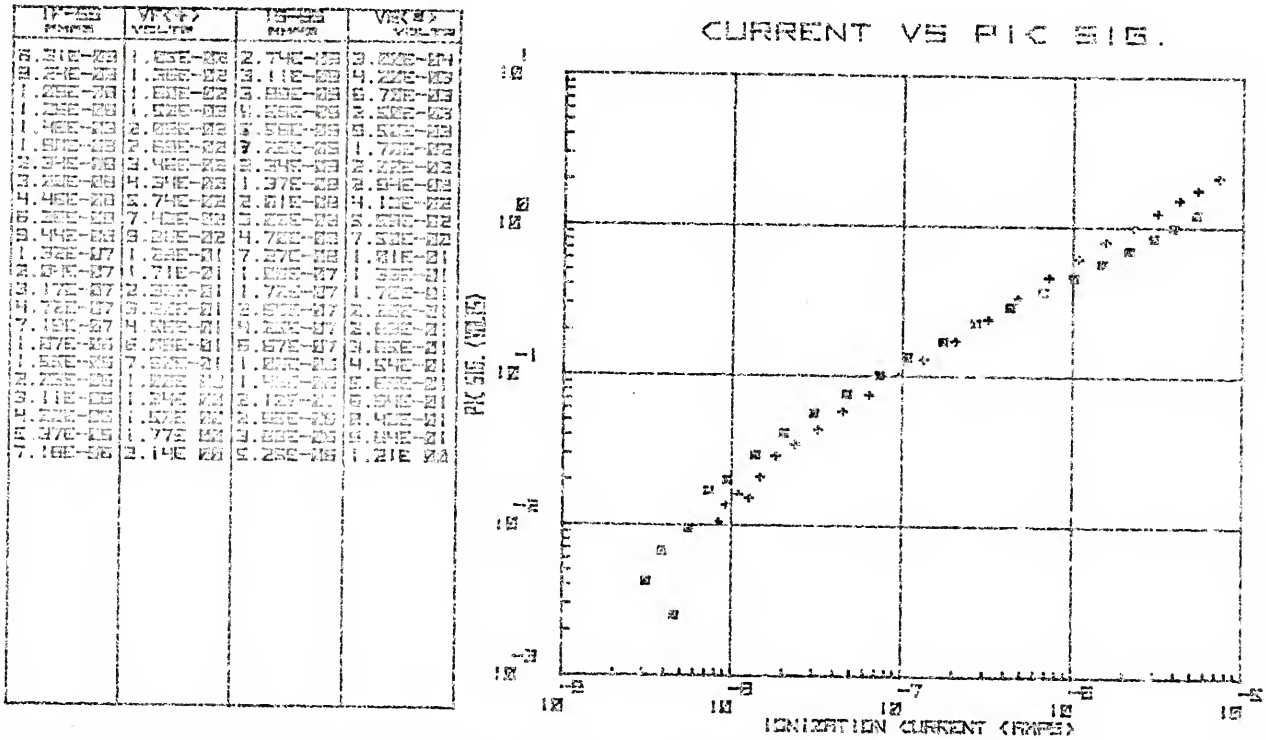

Figure 4-18. PIC signal versus steady state ionization current for 1 atm. Ar-5% N_2-filled neutron-gamma sensitive (+) and gamma sensitive (⊡) chambers at the temperature 91°C.

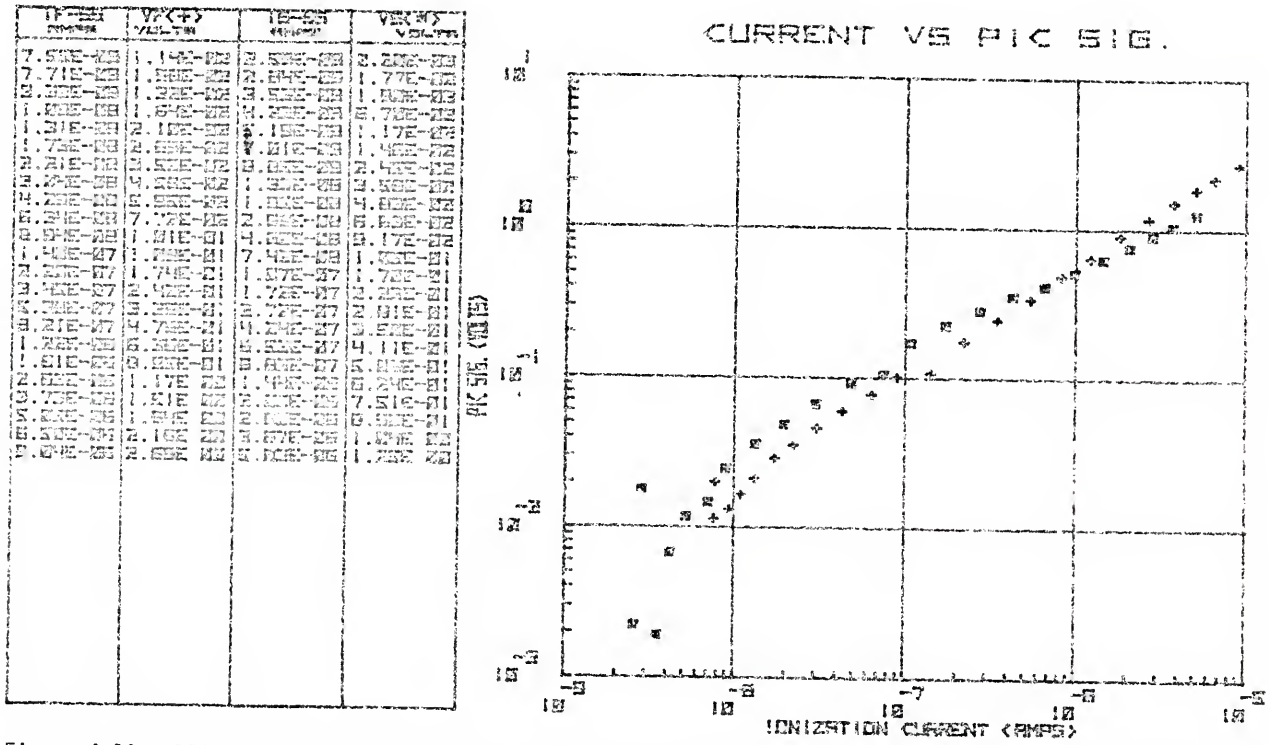

Figure 4-19. PIC signal versus steady state ionization current for 1 atm. Ar-5% N_2-filled neutron-gamma sensitive (+) and gamma sensitive (⊡) chambers at the temperature 152°C.

IP(+) AMPS	VP(+) VOLTS	IP(□) AMPS	VP(□) VOLTS
1.47E-09	1.2ME-02	1.05E-09	4.60E-03
1.55E-09	8.20E-03	1.11E-09	8.20E-04
1.72E-09	8.60E-03	1.18E-09	4.40E-03
1.80E-09	1.20E-02	1.20E-09	6.20E-03
2.15E-09	1.55E-02	1.30E-09	1.40E-02
2.54E-09	2.10E-02	1.54E-09	1.84E-02
3.11E-09	2.77E-02	1.76E-09	2.54E-02
3.85E-09	3.50E-02	2.17E-09	3.50E-02
5.24E-09	4.50E-02	2.82E-09	5.20E-02
7.25E-09	6.60E-02	3.87E-09	7.60E-02
9.57E-09	8.20E-02	5.51E-09	1.15E-01
1.40E-07	1.80E-01	8.00E-09	1.80E-01
2.03E-07	1.37E-01	1.14E-07	2.24E-01
2.87E-07	1.78E-01	1.71E-07	3.40E-01
3.85E-07	2.31E-01	2.67E-07	4.15E-01
5.24E-07	3.18E-01	3.92E-07	5.41E-01
7.85E-07	4.20E-01	5.76E-07	5.76E-01
1.60E-06	5.32E-01	1.64E-06	7.44E-01
2.15E-06	7.70E-01	1.47E-06	9.18E-01
2.17E-06	1.01E 00	2.14E-06	1.30E 00
4.20E-06	1.27E 00	2.60E-06	1.41E 00
5.91E-06	1.51E 00	3.01E-06	1.39E 00
7.44E-06	1.52E 00	5.33E-06	1.61E 00

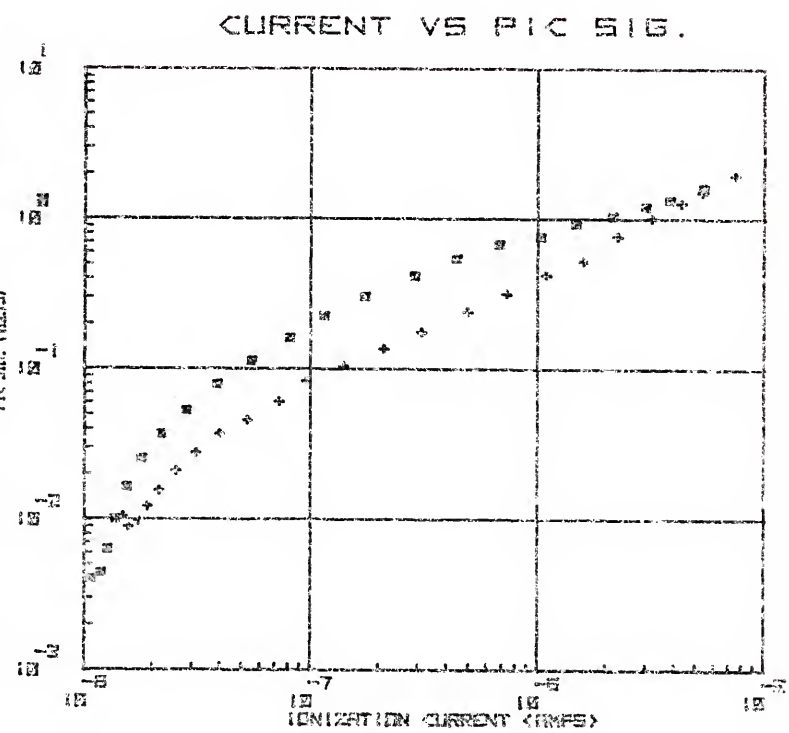

Figure 4-20. PIC signal versus steady state ionization current for 1 atm. Ar-5% N_2-filled neutron-gamma sensitive (+) and gamma sensitive (□) chambers at the temperature 190°C.

IC-SS (AMPS)	VA(+) (VOLTS)	IC-SS (AMPS)	VB(□) (VOLTS)
1.[illegible]E-07	9.[illegible]E-03	9.[illegible]E-08	7.[illegible]E-04
1.[illegible]E-07	1.[illegible]E-02	9.[illegible]E-08	9.[illegible]E-04
1.[illegible]E-07	1.[illegible]E-02	1.[illegible]E-07	5.[illegible]E-03
1.[illegible]E-07	2.[illegible]E-02	1.[illegible]E-07	9.[illegible]E-03
1.[illegible]E-07	2.27E-02	1.[illegible]E-07	1.[illegible]E-02
1.[illegible]E-07	2.[illegible]E-02	1.[illegible]E-07	1.71E-02
1.[illegible]E-07	2.75E-02	1.[illegible]E-07	2.[illegible]E-02
2.[illegible]E-07	3.61E-02	1.11E-07	3.72E-02
2.19E-07	4.[illegible]E-02	1.19E-07	5.[illegible]E-02
3.44E-07	5.34E-02	1.31E-07	8.71E-02
5.72E-07	7.52E-02	1.[illegible]E-07	1.[illegible]E-01
9.15E-07	9.77E-02	1.70E-07	1.67E-01
9.87E-07	1.27E-01	2.13E-07	2.36E-01
1.[illegible]E-06	1.72E-01	2.71E-07	3.31E-01
1.70E-06	2.34E-01	3.[illegible]E-07	4.[illegible]E-01
2.[illegible]E-06	3.[illegible]E-01	5.[illegible]E-07	6.[illegible]E-01
3.[illegible]E-06	4.[illegible]E-01	7.[illegible]E-07	7.47E-01
4.76E-06	6.44E-01	1.11E-06	9.[illegible]E-01
6.[illegible]E-06	8.[illegible]E-01	1.[illegible]E-06	1.[illegible]E+00
8.31E-06	7.61E-01	2.[illegible]E-06	1.31E+00
1.[illegible]E-05	9.[illegible]E-01	3.[illegible]E-06	1.[illegible]E+00
5.[illegible]E-05	1.12E+00	5.[illegible]E-06	1.[illegible]E+00
7.[illegible]E-05	1.41E+00	8.[illegible]E-06	1.[illegible]E+00

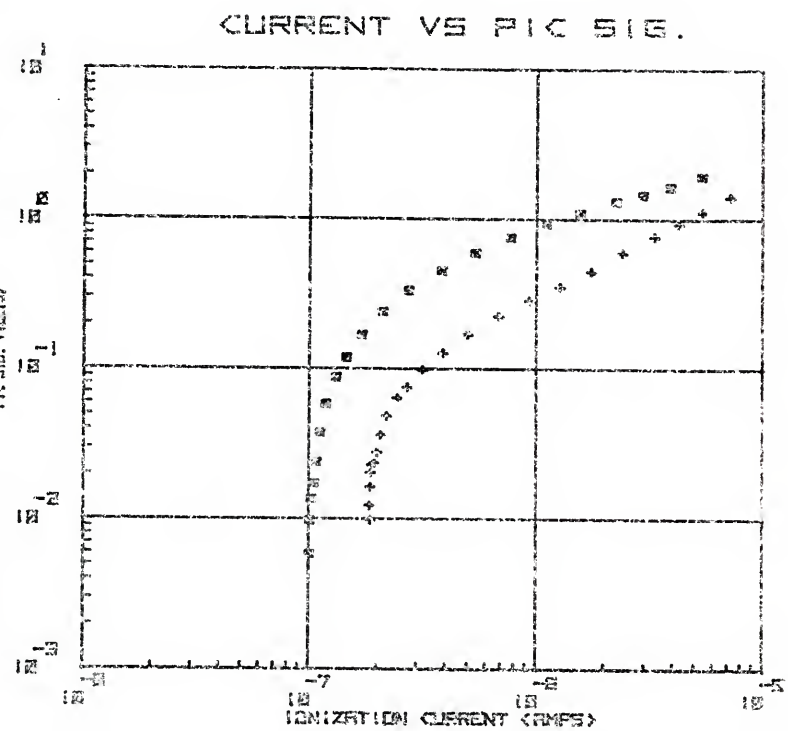

Figure 4-21. PIC signal versus steady state ionization current for 1 atm. Ar-5% N_2-filled neutron-gamma sensitive (+) and gamma sensitive (□) chambers at the temperature 260°C.

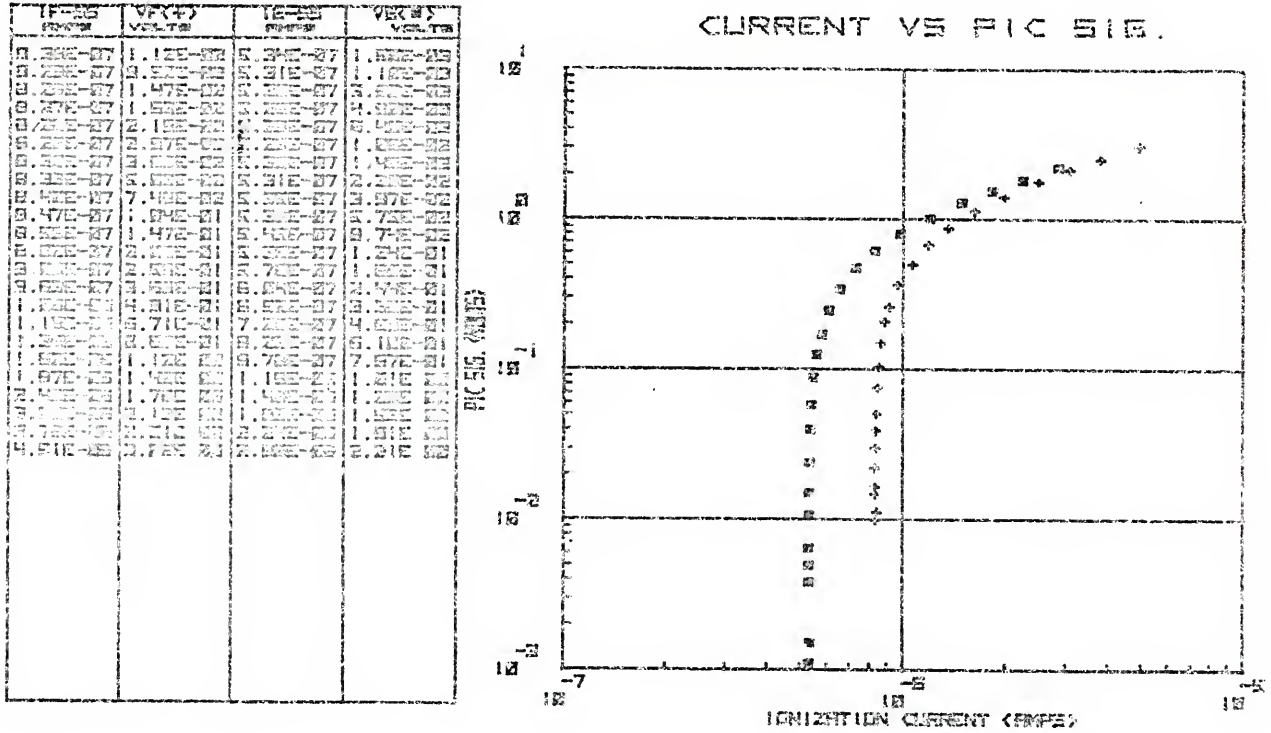

Figure 4-22. PIC signal versus steady state ionization current for 1 atm. Ar-5% N_2-filled neutron-gamma sensitive (+) and gamma sensitive (□) chambers at the temperature 297°C.

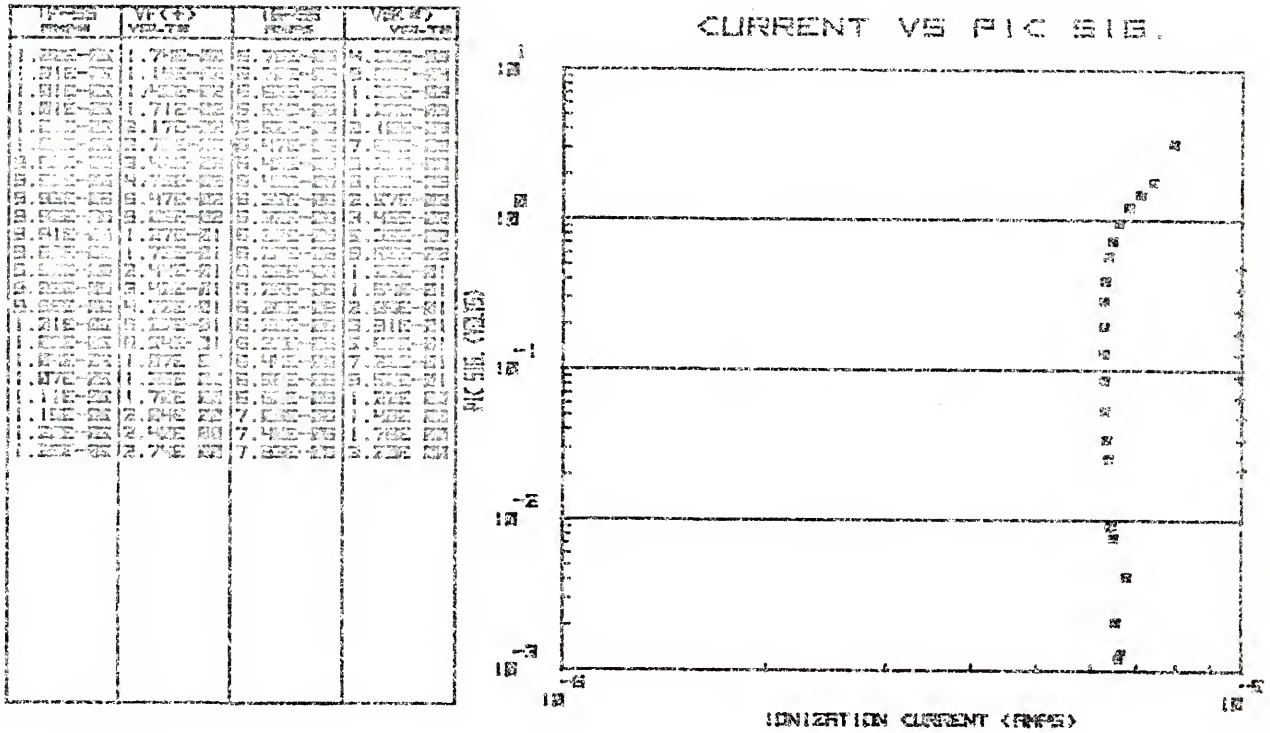

Figure 4-23. PIC signal versus steady state ionization current for 1 atm. Ar-5% N_2-filled neutron-gamma sensitive (+) and gamma sensitive (⊡) chambers at the temperature 377°C.

To glean information from the data more easily, the leakage current was subtracted from all current values and the ratio of $I_{ss}/v(t_c)$ was computed for all data points. Tables 4-2 and 4-3 contain the results for the Ar-N_2 and Ne chambers, respectively. The blank spaces indicate the result obtained was meaningless. Figures 4-24 and 4-25 present the tabulated $I_{ss}/v(t_c)$ ratio at position 3 as a function of temperature for Ne and Ar-N_2 data, respectively.

The reason for calculating the ratio was to smooth out fluctuations in the data caused by vertical and rotational positioning differences between data sets. Since I_{ss} is constant for a given exposure rate, over the temperature range of interest, $v(t_c)$ accounts for the variation in the ratio $I_{ss}/v(t_c)$. If $v(t_c)$ gets larger in the second order region, this indicates that the volume recombination coefficient is decreasing. Note, as well, that as $v(t_c)$ gets larger $I_{ss}/v(t_c)$ gets smaller.

With these facts in mind examine the Ne data in Table 4-2 and Figure 4-24. In particular choose a position where $v(t_c)$ is in the second order region, for instance, position 3. The ratio of $I_{ss}/v(t_c)$ changes considerably over the temperature range of interest. At 25°C the ratio for the gamma chamber is 4.36×10^{-6} while at 477°C it is 1.32×10^{-6}. The same temperature range for the fission chamber gives a ratio range of 4.94×10^{-6} to 1.87×10^{-6}. Note that the relative changes are approximately equal for both chambers. As one will see this is not true for the Ar-N_2 chambers. This indicates the α_2 decreases with increasing temperature for Ne; a fact which appears to contradict Sanders[7] results. Sanders found α_2 constant for Ne from 25°C to 300°C. Examining the data given in the lower part of Table 4-2 (positions 1.5, 2.5, 3, 3.5) more closely, one notes that the ratio is virtually constant

TABLE 4-2
NEON DATA

Vertical Port Position	TEMP	25°C		71°C		129°C		179°C		217°C	
	Chamber	gammaxE9	FissionxE6	gammaxE6	FissionxE6	gammaxE6	FissionxE6	gammaxE6	FissionxE6	gammaxE6	FissionxE6
	Leakage Current	2.44E-12				9.57E-11	2.53E-10	1.93E-09	2.05E-09	1.55E-08	2.13E-08
14		.730	.660	1.03	.867	.521	.642	.456	.630	.521	.642
13		.486	.767	.836	.693	.331	.641	5.96	.692	.800	.714
12		.583	.669	.460	.718	.366	.668	.786	.701	.374	.665
11.5		.572	.775	.707	.804	.362	.706	.611	.651	.305	.561
11		.545	.773	.512	.690	.341	.601	.588	.708	.367	.601
10.5		.732	.855	.661	.743	.435	.673	.456	.640	.377	.687
10		.987	.933	.417	.710	.472	.242	.583	.767	.414	.755
9.5		.945	1.12	.675	.873	.536	.819	.601	.820	.537	.844
9		1.08	1.23	.742	.993	.667	.959	.634	.961	.556	.997
8.5		1.26	1.40	.888	1.15	.778	1.09	.796	1.11	.652	1.02
8		1.47	1.58	.966	1.29	.900	1.26	.923	1.27	.724	1.16
7.5		1.58	1.71	1.16	1.49	1.06	1.46	1.08	1.49	.864	1.44
7		1.69	1.81	1.35	1.69	1.27	1.66	1.22	1.71	.988	1.57
6.5		1.87	1.99	1.53	1.89	1.40	1.85	1.49	1.97	1.17	1.99
6		2.03	2.21	1.83	2.16	1.72	2.07	1.71	2.25	1.43	2.27
5.5		2.35	2.66	2.15	2.54	2.02	2.46	2.09	2.69	1.74	2.80
5		2.61	2.95	2.34	2.78	2.29	2.68	2.40	2.95	2.07	3.11
4.5		3.29	3.39	3.01	3.18	2.79	3.01	3.00	3.30	2.67	3.55
4		3.61	3.80	3.31	3.59	3.18	3.45	3.32	3.62	3.05	3.95
3.5		3.95	4.39	3.76	4.10	3.51	3.78	3.79	4.05	3.62	4.49
3		4.36	4.94	4.31	4.66	4.01	4.25	4.27	4.66	4.15	4.98
2.5		5.40	5.99	5.16	5.55	4.62	5.05	5.01	5.24	4.76	5.92
1.5		6.14	5.87	5.32	6.49	5.55	5.87	5.91	7.00	5.82	6.75

TABLE 4-2 (Cont'd)
NEON DATA

Vertical Port Position	TEMP	282°C		320°C		330°C		432°C	
	Chamber	gammaxE6	FissionxE6	gammaxE6	FissionxE6	gammaxE6	FissionxE6	gammaxE6	FissionxE6
	Leakage Current	2.10E-07	3.23E-07	1.19E-06	1.54E-06	5.76E-06	7.41E-06	1.92E-05	2.32E-05
14		.178	.535	.811	.667		.479	.102	1.00
13		.378	.531						
12		.587	.665		.009				
11.5		604	.650		.048				
11		.709	.746						
10.5		.612	.808		.065				
10		.553	.835		.214				
9.5		.470	.833	.009	.355				
9		.479	.916	.115	.424				
8.5		.491	.978	.215	.557				
8		.558	1.09	.297	.607	.046	.197		
7.5		.588	1.22	.338	.710	.223	.419		
7		.648	1.40	.400	.820	.339	.627		
6.5		.733	1.64	.498	.968	.408	.841		.240
6		.850	2.12	.589	1.12	.516	1.04	1.29	.413
5.5		.972	2.33	.698	1.31	.656	1.28	.256	.590
5		1.13	2.72	.812	1.50	.736	1.43	.476	.849
4.5		1.39	3.05	.961	1.80	.869	1.68	.678	1.09
4		1.62	3.49	1.15	2.08	1.10	2.44	.913	1.35
3.5		1.89	3.95	1.36	2.44	1.22	2.58	1.12	1.62
3		2.19	4.52	1.60	2.82	1.43	2.88	1.32	1.87
2.5		2.54	5.22	1.87	3.52	1.85	3.23	1.76	2.09
1.5		3.23	6.02	2.37	4.07	2.28	3.76	2.19	2.38

TABLE 4-3
ARGON DATA

Vertical Port Position	TEMP	25°C		91°C		152°C		190°C		200°C	
	Chamber	gammaxE6	FissionxE6	gammaxE6	FissionxE6	gammaxE6	FissionxE6	gammaxE6	FissionxE6	gammaxE6	FissionxE6
	Leakage Current	8.35xE-12	3.56xE-12	2.28xE-9	2.01xE-9	2.13xE-9	1.25xE-9	1.02xE-8	8.38xE-9	9.90xE-8	1.00xE-7
14		.271	.556		.690	.209	.553	.115	606		
13		.170	.465	.198	.531		.326		.802		.410
12		.228	.400	.240	.556	.736	.611	.362	.903	.269	.403
11.5		.210	.383	.919	.696	.311	.563	.289	.863	.181	.370
11		.252	.418	.343	.603	.261	.567	.339	.836	.222	.419
10.5		.225	.416	.293	.555	.335	.554	.316	.611	.345	.599
10		.268	464	.353	.619	.274	.595	.303	.824	.374	.708
9.5		.307	.523	.388	.690	.311	.636	.314	.844	.303	.739
9		.339	.529	.433	.742	.360	.700	.340	.966	.320	.818
8.5		.483	.791	.439	.829	.417	.805	.364	1.06	.369	1.03
8		.593	.846	.597	.937	.501	.870	.398	1.06	.337	1.20
7.5		.748	.930	.596	1.01	.688	1.29	.441	1.25	.407	1.58
7		.837	1.07	.777	1.18	.613	1.25	.465	1.48	.406	1.63
6.5		.986	1.24	1.00	1.32	.761	1.42	.538	1.70	.529	1.88
6		1.17	1.41	1.17	1.40	.952	1.60	.668	2.00	.633	2.23
5.5		1.40	1.62	1.47	1.57	1.21	1.71	.794	2.28	.782	2.63
5		1.69	1.91	1.82	1.76	1.58	1.91	.988	2.56	.862	3.10
4.5		1.95	2.10	2.20	1.96	1.92	2.02	1.24	3.04	1.09	3.52
4		2.26	2.40	2.60	2.22	2.30	2.25	1.60	2.90	1.26	3.74
3.5		2.62	2.88	3.05	2.50	2.72	2.48	2.04	3.13	1.64	4.11
3		2.97	3.24	3.50	2.77	3.12	2.74	2.47	3.38	1.97	4.38
2.5				3.94	3.04	3.52	2.99	2.85	3.84	2.31	4.66
1.5				4.36	3.36	4.02	3.37	3.35	3.85	2.72	4.94

TABLE 4-3 (Cont'd)
ARGON DATA

Vertical Port Position	TEMP Chamber	297°C		377°C	
		gammaxE6	FissionxE6	gammaxE6	FissionxE6
	Leakage Current	5.32xE7	8.31xE-7		
14					
13					
12					
11.5					
11					
10.5					
10					
9.5					
9			.118		
8.5			.149		
8		.130	.190		
7.5		.183	.249		
7		.246	.302		
6.5		.292	.353		
6		.350	.472		
5.5		.416	.528		
5		.475	.604		
4.5		.558	.702		.203
4		.656	.815		.352
3.5		.740	.942		.514
3		.842	1.06	.212	.658
2.5		.941	1.18	.357	.749
1.5		1.05	1.34	.384	.829

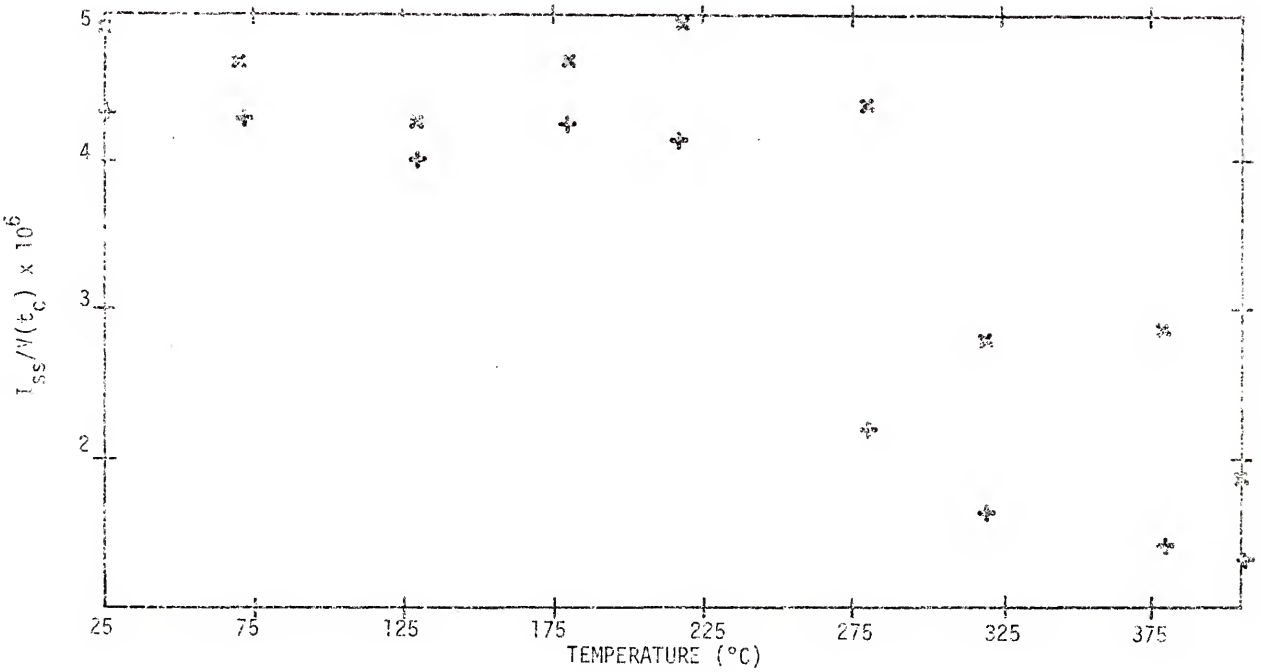

Figure 4-24. PIC signal versus temperature for 2 atmosphere Ne-filled neutron-gamma sensitive (x) and gamma sensitive (+) chambers at position 3.

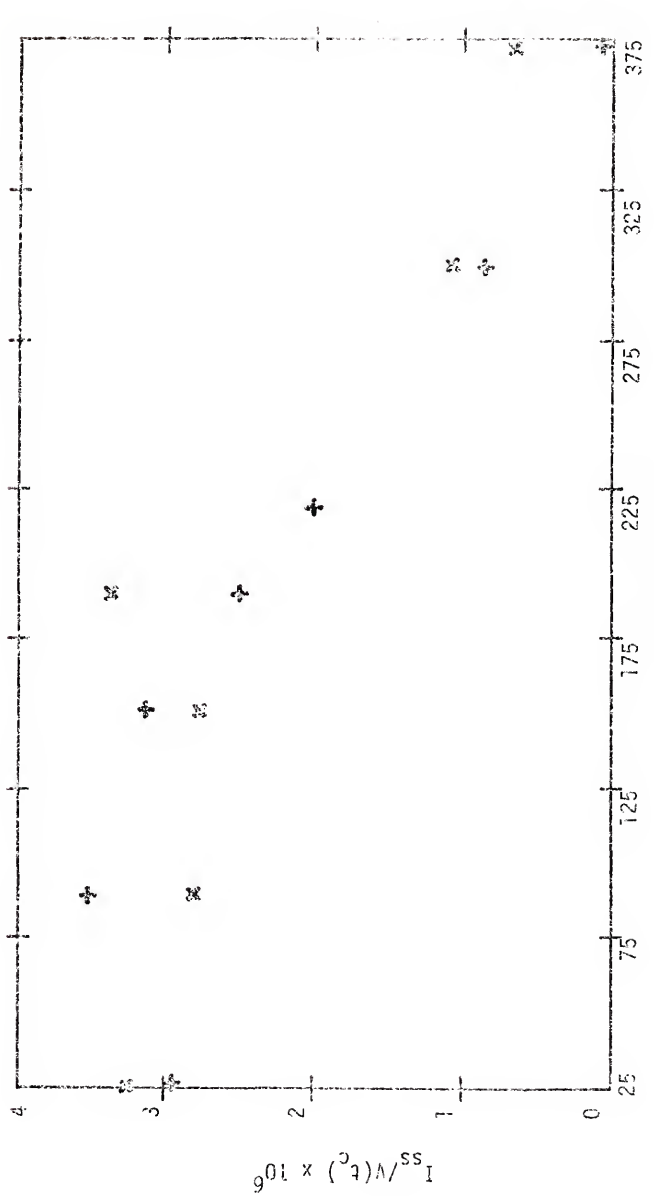

Figure 4-25. PIC signal versus temperature for 1 atmosphere AR-5% N_2-filled neutron-gamma sensitive (x) and gamma sensitive (+) chambers at position 3.

up to 282°C. At 282°C it takes a sudden drop and continues down over the rest of the temperature range. Thus rather than contradicting Sanders data, it validates his conclusion to some extent that α_2 for Ne is essentially constant from 25°C to approximately 300°C. Note also that a 1 atmosphere chamber was used in Sanders experiment while the ones used here contained 2 atmospheres of Ne.

The gradual decrease in the ratio at a given temperature is due to the transition between weak linear diffusional losses and stronger volume recombinational losses as the steady state ion density increases.

Table 4-3 contains the Ar-N_2 data. For the highest exposure rates, where volume recombination predominates, the $I_{ss}/v(t_c)$ ratio changes by a factor of 10 for the gamma chamber and by a factor of 5 for the fission chamber. There is no theoretical explanation for this if both chambers were prepared in the same manner and filled with the same gas. A possible explanation is that these chambers were not thoroughly baked and pumped before filling. The fission chamber, having its walls coated with pure uranium, maintained a purer gas mixture as the temperature was raised because the gas impurities in the walls were trapped by the coating. The gamma chamber, however, having no such protection, had wall trapped gas impurities mixed in with the Ar-N_2 fill gas. Such impurities would, in general, enhance the temperature dependence of α_2, an effect which is apparent in the data.

Little was said of the transition and first order data regions for two reasons. The first being, it is a well known fact that diffusion, which controls losses in the first order region, is both temperature and pressure dependent in rather complex ways.[11] Thus a simple explanation of the results does not exist and it would be inappropriate to go into it

in this paper, since it is not needed and many excellent works on diffusion have been published. The second reason is that for practical reactor operation gamma compensation is not necessary until an exposure rate of greater than 10^5 R/hr is experienced. As one can see in figure 4-4, above 10^5 R/hr second order effects predominate.

Sources of Errors

The main source of error in this experiment was detector positioning. A ±5% error in positioning produced as much as a ±15% error in the measured signal. The reason for the magnification was the rapid variation of flux with position. In the temperature measurements the positional error became even more aggravated due to the oven. The oven was allowed some rotational freedom as it was moved vertically. Thus, the chambers were rotated in the horizontal plane with respect to the source. This effect was minimized when the styrofoam mold was used, but when the oven was used, appreciable (±5%) exposure rate fluctuations were experienced at the chambers due to self shielding. This variation accounts, in part, for the apparent staggered look of the data tabulated in Table 4-2 and 4-3. Only trends are meaningful in this data and point by point comparison should be avoided.

Another source of error in measuring $v(t_c)$ was the drift in the base line caused by the temperature dependence of the impedance switching transistors (10 mV/°C). This error was almost impossible to accurately determine. However, the base line was monitored before and after each set of measurements, if it was found to have drifted more than ± 10 mV the set of data was discarded and the measurement repeated.

As stated in the first part of the chapter the electronics remained both linear and accurate to within ±2%, over the 3 months the system was used.

In measuring $v(t_c)$ a source of error other than instrument error was present. I_{ss}, which contributes to $v(t_c)$ only minutely at low exposure rates, at the high exposure rates could begin to significantly contribute to the $v(t_c)$ measured. Ideally $v(t_c)$ should be constituted of only the steady state ion density collected. The equation which describes the I_{ss} current contribution is,

$$v_{ss}(t) = I_{ss}R\ (1 - \exp(-t/RC)),$$

where RC is the circuit time constant. For $t << RC$ this reduces to

$$v_{ss}(t) = I_{ss}R.$$

Note that $v_{ss}(t)$ can be reduced by reducing R, just as long as $t << RC$. Also, to avoid affecting $v(t_c)$ adversely RC must remain significantly greater than t_c. In this experiment R was 20 MΩ, C was 400 pf and t_c was 100 μsec. Thus RC was 8 msec, a factor of 8000 greater than t_c. At the high exposure rates v_{ss}(100 μsec) constituted approximately 5% of the measured $v(t_c)$. This could have been reduced by a factor of approximately 20 by reducing R to 1 MΩ. Such a reduction would have had a minimal effect on the true value $v(t_c)$.

Another possible source of error incurred during the neon chamber temperature measurements involved the 2 foot air coax used to connect the chamber to the RG62U cables coming from the HVP. Since approximately a two inch section of the air coax was partially heated during the experiment the change in the characteristics of the air coax with temperature could possibly have had a measurable effect on the apparent response of the neon chamber. However, it is felt that due to the gas kinetic characteristics of air and the relatively small volume involved, the air coax temperature effect on the measured signal was negligible.

CHAPTER V
CONCLUSIONS

To verify the Pulsed Ion Chamber applicability to the measuring of the full range of reactor power, three basic steps were required. A computer based, solid state, dual chamber PIC system had to be designed and built. Gamma compensation for the expected mixed order (linear and/or second order) response region had to be clearly verified. The PIC mode chamber response had to be proven to be independent of temperature over a range of 25 to 500°C.

The design and building of the computer based PIC system took considerable time and effort, but the end result was success. It met all the design requirements and more. Its versatility simply as a plasma diagnostic tool is apparent. One has full control over all pulsing-sampling sequences, as one can see in figure 3-3 all the timing sequence potentiometers are on the front panel. The system is free from the time jitter and position orientation problems which plagued the most advanced mercury wetted reed pulsers previously used. The impedance switching circuit has a response time on the order of 50 nsec, due to the use of the most advanced gigahertz switching transistors. This in itself is an improvement of a factor of 5 over the previous systems. Thus the system is a significant advancement of the PIC state of the art.

Verifying the feasibility of gamma compensation was accomplished relatively easily using the PIC computer based system. Compensation, at

a given temperature for the exposure rates where compensation would be required, can be obtained to within ±2% of the total gamma signal.

The PIC mode chamber response was proven to be temperature dependent over the range of 25 to 500°C for Ne as well as the Ar-N_2 fill gas mixture. However, as stated earlier, the Ne response was constant up to ~282°C, this constant range could be extended by reducing the pressure of the Ne fill gas. The 300°C temperature range is the operating range of current light water reactors. Thus this PIC system offers all the required characteristics and more for an in-core wide range neutron measuring system for present light water reactors.

A fill gas whose PIC response is independent of temperature over the 25°C to 500°C range must be found before the system could realistically be applied to power measurements in the new, more advanced HTGR and LMFBR reactors. Seeing that this is apparently the only remaining stumbling block to the use of the PIC system for wide range reactor power measurements in these reactors a concentrated effort to find a suitable gas should be launched.

In conclusion, since new findings and advancement of the state-of-the-art, both of which have been accomplished here, are the essence of research, this was indeed a successful endeavor.

APPENDIX

HP 9821 Codes

The following HP9821 programs were used to control the PIC system, read and record data, perform data analysis, and finally output the data in plot form.

PIC System Data Recording Code

This code records the I_{ss}, $v(t_c)$ and R/hr data used in this thesis.

```
 0:  PRT "THIS PROGRAM"
 1:  PRT "RECORDS S.S."
 2:  PRT " CURRENT VS. PIC"
 3.  PRT "VOLTAGE SIGNAL"
 4:  PRT "DATA AND STORES"
 5:  PRT "IT IN FILE"
 6:  PRT "GIVEN."
 7:  SPC 3
 8:  ENT "WTB NO. C-MODE 1", R12
 9:  ENT "WTB NO. C-MODE 2", R13
10:  ENT "VOLT FULL SCALE", R7
11:  ENT "VOLTS ZERO SCALE", R6
12:  ENT "I FULL SCALE?", R10
13:  ENT "I ZERO SCALE?", R9
14:  21 → R16; 0 → R17
```

In the above statements the expected value limits of $v(t_c)$ and I_{ss} are input as well as the range control numbers for the Keithley 419 picoamp; statements 8 and 9.

```
15:  WTB 1, 192
16:  CMD "?V5"; FMT *; RED 13, A
17:  1 → X
18:  RED 3, Y, Z
19:  X + 1 → X; IF x ≤ 200; JMP -1
20:  CMD "?V5"; FMT *; RED 13, B
21:  B-A → C; IF C > 100; INT (C/100) * 60 + (C-INT (C/100) * 100) → C
22:  C * 1E6/200 → R5; FLT 5; PRT "PERIOD IN 10-6 SECONDS ---", R5
```

Statement 15 contains the command which switches the system into the PIC mode. The remainder of this section measures the period of the system utilizing the HP clock which is addressed in statements 16 and 20.

```
23:  ENT "POSITION ?", X
24:  "2"; WTC 1, R12; R3 → X
25:  6.226376 + .403346 X - .193881x ↑ 4 → Y
26:  Y + 1.168232E - 4X ↑ 5 - 3.396338E - 6X ↑ 6 + 4.052068E - 8X ↑ 7 → Y
27:  10 ↑ Y → R (R16 + 4)
```

The vertical port position is entered by the experimenter and the R/hr is computed from the seventh order curve fit described in Chapter IV.

Statement 24 switches the system into the steady state mode in order to measure I_{ss} for channel 1(I_{ss1}).

```
28:  "3"; GSB "DELAY"
29:  RED 3, X, Y
30:  IF Y ≤ 200; IF R12 ≤ 170; R12 + 1 → R12; GET "2"
```

```
31:  IF Y > 3000; IF R12 > 160; R12 - 1 → R12 GTO "2"
32:  GSB "DELAY"
33:  RED 3, X, Z
34:  IF ABS (Z-Y) > 60; GTO "3"
35:  0 → C
36:  RED 3, X, Y
37:  Z + Y → Z; C + 1 → C; IF C ≤ 8; JMP - 1
38:  Z/10 → Z
39:  Z* .0033333 * 10 ↑ (158 - R12) → RR16
40:  IF R12 = 165; RR16 - .1E-7 → RR16; GTO "4"
41:  IF R12 = 166; RR16 - .05E - 8 → RR16; GTO "4"
42:  IF R12 = 167; RR16 * 1E9 → X
43:  IF R12 = 167; .03948 + .8529X + 7968E - 6 * X ↑ 2 - 4.202E - 4 * X ↑
     3 → Y; Y * 1E - 9 → RR16
```

This section measures I_{ss1} 10 times and then computes and stores the average.

```
44:  "4"; WTB 1, R13
45:  GSB "DELAY"
46:  RED 3, X, Y
47:  IF Y ≤ 200; IF R13 ≤ 106, R13 + 1 → R13; GTO "4"
48:  IF Y > 3000; IF R13 > 90; R13 - 1 → R13; GTO "4"
49:  GSB "DELAY:
50:  RED 3, X, Z
51:  IF ABS (Y - z) > 60; GTO "4"
52:  0 → C
53:  RED 3, X, Y
54:  Z + Y → Z; C + 1 → C; IF C ≤ 8; JMP - 1
```

```
55:  Z/10 → Z
56:  Z * .003333 * 10 ↑ (94 - R13) → R (R16 + 2)
57:  R (R16 + 2) → X
58:  IF R13 = 101; X ← .1E-7 → R (R16 + 2); GTO "B"
59:  IF R13 = 102; X ← .05E-8 → R (R16 + 2); GTO "B"
60:  IF R13 ≠ 103; GTO "B"
61:  X * 1E9 → X; .03948 + .8529X + 7968E-5 * X ↑ 2 - 4.202E-4 * X ↑ 3 → Y
62:  Y * 1E-9 → R (R16 + 2)
```

This section measures and stores the I_{ss} value for channel 2.

```
63:  "B"; WTB 1, 192
64:  0 → C; 0 → X; 0 → Z; 0 → R1 8; 0 → R19
65:  35 → X; GSB "DELAY"
66:  RED 3, Y, X; RED 5, Y, Z
67:  X + R18 → R18; Z + R19 → R19; C + 1 → C; IF C ≤ 9; JMP -1
68:  R18/10000 → R (R16 + 1); R19/1000 → R (R16 + 3)
69:  FLT 4; PRT R (R16 + 4), R (R16 +1), RR16, R (R16 + 3), R (R16 +2);
     R16 + 6 → R16; SPC 1
```

$v(t_c)$ for channels 1 and 2 are measured and stored in this section.

Note 10 values of each are measured and then averaged together.

```
70:  ENT "MORE?  YES → 1 NO → 0", Y
71:  ENT "POSITION?", R3
72:  IF Y > 0; GTO "2"
73:  ENT "NEW SET? Y → 1 NO → 0", Y
74:  IF Y > 0; R16 → RR17; R17 + 1 → R17; GTO "2"
75:  R16 → RR17
76:  ENT "TAPE?", A," FILE?", A
77:   RCF A, R (R16 - 1)
78:  GTO "END"
```

This section asks if more data are to be taken. If so, the cycle is repeated. If not the data are stored on tape in the specified file.

```
79:  "DELAY"
80:  CMD "?V5"; FMT *; RED 13, A
81:  "0"; CMD "?V5"; RED 13, B
82:  IF X ≠ 35; 10 → X
83:  IF B-A ≤ X; GTO "0"
84:  RET
85:  "END"; END
```

This is a subroutine addressed after switching from channel to channel or mode to mode. It delays the data recording for 10 to 35 sec to allow the system to stabilize.

Curve Fitting By Chebyshev Polynominals

This program[10] fits a least-squares curve to a set of given data points (x_1, y_1), (x_2, y_2),..., $(x_n, y_n,)$ where the x_i lie in an interval (a, b) and are equally spaced. The user specifies a degree m and the program outputs the coefficients a_0, a_1,..., a_m of a polynomial $P(x) = a_0 + a_1x + \ldots + a_mx^m$ passing near or through each input point.

The program determines the a_i by considering P(x) as a linear combination of Chebyshev polynomials $T_i(x)$, $P(x) = c_0T_0(x) + c_1T_1(x) + \ldots + c_mT_m(x)$ and applying the least-squares criterion to the expression $S = \sum_{i=1}^{n} y_1 - P(x)^2$ to give a system of simultaneous equations $\frac{\partial S}{\partial cj} = 0$, $j = 0, 1, \ldots, m$ from which the c_i can be determined. Calculation of the c_i is facilitated by using the orthogonality properties of the Chebyshev

polynomials and evaluating P(x) at special points

$\bar{x}_i = \frac{\cos(2i - 1)\pi}{2(m + 1)}$ within the interval (-1, 1) to force off-diagonal elements to be zero in this system of equations. Corresponding values $\bar{y}_i$ are needed in the system of equations in order to be able to solve for the c_i. The program obtains these by applying a linear transformation to the x_i to bring the x_i within the interval (-1, 1) and then using these transformed values and applying the Lagrange interpolation formula to the $\bar{x}_i$ to obtain the $\bar{y}_i$. The system of equations is then easily solved for the c_i. The program then applies a linear transformation to $\bar{x}$ to change the expression $P(\bar{x}) = c_0T_0(\bar{x}) + c_1T_1(\bar{x}) +...+ c_mT_m(\bar{x})$ to the form $P(x) = a_0 + a_1x +...+a_mx^m$ over the original interval (a, b).

```
 0:  TBL 4; ENT "DEGREE?", Z + 1 → R6, "X1?", R8 → X, "DELTA X?", R9;
     CFG 13; TBL 2
 1:  PRT "DEGREE"; SPC 1; PRT Z; SPC 2; PRT "X", "Y"; SPC 1; 12 → R0 → Z
 2:  ENT "Y?", RZ; IF FLG 13 = 0; PRT x, RZ; SPC 1; X + R9 → X; Z + 1
     → Z → R1; JMP 0
 3:  SPC 1; PRT "COEFFICIENTS"; SPC 1
 4:  (((R1-12 → R7) + R (1 → A) → R2) + R6 → R3) + R6 → R4
 5:  COS ((π/2) (2A-1)/R6) → R (R6-A + R2); JMP (A + 1 → A) > R6
 6:  R7 - 1 → A; 2/A → B; -1 → RR1; R1 → C
 7:  RC + B → R (C + 1); JMP (C + 1 → C) = R2 -1
 8:
 9:
10:  0 → A; 1 → B
```

```
11:  IF R (R2 + A) > R (R1 + B); B + 1 → B; JMP 0
12:  B ÷ (B = 1) - (B = R7 -1) → C
13:  (R7-1) (R (R2 + A) - R (R1 + C -1))/2 → Y
14:  -Y (Y - 1) (Y - 2) R (R0 + C - 2 → C)/6 + (YY -1) (Y - 2) R (C + 1)/2 → Z
15:  Z - (T + 1) (Y - 2) YR (C + 2)/2 + Y (YY - 1) R (C + 3)/6 → R (R4 + a)
16:  IF R6 ÷ (A + 1 → A); GTO -5
17:
18:
19:
20:  0 → A
21:  0 → Y; 0 → B; IF A = 1; GTO 25
22:  IF A > 1; GTO 27
23:  Y + R (R4 + B) → Y; JMP (B + 1 → B) > R6 -1
24:  GTO 31
25:  Y + R (R2 + B) R (R4 + B) → Y; JMP (B + 1 → B) > R6 ÷ 1
26:  GTO 31
27:  1 → RR1
28:  R (R2 + B) → R (R1 + 1); 2 → C
29:  2R (R2 + B) R (R1 + C-1) -R (R1 ÷ C-2) → R (R1 + C); JMP (C + 1 → C) > A
30:  Y ÷ R (R4 + B) R (R1 + A) → Y; IF (B + 1 → B) ≤ R6 -1; GTO 28
31:  2Y/Ry → R (R3 + A); IF (A + 1 → A) ≤ R6 -1; GTO 21
32:  RR3/2 → RR3
33:  (R8 → C) + R9 (R7 - 1) → B
34:  (B + C)/2 → R10; (B - C)/2 → R11
35:  RR3 → RR4; R (R3 + 1) → R (R4 + 1); 0 → C
36:  IF R6 ≤ 2; GTO 46
37:  0 → R (R1 + C) → R (R0 + C) → R (R4 + C + 2); JMP (C + 1 → C) > R6 -1
```

```
38:  1 → R (R1 + 1); 2 → C
39:  COS (πC/2) → RR0; 1 → B
40:  2R (R1 + B - 1) -R (R0 + B) → R (R0 + B); JMP (B + 1 → B) > C
41:  0 → B
42:  R (R4 + B) + R (R3 + C) R (R0 + B) → R (R4 + B); R (R1 + B) → A;
     R (R0 + B) → R (R1 + B); A → R (R0 + B)
43.  IF (B + 1 → B) ≤ C; GTO 42
44:  IF (C + 1 → C) ≤ R6 - 1; GTO 39
45:
46:  RR4 → RR0; 1 → C
47:  0 → R (R0 + C); JMP (C + 1 → C) = R6
48:  1 → C
49:  R (R0 + C) + R (R4 + C)/R11 + C → R (R0 + C); 1 → A → R5 → B; C + 1 → Y
50:  B → X; XR5 → R5; R5R11 + C → Z; A (Y - X) → A
51:  R (R0 + C - B) + A*R10 + B*(-1) + B*R (R4 + C)/Z → R (R0 + C -B); IF
     (B + 1 → B) ≤ C; GTO 50
52:  IF (C + 1 → C) ≠ R6; GTO 49
53:  0 → A
54:  PRT A, R (R0 + A); SPC; JMP (A + 1 → A) = R6
55:  R0 → R7; PRT "----------------"; SPC 13
56:  GTO 0
57:  END
```

Compensation Code

This program was written to determine how accurately gamma compensation could be achieved utilizing digital computer methods rather than analog methods.

```
 0:  PRE "--- DATA ---"; SPC 2; PRT "R/HR"; SPC 1; PRT "V ''3''", "V ''4''"
     ; SPC 1
 1:  PRT "R = F (V3)", "R = F (V4)"; SPC 1
 2:  PRT "% DIF of V3 to V4"; SPC 1
 3:  PRT "%/DIF. to R/HR"; SPC 3
 4:  21 → R16; 0 → R17
 5:  WTB 1, 192
 6:  "A"; ENT "POSITION ?", X; IF X ≤ 0; GTO "L"
 7:  6.226376 + .603346X - .193881X↑2 + .02637X↑3→Y
 8:  Y - .00220673X↑4 + 1.168232E-4X↑5 - 3.396338E -6X↑6 + 4.052068E-8X↑7→Y
 9:  10 ↑ Y → RR16
10:  0 → C; 0 → X; 0 → Z; 0 → R1 S; 0 → R19
```

In the above section the experimenter enters the vertical port position and the exposure rate is calculated and stored.

```
11:  35 → X; GSB "DELAY"
12:  RED 3, Y, X; RED 5, Y, Z
13:  X + R18 → R18; Z + R19 → R19; C + 1 → C; IF C ≤ 9; JMP -1
14:  R18/1000 → R (R16 + 1); R19/10000 → R (R16 + 2)
15:  LOG R (R16 + 1) → X
16:  5.1661489 + 1.4982995X + .4589825X↑2 - .2015837X↑3 - .458746X↑4 → Y
17:  Y + .2037761X↑5 + .36659235X↑6 + .08162451X↑7 → Y
18:  - 9.80343538E-3X↑8 + Y → Y; 10↑Y → R (R16 + 3)
19:  LOG R (R16 + 2) → X
20:  5.635509 + 1.53211X + .15001044X↑2 - .32412528X↑3 → Y
21:  Y + .04883571X↑4 + .413/684X↑5 + .25185536X↑6 → Y
22:  Y + 052733125X↑7 + .002576072X↑8 → Y; 10↑Y → R (R16 + 4)
23:  FLT 4; PRT RR16; SPC 1; PRT R (R16 + 1), R (R16 + 2); SPC 1; 3 → X
```

In this section $v(t_c)$ for both channels is measured. These values are then put into the curve fit equations for $v(t_c)$ vs R/hr; equations 4-1 and 2.

```
24:  PRT R (R16 + X); X + 1 → X; IF X ≤ 4; JMP 0
25:  SPC 1; FXD 4; PRT (R (R16 + 3) -R (R16 + 4))/R (R16 + 3)
26:  RR16 → X; FXD 4; SPC 1; PRT (R (R16 + 3) -X)/X, (R (R16 + 4) -X)/X
27:  R16 + 5 → R16; SPC 3
38:  GTO "A"
29:  "1"; R16 → RR17
30:  ENT "TAPE ?", A," FILE ?", A
31:  RCF A, R (R16 - 1)
32:  GTO "END"
33:  "DELAY"
```

The compensation values tabulated in tables 4-1 and -2 are then calculated and stored.

```
34:  CMD "?V5"; FMT *; RED 13, A
35:  "0"; CMD "?V5"; RED 13, B
36:  IF X ≠ 35; 10 → X
37:  IF B-A ≤ X; GTO "0"
38:  RET
39:  "END"; END
```

This is a subroutine used to delay the computer 35 sec between measurements.

Plotting Routine

The following in the data output plotting routine used to produce figures 4-8 through 4-23.

```
 0:  PRT "PROG. PLOTS I VS."
 1:  PRT "PIC VOLTAGE SIG."
 2:  PRT "DATA FROM FILE"
 3:  PRT "GIVEN."; SPC 3
 4:  ENT "TAPE ?", B; ENT "PLOT FILE ?", A; LDF A
 5:  SCL -8200, 11000, -2000, 11000
 6:  LTR 2000, 10600, 321
 7:  PLT "CURRENT VS PIC SIG."
 8:  0 → X ; 0 → Y
 9:  PEN; PLT X, Y; 1 → A; R9 → B
10:  1000/(-LOG R9 + LOG R10) → R11
11:  (-LOG R9 + LOG (B * A)) * R11 → X
12:  PLT X, Y; PLT X, Y + 100; PLT X, Y
13:  A + 1 → A; IF A ≤ 9; JMP -2
14:  B * 10 → B; 1 → A; IF 10000 > (-LOG R9 + LOG (B*A)) * R11; JMP -3
15:  PLT 10000, Y
16:  PEN; 1 → A; R6 → B; 0 → X; 0 → Y; PLT X, Y
17:  10000/(-LOG R6 + LOG R7) → R8
18:  (-LOG R6 + LOG (B * A)) * R8 → Y
19:  PLT X, Y; PLT X + 10 0, Y; PLT X, Y
20:  A + 1 → A; IF A ≤ 9; JMP -2
21:  B * 10 → B; 1 → A; IF 10000 > (-LOG R6 + LOG (B * A)) * R8; JMP -3
22:  PLT x, 10000
23:  10000 → X; 0 → Y
24:  PEN; PLT X, Y; PLT X, Y + 10000; PLT X - 10000, Y + 10000; PEN
25:  R9 → B; 0 → Y
26:  (-LOG R9 + LOG B) * R11 → X; B * 10 → B; IF B > R10; JMP 2
```

```
27:  PLT X, Y; PLT X, Y  + 10000; PEN; JMP -1
28:  R6 → B; 0 → X
29:  (-LOG R6 + LOG B) * R3 → Y; B * 10 → B; IF B > R7; JMP 2
30:  PLT X, Y; PLT X + 10000, Y; PEN; JMP - 1
31:  R6 → B
32:  -1000 → X; LOG B → A
33:  (-LOG R6 + LOG B) * R8 - 100 → Y
34:  LTR X, Y, 211; PLT "10"
35:  LTR X + 300, Y + 300; FXD 0; PLT A; A + 1 → A; IF A ≤ LOG R7; 10 * B
     → B; JMP -2
36:  LTR 3000, - 900, 211
37:  PLT "IONIZATION CURRENT (AMPS)"
38:  R9 → B; -600 → Y; LOG B →  A
39:  (-LOG R9 + LOG B) * R11 -300 → X
40:  LTR X, Y, 211; PLT "10"
41:  LTR X + 300, Y + 300; FXD 0; PLT A; A + 1 → A; IF A ≤ LOG R10; 10
     * B → B; JMP -2
42:  LTR -1200, 4300, 212
43:  PLT "PIC SIG. (VOLTS)"
44:  LTR - 7800, 10800, 211
45:  PLT "IG-SS VG(+) IF-SS VF ( )"
46:  -2200 → X; 10890 → Y; PLT X, Y; PEN
47:  PLT X + 50, Y + 50; PLT X + 50, Y - 50; PLT X - 50, Y - 50; PLT X - 50,
     Y - 50; PLT X + 50, Y + 50; PEN
48:  LTR -7900, 10600, 111
49:  PLT "AMPS VOLTS AMPS VOLTS"
```

```
50:  11000 → Y; -600 → Z; PLT -8200, Y; PLT -8200, Z; PLT -6545, Z; PLT
     -6545, Y; PLT -4890, Y
51:  PLT -4890, Z; PLT -3235, Z; PLT -3235, Y; PLT -8200, Y; PLT -1580, Y;
     PLT -1580, Z; PLT -8200, Z
52:  PEN; PLT -8200, 10480; PLT -1580, 10480
53:  10350 → Z; 21 → A; 0 → R12; A → R12
54:  "0"; ENT "CHANGE PEN?", C
55:  Z -250 → Z
56:  "1"; LTR -8100, Z, 21; FLT 2; PLT RR13
57:  LTR -6460, Z; FLT 2; PLT R (R13 + 1)
58:  LTR -4790, Z; FLT 2; PLT R (R13 + 2)
59:  LTR -3135, Z; FLT 2; PLT R (R13 + 3)
60:  Z -300 → Z; R13 + 4 → R13; IF R13 + 1 ≤ RR12; GTO "1"
61:  "2"; A + 1 → B; IF RA ≤ 1E-14;; GTO "3"
62:  IF RA ≤ R9; GTO "3"
63:  IF RA > R10; GTO "3"
64:  IF RB ≤ R6; GTO "3"
65:  IF RB > R7; GTO "3"
66:  (-LOT R6 + LOG RB) * R8 → Y; (-LOG R9 + LOG RA) * R11 → X; PLT X + 50, Y
67:  PLT X-50, Y; PEN; PLT X, Y + 50; PLT X, Y - 50; PEN
68:  "3"; A + 3 → C; A + 2 → B
69:  IF RB ≤ 1E - 14; GTO "4"
70:  IF RC ≤ R6; GTO "4"
71:  IF RC > R7; GTO "4"
72:  IF RB ≤ R9; GTO "4"
73:  IF RB > R10; GTO "4"
74:  (-LOG R6 + LOG RC) * R8 → Y; (-LOG R9 + LOG RB) * R11 → X; PLT X, Y;
     PEN; PLT X + 50, Y + 50
```

```
75:  PLT X + 50, Y - 50; PLT X - 50, Y - 50; PLT X - 50, Y + 50; PLT
     X + 50, Y + 50; PEN
76:  "4"; A + 4 → A; IF A + 1 ≤ RR12; FTO "2"
77:  R12 + 1 → R12; IF R12 ≤ 4, IF RR12 > 0; GTO "9"
78:  STP; END
```

REFERENCES

1. Popper, G. F. and Lipinski, W. C., "Wide Range Counting-Campbelling Neutron Flux Detection System," ANL-7224 (1967).

2. Harrer, J. M. and Beckerley, J. G., Nuclear Power Reactor Instrumentation Systems Handbook, Volume I and II, T.I.C., U.S.A.E.C. (1973).

3. Sprague, K. E., "Nuclear Seeded ^{3}He Plasma," Master's Thesis, University of Florida (1966).

4. Markwell, F. A., "The Application of the Pulsed Ionization Chamber to Reactor Power Measurements," Master's Thesis, University of Florida (1971).

5. Kaiser, B. J., "Pulsed Ion Chamber Wide Range Radiation Field Monitor," Masters Thesis, University of Florida (1975).

6. Heravi, I., "Steady State Density and Collection Systematics for Positive Ions in the Pulsed Ion Chamber," Master's Project, University of Florida (1976).

7. Cooper, J. L., "Gamma Compensated Pulsed Ionization Chamber," Master's Thesis, University of Florida (1972).

8. Sanders, G. H., "Gas Systems Development and PIC Measurements for Gas Kinetics Studies of He-N_2 and He-Ne Mixtures," Master's Thesis, University of Florida (1972).

9. Ellis, W. H., "Gamma Compensated Pulsed Ionization Chamber Wide Range Neutron/Reactor Power Measurement System," U. S. Navy Patent Disclosure, Navy Case No. 57,018 (1973).

10. Shan, S. Kuo, Numerical Methods and Computers, Addison - Wesley, Reading, Massachusetts (1965).

11. Loeb, L. B., Basic Processes of Gaseous Electronics, University of California Press, Berkley, (1961)

BIOGRAPHICAL SKETCH

Bruce John Kaiser was born July 10, 1950, in Picton, Ontario, Canada. He attended grade school at St. Michael's in Belleville, Ontario, and high school at Cardinal Gibbons in Fort Lauderdale, Florida. His college career began with two years at Loyola of Montreal where he was awarded a scholarship for maintaining a high scholastic average. At the end of two years he transferred to the University of Florida, from where he was graduated in 1972 with an honors B.S. degree in physics.

He entered the University of Florida Graduate School in September 1972 and was supported for one year by a N.E.W. traineeship and then by a University of Florida teaching assistantship. In June 1975, he received his master's degree in Nuclear Engineering Sciences. He then continued his schooling at the University of Florida being financially supported by a teaching assistantship and later by a Northwest College and University Association for Science fellowship. The main body of his reseach was completed at the Hanford Engineering and Development Labs run for ERDA by the Westinghouse Hanford Company.

He married Michele Ritzmann of Miami, Florida, on June 16, 1973. His hobbies include electronics associated with high fidelity sound reproduction, wild life photography, archery, fishing, and woodworking.

His interests professionally lie in applied nuclear engineering reseach, and it is for this reason he continued his education at the

University of Florida, seeking a doctorate degree in nuclear engineering. He is currently seeking a job in his field of expertise.

I certify that I have read this study and that in my opinion it conforms to acceptable standards of scholarly presentation and is fully adequate, in scope and quality, as a dissertation for the degree of Doctor of Philosophy.

W. H. Ellis, Chairman
Associate Professor of Nuclear Engineering Sciences

I certify that I have read this study and that in my opinion it conforms to acceptable standards of scholarly presentation and is fully adequate, in scope and quality, as a dissertation for the degree of Doctor of Philosophy.

E. E. Carroll, Co-chairman
Professor of Nuclear Engineering Sciences

I certify that I have read this study and that in my opinion it conforms to acceptable standards of scholarly presentation and is fully adequate, in scope and quality, as a dissertation for the degree of Doctor of Philosophy.

N. J. Diaz
Associate Professor of Nuclear Engineering Sciences

I certify that I have read this study and that in my opinion it conforms to acceptable standards of scholarly presentation and is fully adequate, in scope and quality, as a dissertation for the degree of Doctor of Philosophy.

G. R. Dalton
Professor of Nuclear Engineering Sciences

I certify that I have read this study and that in my opinion it conforms to acceptable standards of scholarly presentation and is fully adequate, in scope and quality, as a dissertation for the degree of Doctor of Philosophy.

W. Mauderli
Professor of Radiation Physics

I certify that I have read this study and that in my opinion it conforms to acceptable standards of scholarly presentation and is fully adequate, in scope and quality, as a dissertation for the degree of Doctor of Philosophy.

C. K. Day
Engineer, Westinghouse Hanford Company

This dissertation was submitted to the Graduate Faculty of the College of Engineering and to the Graduate Council, and was accepted as partial fulfillment of the requirements for the degree of Doctor of Philosophy.

June, 1977

Dean, College of Engineering

Dean, Graduate School